EXPERIMENTAL AND ANALYTICAL STUDY
ON THE STABILITY OF A BOUNDED JET
AT LOW REYNOLDS NUMBERS

By

JUAN L. LOPEZ

A DISSERTATION PRESENTED TO THE GRADUATE COUNCIL OF
THE UNIVERSITY OF FLORIDA IN PARTIAL
FULFILLMENT OF THE REQUIREMENTS FOR THE DEGREE OF
DOCTOR OF PHILOSOPHY

UNIVERSITY OF FLORIDA
1977

To my wife Elsa

ACKNOWLEDGEMENTS

TABLE OF CONTENTS

TABLE OF CONTENTS (Continued)

TABLE OF CONTENTS (Continued)

Page

LIST OF FIGURES

LIST OF FIGURES (Continued)

LIST OF SYMBOLS

(Arranged in Alphabetical Order)

A_0 cross-sectional area (unobstructed)

A_1 cross-sectional area (obstructed)

c complex axial wave velocity

$\bar{c}$ dimensionless axial wave velocity

C viscometer calibration constant

d interface distance

D_0 test section diameter (unobstructed)

D_1 constriction diameter

e model eccentricity

H step height

Hz Hertz

I_m modified Bessel function of the first kind

K_m modified Bessel function of the second kind

k axial wavenumber

$\hat{k}$ unit vector in the z direction

L_D length of the turbulence region when close to the constriction

m azimuthal wavenumber

p total pressure

$p(r)$ amplitude of the pressure fluctuation

$\hat{p}$ pressure fluctuation

P_0 mean flow pressure

$\vec{q}$ total velocity vector

Q   flow rate

r   radial cylindrical coordinate

R   interface distance, $R = R_2 - R_1$

Ro   boundary position

Re   Reynolds number based on unobstructed pipe diameter Do

s   asymmetric parameter

t   time of fall

T   temperature in ^{o}C

u   longitudinal velocity component

$\hat{u}$ longitudinal fluctuation velocity

u(r) amplitude of the radial velocity fluctuation

U   longitudinal component of the mean flow velocity

Uo   mean flow centerline velocity

U   mean flow orifice velocity

v   transverse component of velocity

$\hat{v}$ transverse fluctuation velocity

V   transverse component of the mean flow velocity

w   axial velocity fluctuation

W(r) axial velocity distribution

Wo   mean flow centerline velocity in cylindrical coordinates

x   longitudinal rectangular coordinate

y   transverse rectangular coordinate

Zo   constriction length

LIST OF SYMBOLS (Continued)

Greek letters

δ velocity profile parameter, $\delta = d_1/(d_2-d_1)$

θ angular cylindrical coordinate

μ fluid viscosity

ν kinematic viscosity

ρ fluid density

σ disturbance growth rate

τ_w wall shear stress

ϕ perturbation amplitude

ψ Stoke's stream function

ω complex amplification factor

Subscripts

i   imaginary part

r   real part

N   normalized variable

Symbols not listed here have all been described in the text when used for the first time.

Abstract of Dissertation Presented to the
Graduate Council of the University of Florida
in Partial Fulfillment of the Requirements for the
Degree of Doctor of Philosophy

EXPERIMENTAL AND ANALYTICAL STUDY ON THE
STABILITY OF A BOUNDED JET AT LOW REYNOLDS NUMBERS

By

Juan L. Lopez

June, 1977

Chairman: Dr. Ulrich H. Kurzweg
Major Department: Engineering Science, Mechanics, and
Aerospace Engineering

A series of steady flow experiments is described, in
which important hydrodynamics factors, including onset of
instabilities and transition to turbulence are considered
for the axisymmetric jet formed downstream of symmetric
constrictions in circular pipes. Results were obtained
for several ratios of test section to constriction dia-
meter, within a Reynolds number ($Re=UoDo/\nu$) range from
approximately 50 to 2000. The critical Reynolds number
for onset of velocity undulations was evaluated for a
wide range of area ratios using a non-disturbing flow vis-
ualization technique, based on the double refracting
properties of an aqueous colloidal solution of White
Hector bentonite.

It was found that the critical Reynolds number was independent of the test section diameter and a function of the dimensionless area ratio. Different types of instabilities were noticed and the flow characteristics changed rapidly with increasing flow velocity.

A brief comparison with previous investigations on the onset of sound showed a definite correlation with the onset of undulations in the present experiment, but onset of sound appeared to occur at a more advanced stage of flow disturbances, beyond the onset of instabilities.

Experimental observations also demonstrated the existence of different modes of instability propagation. Of particular interest was some type of helical motion which usually appeared at some distance from the orifice. At sufficiently large flow rates the jet broke down into turbulence, producing a localized turbulent region of highly irregular motion bounded by laminar disturbed flow on both sides. The relative position of this region with respect to the jet orifice was measured for several geometrical conditions. Pressure drop measurements were taken across the obstructed pipe section using distilled water and a solution of polyethylene oxide. Results demonstrated a strong influence of geometry and area ratio upon pressure drop measurements on flows through pipe constrictions.

Inviscid stability analysis was applied to study the

propagation of symmetrical and non-symmetrical disturb-
ances in rectangular and cylindrical geometry, and the
wave phase velocity and growth rate computed for several
velocity profiles. Numerical calculations showed a
non-vanishing growth rate for the dimensionless wavenumber
range $o < kd < 1.30$, where d is interface layer thickness.
Maximum growth rate usually occurred for kd approximately
0.80 and of magnitude very sensitive to the shear-layer
thickness.

The stability of an unbounded cylindrical jet was
examined and the instability amplification evaluated at
various downstream positions. Results validated some of
the experimental observations by showing the growth rate
to be larger for axisymmetric disturbances near the jet
orifice, but, larger for non-axisymmetric modes at positions
further downstream, where the jet has partially diffused.
Observed instability wave lengths correlated with the
corresponding wavenumber for maximum amplification as
predicted by inviscid analysis.

CHAPTER I
INTRODUCTION

The Problem of Transition to Turbulence

In 1839 the German engineer Hagen published results
of experiments on the flow of water through cylindrical
glass tubes, reporting observations on the transition
region between steady and irregular flow. This seems
to be one of the first times that the transition phenom-
enon and the existence of turbulence have been expressly
reported in the literature.

In his fundamental investigations 1879-1833, O.
Reynolds distinguished between "steady" and "sinuous"
fluid motion, and introduced a dimensionless quantity
characterizing homogeneous incompressible viscous flow.
This is Reynolds number, $Re = U\, Do/\nu$ (U = mean flow velocity;
Do = tube diameter; ν = kinematic viscosity) usually inter-
preted as the ratio of the inertial to the viscous forces
has been used since Reynolds' experiments to indicate the
state of a fluid motion, with transition to irregular
motion occurring at a certain value.

Experimental and analytical studies of the transi-
tion phenomenon have been numerous since the end of the
last century, most of them related to the incidence of
turbulence in relation to flow through straight pipes

1

and channels. Schiller (1921) reported that if the flow
is highly disturbed at the tube entrance and provided
the entrance length is long enough there occurs an instan-
taneous increase of the flow resistance when a critical
Reynolds number is exceeded. This discontinuity of the
flow resistance was currently interpreted as an instan-
taneous onset of turbulence. Tollmien (1929) computed
the neutral stability curve for the boundary layer on a
flat plate using the theory of instability to small
oscillations. Tatsumi (1952) using Tollmien's method,
obtained a lowest possible critical Reynolds number of
approximately 9700 for Poiseuille flow.

Binnie (1945, 1947) reported the appearance of flow
disturbances by visual observations using the stream
double refraction technique at a Reynolds number close
to 1970, with continuous turbulence established at 2900.
Lindgren (1957) made similar studies and the interpreta-
tion of these observations suggests that the transition
phenomenon in viscous flow does not occur instantaneously
at some specific Reynolds number but rather within a
transitional Reynolds number range.

While there are numerous experiments on transition in
cylindrical test sections, there appears to be no exten-
sive data published concerning the critical Reynolds
number at which an axisymmetric jet becomes unstable, or,
the characteristics and position of the stationary turbu-

lent region formed downstream of a jet orifice.

The present investigation has been directed to investigate the flow characteristics for a jet in the presence of rigid boundaries. The jet was formed by symmetric constriction sections of various diameters within the test pipe. The method of observation was based on the streaming double refraction properties of White Hector Bentonite. An inviscid stability analysis was then applied to determine the mode of disturbance propagation that grows most rapidly at large Reynolds number. The analysis was applied to study the propagation of symmetrical and non-symmetrical disturbances, the wave phase velocity, and instabilities growth rate for the approximated symmetrical velocity profiles.

The Reynolds number at the onset of undulations was compared with some available date from previous investigations and with the conditions for the onset of sound in cylindrical sections with flexible walls.

Previous Investigations

The first major contribution to the study of hydro-dynamical stability can be found in the theoretical papers of Helmholtz (1868). Previous to this time, many scholars had certainly become aware of the question but their efforts did not progress beyond the stage of

description. After the findings of Helmholtz, the com-
bined efforts of Reynolds (1883), Kelvin (1880) and
Rayleigh (1878) produced a rich harvest of knowledge.
Lord Rayleigh, between 1878 and 1917 published a great
number of papers on this subject and was able to prove
that the existence of a point of inflexion on the velo-
city profile constitutes a necessary condition for the
occurrence of instability in inviscid fluid flow. Much
later Tollmien (1926) succeeded in showing that this
constitutes also a sufficient condition for the amplifi-
cation of disturbances.

The key stability equation was arrived at indepen-
dently by Orr (1907) and by Sommerfeld (1908). At this
stage, it was generally believed that the study of
infinitesimal small pertubations would lead to some
definite answers to the problem of transition from lam-
inar to turbulent flow. Tollmien (1929) using the Orr-
Sommerfeld stability equation calculated the first
neutral eigenvalues for two-dimensional boundary layer
flow. Soon the same road led Schlichting (1932) to
further evaluation of critical Reynolds number and ampli-
fication rates of disturbances.

Later, Lin (1945) reviewed and improved the mathe-
matical procedures and laid the foundations for a
general expansion of the stability analysis.

At this time the stability of plane Poiseuille
flows had become a particularly controversial issue

and Lin put it in order by his new and more general analysis. Also at this time a new tool, the digital computer, became available for the analysis of hydro-dynamic stability. After a great deal of effort it became apparent that the theory of amplification of small flow perturbations could not explain the transi-tion to turbulent flow.

The efflux of a laminar jet from an orifice in the absence of solid boundaries was treated by Bickley (1939) applying boundary layer theory. The velocity profiles determined by Bickley were correlated with experiments by Andrade (1939) confirming the theoretical predictions. It was also determined that the jet becomes unstable at very low orifice Reynolds number.

The laminar circular jet was treated by Schlichting (1933), and Tollmien (1926) determined the velocity distribution for the circular turbulent jet using Prandtl's mixing-length theory, both cases for jets immersed in a medium with no radial boundaries. Experi-mental results on circular jets were given by W. Zimm (1921) and P. Ruden (1933). The immersed free jet, which occures when a fluid is discharged from a nozzle or orifice far from any solid boundaries, becomes completely turbulent a short distance from the point of discharge producing strong mixing with the surrounding fluid.

A. J. Reynolds (1962) conducted experiments on the instabilities of a liquid-into-liquid jet directed into a large tank of water. The experiments were performed with the purpose of resolving observational discrepancies reported by Schade and Viilu (See Reynolds, 1962). Schade reported that a long rectilinear jet could be maintained until the Reynolds number (based on orifice diameter) was a few hundreds. Viilu (1960) reported, after careful experiments at low flow rates, a value of 11 for the Reynolds number at breakdown. Reynolds (1962) in his observations encountered a surprising variety of flows, among them, "pedal" breakdown, "sinuous" oscillations, and "shearing" puffs. According to his observations while it was difficult to obtain steady jets at relative low Reynolds numbers, progressively longer jets could be maintained as the Reynolds number increased toward 150. For Reynolds numbers above 300, jets became disordered near the nozzle, although not so near as in the range between 10 and 30.

The stability of the two-dimensional laminar free jet against infinitesimal antisymmetric disturbances was treated by Tatsumi and Kakutami (1958), obtaining a curve of neutral stability separating the regions of stable and unstable flow in the (k, Re) plane, where k is the oscillation wave number. Calculation showed that the free jet becomes unstable at very low Reynolds number of less than 10.

Batchelor and Gill (1962) made a general mathematical analysis of the stability of axisymmetric jets for homogeneous unbounded fluids. A condition similar to Rayleigh's about the inflexion point was shown to be a necessary condition for instability, also it was shown that the propagation of non-axisymmetric mode of oscillations were favored for velocity profiles varying slowly with respect to the radial coordinate, as observed previously by Reynolds (1962).

Recently the breakup of a free liquid jet was studied by Taub (1976) using a high resolution optical probe technique.

Investigations on Jets in the Presence of Rigid Boundaries

Most of the experiments in connection with the flow of fluids through orifices in bounded regions have been directed toward the establishment of the orifice as a flow meter device. The flow of fluids through locally constricted regions has been extensively investigated both experimentally and theoretically in recent years for the purpose of determining characteristics of flow through constrictions in arteries, commonly referred to as stenosis.

The characteristics of the flow of fluids through pipe orifices within the transitional region between steady laminar and turbulent flow have been described

by Johansen (1929). The flow pattern downstream of the orifice was studied by means of a dye in distilled water. Johansen found that the magnitude of the Reynolds number for a given event or type of flow increased progressively as the orifice to pipe diameter ratio was increased. Also it was possible to relate many of the pressure drop characteristics to features of the flow pattern observed visually.

In the last two decades the flow passing an abrupt expansion has been studied experimentally by many researchers. Abbott and Kline (1962) observed the turbulent flow over single and double steps in rectangular sections, determining the length of separation. Meisner and Rushmer (1963) studied the disturbed region downstream of the expansion using a colloidal suspension of White Hector Bentonite.

The effects on fluid flow produced by a geometry change, of a constricted region in a pipe were determined by Robbins and Bentov (1967) with the purpose of identifying the most influential factors in stenotic flow. Back and Roschke (1972) in an experimental investigation on the flow of water through an abrupt circular-channel expansion described the position of the reattachment point as a function of the upstream Reynolds number within the range of transition to turbulence.

Experimental studies on instabilities and velocity distribution downstream of a constricted flow region were reported by Durst, Melling and Whitelaw (1974), in a rectangular symmetric expansion, and by Iribarne, Frantisak, Hummel, and Smith (1972) in a cylindrical symmetric expansion.

Pressure drop measurements across constricted regions simulating stenosis have been made by Young and Tsai (1973) and by Seeley and Young (1976), while the turbulence spectra were obtained for flows downstream of the constriction by Kim and Corcoran (1974).

Numerical computations and correlation with experiments were reported by Macagno and Hung (1967) for a circular conduit with an abrupt expansion, and by Lee and Fung (1970) for local constrictions with smooth axisymmetric expansions at low Reynolds number flows.

Morgan and Young (1974) using an integral method approach presented a solution to the problem of incompressible flow through an axisymmetric constriction for low Reynolds number flows below the onset of turbulence. The results showed that even a mild constriction can cause a radical alteration in flow characteristics which become more drastic with constriction ratio and increasing Reynolds number.

Later Aillo and Trefil (1976) studied the entrance flow problem by linearization of the convective derivative

to evaluate the establishment of Poiseuille flow in locally constricted tubes.

Physiological Implications, Blood Flow

While most of the flows we encounter in daily life are turbulent; many biological flow systems appear designed to function within the laminar regime. The possible occurrence of turbulence in hemodynamics has been with us for a long time. Physiologists, biophysicists and more recently fluid dynamicists have speculated and performed experiments to determine the flow characteristics of the circulatory system.

A good review of the differences between turbulent and laminar flow and previous research work in the area of circulatory blood flow is given by Robertson and Herrick (1975). The mentioned paper discusses the conditions under which turbulence may be expected to occur in flowing blood in vivo, and makes an attempt to classify the flow as laminar, disturbed or turbulent; with blood flow being mostly of the dissipating type and not permanent or self-preserving turbulence.

Considerations of turbulent motion in hemodynamics are complicated by several factors usually not encountered in other fluid dynamic studies. In vivo blood flows are maintained by pulsatile pressure gradients, and take place in tubes with flexible walls, which are

tapered, and not long enough between bifurcations to permit establishment of fully developed turbulent flow conditions.

At low shear, blood behaves as a non-newtonian fluid with a yield stress (Charm, 1972). Blood also contains suspended particles (erythrocytes, leucocytes and platelets) and is not considered a homogeneous medium.

The physiological range of average flow Reynolds numbers is usually considered to be below 2000, but due to the pulsating nature of the flow, Reynolds numbers above this value do occur. McDonald (1960) estimated peak Reynolds numbers in the aorta of humans and animals noting values in the range 2400 to 10000. We must remind ourselves that although Reynolds numbers of this magnitude actually occur in the blood circulatory system, these occurrences will be over very short periods of time and over short tube lengths, so that conditions for fully developed turbulence are not satisfied.

Stenotic Flow

The partial occlusion of arteries due to stenotic obstruction is one of the most frequently occurring abnormalities in the circulatory system. The causative factors for the initial development of arterial lesions, leading to stenoses, are not well understood, but regardless of

the cause it is clear that once an obstruction has developed the flow characteristics will change and hydrodynamic factors will play an important role as the stenosis continues to develop.

Flow through local constrictions has been widely studied analytically, numerically and experimentally using models of different geometries simulating stenoses. Macagno and Hung (1967) used computer solutions of the vorticity-transport equation for two-dimensional viscous flow through a conduit expansion, and Lee and Fung (1970) made numerical calculations on the problem of flow in constructed tubes.

Meisner and Rushmer (1963), Back and Roschke (1972), Durst, Melling and Whitelaw (1974), made experimental studies on the flow behavior through cylindrical and rectangular expansions, while Young and Tsai (1973) measured the pressure loss for flows through tube con-strictions. These researchers among many others con-cluded that the most improtant factors having potential physiological significance in the flow of blood through a constricted artery are

(a) Resistance of the constriction to the flow characterized by an increased pressure drop across the constricted region as determined by Young and Tsai (1973) and Seely and Young (1976). Consequently the heart would have to work harder to maintain a required blood supply to the circulatory system.

(b) Damage to the wall tissues produced by turbulent velocity fluctuations in the flow which are created downstream from the stenosis. Fry (1968) reported a possible damage to the endothelium by increased velocity gradient at the wall in arterial blood flow. Morgan and Young (1974) conducted theoretical studies in the wall shear distribution. These results revealed significant alterations caused by severe contractions producing an order of magnitude increase in the maximum shearing stress at low Reynolds number and two orders of magnitude in the moderate range, (about 100), with separation in the downstream diverging section producing a reversal in the wall shearing stress.

(c) The nearly stagnant conditions in the separated region may significantly affect vessel-to-blood mass transfer as reported by Caro (1971) and possibly affect the tissue properties in that region.

(d) Localized turbulence appearing downstream the constricted region. Eddy formation and turbulence were identified by Meisner and Rushmer (1963) using flow visualization methods. The vibrations transmitted to the wall were studied by Foreman and Hutchison (1970) and the fluctuation frequency spectrum measured by Kim and Corcoran (1974) distal (downstream) to a simulated stenosis.

(e) Noise production attributed to the appearance of turbulent motion downstream of a stenosis. This characteristic can be used as a diagnostic tool (phonangiopraphy) for assessing the degree of narrowing of a blood vessel as suggested by Lees and Dewey (1970).

One of the most dramatic consequences associated with a stenosis is the commonly observed enlargement which occurs in the low pressure region distal to a stenosis. Radiologically this post-stenotic dilation (PSD) is often easier to identify than the stenosis, and may be caused by wall damage induced by turbulence (Foreman, 1970). Roach (1963a) indicated that turbulence was the causative agent in PSD developed in dog arteries after artificially producing stenoses in the femoral and carotid arteries with a nylon band. The alterations to the arterial wall which eventually becomes more distensible seems to be related to the flow distortions produced by the stenosis, affecting in some undetermined way the elastin and intercollagen links (Roach, 1963b).

While most authors seem to believe that the flow distortions produced by the stenosis is turbulence, others have questioned this conclusion. Bruns (1959) suggested that turbulence is a random phenomenon and cannot create enough energy to produce sound (murmurs). He proposed that vortex formation (a Karman Trail) was the most likely cause of murmurs and post-stenotic dilatations in arteries.

Another group (Robicsek et al., 1958; Rodbard et al., 1967) feels that cavitation is the most likely cause of murmurs and hence of PSD.

Our intention in bringing the problem of flow through an occluded artery was not an attempt to explain and solve a physiological problem, but to try to relate our experiments in locally constructed tubes and our analytical results to an interesting problem which is not fully understood. We feel that the results obtained during the present investigation on the onset of disturbances, the position of localized turbulence and the pressure drop measurements under steady flow conditions can supply useful information about stenotic flow and provide a good example to which experimental and analytical engineering techniques can be applied to other sciences.

CHAPTER II
EXPERIMENTAL APPARATUS

Description of the Experimental Apparatus and Procedure

Preliminary investigations were conducted using a
very simple experimental apparatus, consisting mainly of
straight rectangular test sections connected directly to
an electric pump and a storage tank, forming a closed
loop. These transparent rectangular test models were
made of three separated sections of acrylic glass, joined
together, with the rectangular channel and constriction
located in the midsection. Two constrictions were made,
one with sharp edges and the other with rounded edges,
both 3.0 cm long, with a channel to orifice diameter
ratio of 1/4 and a channel width of 0.63 cm. These two-
dimensional constrictions consisted of a slit which
extended to the full depth of the flow section.

The optical properties of a solution of a commercial
dye, Milling Yellow, were used to observe the flow
pattern produced by the presence of the channel constric-
tion. The Milling Yellow solution exhibited excellent
birefringent properties, showing a clearly visible inter-
ference pattern when viewed through crossed polarizers,
but unfortunately the solution also exhibited a strong
non-newtonian behavior, and the viscosity was not only a
function of shear stress but was also sensitive to changes
in temperature.

The test section was connected to the pump and the storage tank using tygon vinyl tubing. Care was taken to taper and smooth the inside of the connecting section between the cylindrical tubing and the rectangular inlet to the test section, in order to prevent unnecessary disturbances of the flow patterns at these points.

The experimental observations in the constructed rectangular channels can be summarized as follows: At very low flow rates the over-all flow field remained laminar. This situation was characterized by undisturbed alternating dark and light lines. As the flow rate was increased the central core became disturbed and then small localized eddies appeared. A few diameters down-stream from the localized disturbed region, the disturb-ances were damped and the flow again assumed laminar characteristics. As the flow rate was increased, the eddies formed closer to the jet orifice and the turbulence activity became more pronounced. For high flow rate tur-bulence occurred over a wider region starting at the orifice, but decaying back to stable flow several dia-meters downstream from the constriction. No turbulence was observed upstream of the constricted area.

A stability problem similar to that experienced in fluidic devices was observed. The jet profile in the expansion region showed preference to reattach to one of the walls first, producing asymmetric flow condition.

The observations made in the rectangular cross-section models using the Milling Yellow solution were primarily of a qualitative nature and served only as a preliminary step to more refined experiments using cylindrical test sections.

The arrangement of the experimental equipment for the investigations on flows through cylindrical test sections is shown in Figures 2.1, 2.2a, b. The liquid flow system consisted of an overhead tank, whose level was maintained by continuously pumping the fluid from the storage tank with 1/35 hp 3000 rpm pump, permitting the excess fluid to return to the lower tank through an overflow pipe. This way a truly constant head pressure maintained the flow through the test pipe.

Fluid from the overhead tank flowed through an entrance tube, 130.2 cm long. before entering the test section. The function of the entrance section was to insure the decay of entrance disturbances and the developing of a parabolic flow profile prior to the constriction entrance. Entrance section and all test sections were made of commercially smooth extruded acryllic tubes.

Several test section diameters were used during the experiment as described in Table 1. Their average diameters did not vary more than approximate 1% from the value specified by the manufacturer, but local variations (up to 6%) were noticed in some cases. The average diameter of each tube was determined by filling the tube

with distilled water and measuring the weight of the fluid. Test sections were joined to the entrance and return sections using flanges made of plexiglas, the constriction placed between the entrance and the test section as indicated in the upper right-hand corner of Figure 2.1. The return section drained the fluid into the storage tank forming a re-circulating system.

Flow rate was regulated by a needle valve which allowed very fine adjustments in the fluid velocity. Flow rate was measured with a spherical float flowmeter, manufactured by Gilmont Instruments, Inc., with a water flow range of 30 - 1900 ml/min.

The entrance and the test sections were firmly fixed to a heavy test bench to avoid any external mechanical vibrations, and was mounted horizontally. Connecting tubing between different sections were made of 3/4" ID (1.905 cm) tygon vinyl hose. Also two calibration compartments (of known volumes) were included as part of the storage or collecting tank and, used to calibrate the flow meter and to measure the flow rate outside the flowmeter capabilities.

An important point in the arrangement and design of the experimental apparatus was the avoidance of pressure fluctuations or mechanical vibrations that could induce premature fluid oscillations. It was observed that very small vibrations of the apparatus induced propagation of

instabilities when the fluid was close to the critical
point. For this reason the test bench was mounted on
rubber and rubber strips introduced between the rigid
test tubes and the bench tubes supporter. Measurements
of the critical flow rate (onset of velocity undulations)
were only made when external disturbances were at a
minimum.

Temperature was measured with a thermometer located
prior to the entrance section, and all readings were
taken at room temperature between 24.0° and 25.0° C.
The apparatus described allowed for a complete re-circu-
lating system, very easy to operate and to maintain. At
the beginning of each experiment the fluid was circulated
for a few minutes through the apparatus to obtain homo-
geneous flow conditions.

A Gravity tank
B Flowmeter
C Thermometer
D Entrance section (130.2 cm)
E Test section (57.1 cm)
F Polarizer-Analyzer
G Needle valve
H Control valve
I Calibration compartments
J Storage tanks
K Pump
L Constriction
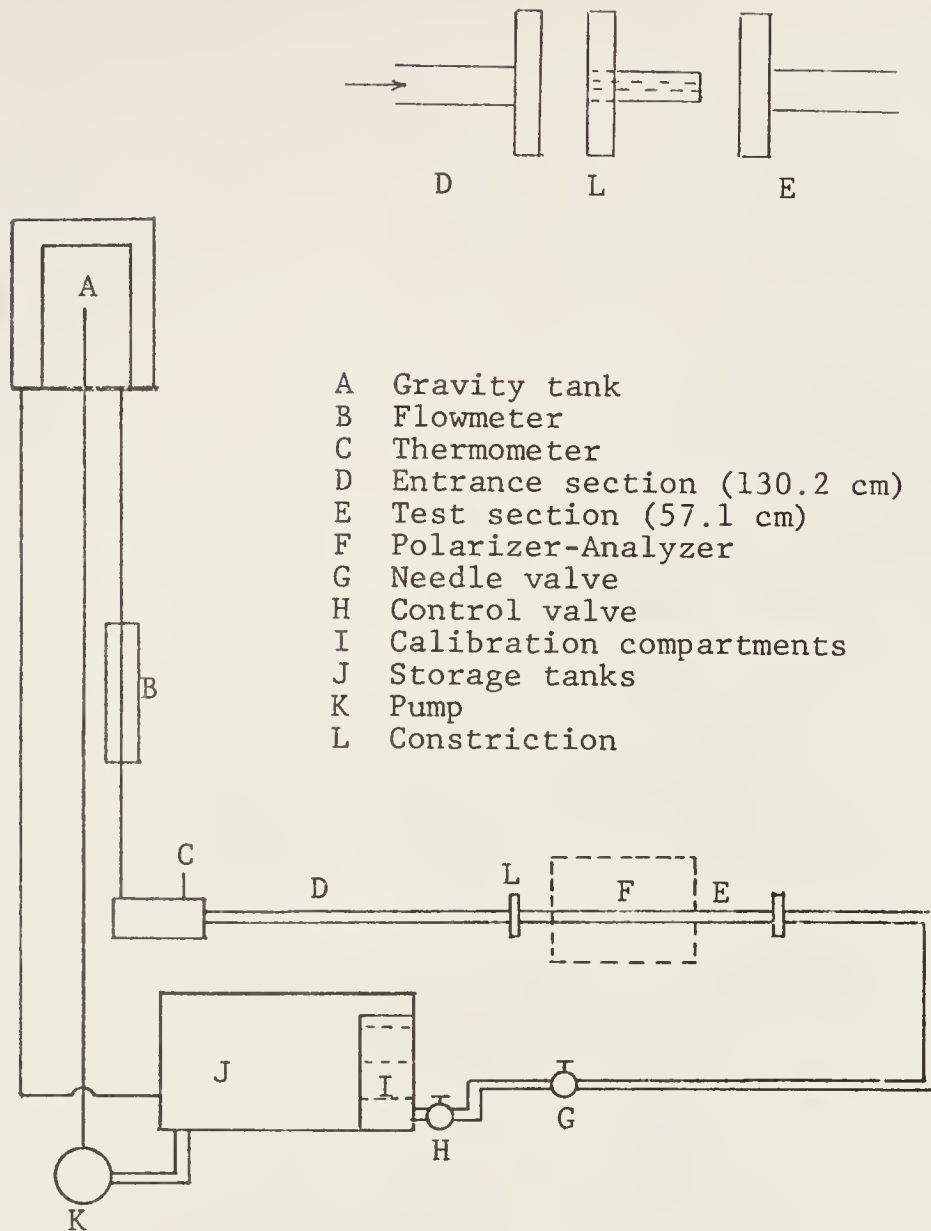
Figure 2.1   Diagram of the experimental apparatus
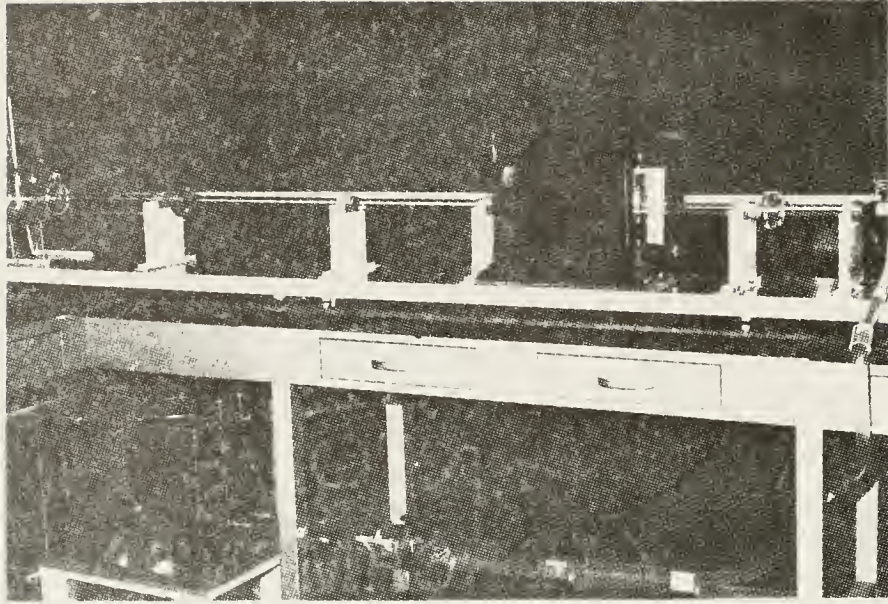
Figure 2.2a   Experimental Apparatus
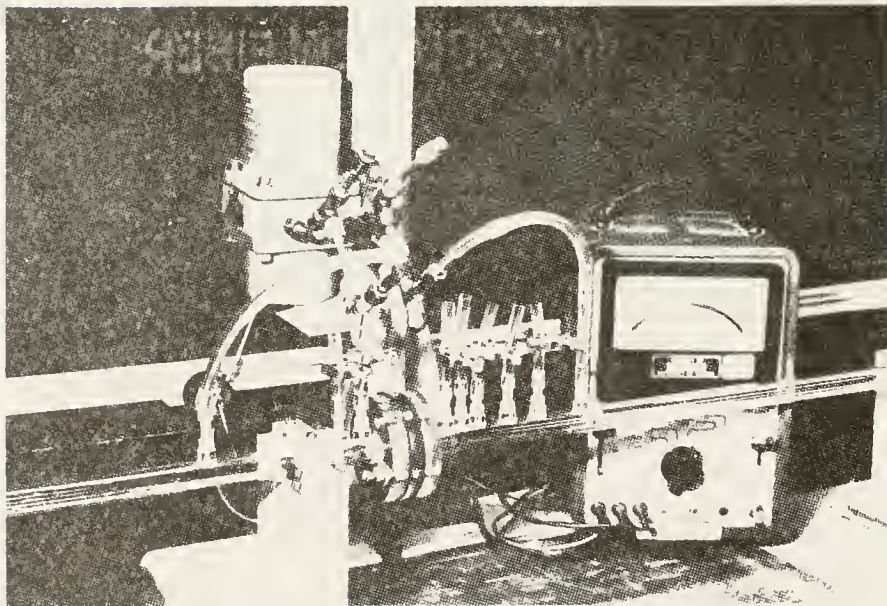
Figure 2.2b   Apparatus for Pressure
                   Drop Measurements
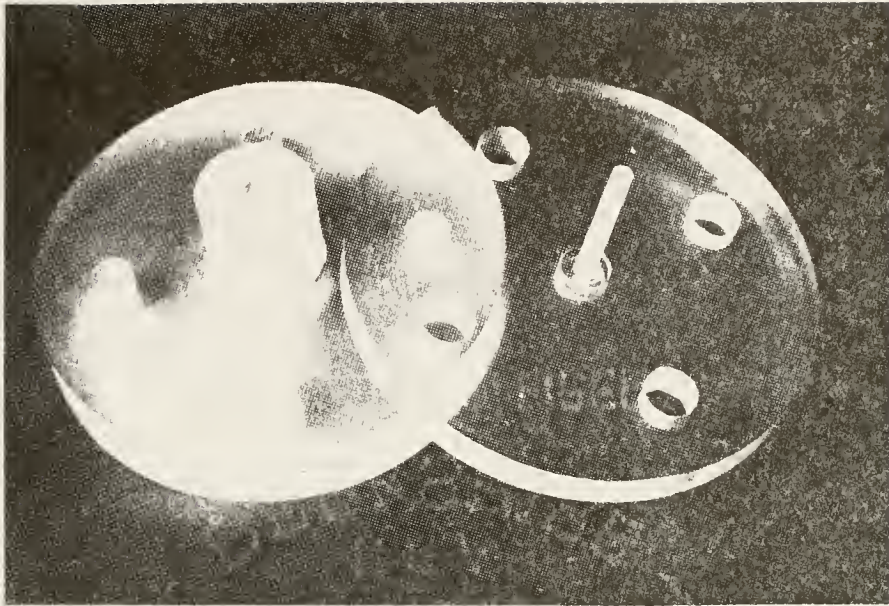
Figure 2.3a Constriction Models

Figure 2.3b Model with Rounded Edges

TABLE I
Constrictions Models and Test Sections

Model No.	Pipe D_o (cm)	Orifice D_1 (cm)	Diameter Ratio D_1/D_o	Area Radio A_1/A_o	% Constricted
1	1.905	0.16	0.08	0.007	99.3
2		0.32	0.17	0.028	97.2
3		0.63	0.33	0.11	89
4		0.95	0.50	0.25	75
5		1.11	0.58	0.34	66
6		1.27	0.67	0.44	56
7 7(R)	1.27	0.16	0.125	0.016	98.4
8 8(B) 8(R)		0.32	0.25	0.063	93.7
9		0.48	0.375	0.14	86
10 10(B) 10(R)		0.63	0.50	0.25	75
11		0.95	0.75	0.56	44
12		1.03	0.81	0.66	34
13		1.19	0.94	0.88	12
14	0.952	0.16	0.17	0.028	97.2
15		0.32	0.33	0.11	89
16		0.63	0.67	0.44	56
17		0.71	0.74	0.55	45
18		0.74	0.78	0.61	39
19	0.635	0.16	0.25	0.062	93.8
20		0.24	0.37	0.14	86
21		0.32	0.50	0.25	75
22		0.40	0.62	0.39	61
23	0.317	0.079	0.25	0.062	93.8
24		0.16	0.50	0.25	75
25		0.24	0.75	0.56	44

(*) R: Rounded edges

  B: Beveled edges

Cylindrical constriction models were made of cast acrylic rods, machined to the test section diameter, and cemented to a plexiglass flange. Different holes were drilled and polished to the specific values of the desired area ratios as described in Table I. In order to study the effect that a different constriction geometry had on the flow characteristics, some of the constrictions were made with rounded or beveled corners as shown in Figures 2.3a and 2.3b; all models were 3 cm long.

During the flow visualization experiment the flow was normally illuminated by a 60-watt sodium vapor lamp, from which light passed through a polarizer - analyzer system.

<u>Preparation and Physical Characteristics of</u>
<u>Bentonite Solutions</u>

An aqueous suspension of White Hector Bentonite, supplied by Tansul Industries, showed good stream-double refraction properties even at very low Bentonite concentration, with a density and viscosity very close to that of water, as described in Appendix A. A decision was then made to use Bentonite solutions instead of Milling Yellow to avoid the non-newtonian behavior of the latter.

Several stock solutions of Bentonite were prepared during the course of the experiment, all using the same procedure, and their density and viscosity determined over a wide range of shear stress and temperature.

The procedure to prepare a 5% concentration stock solution was to slowly dissolve the bentonite powder in distilled water at room temperature, agitating continuously until all bentonite lumps had been dissolved and the bentonite particles well dispersed. To prepare the working solution the procedure was to dilute the 5% stock solution with distilled water until the desired 0.5% concentration was reached.

After standing for a few days solid material that did not go into suspension precipitated to the bottom of the container and the remaining solution was decanted. To determine the final concentration, a sample was heated in an oven at 82°C for about 20 hours, until all the liquid evaporated. By proper weighing with a Sartorius balance (accuracy 0.1 mg) the amount of solid in suspension was determined to be approximately 0.20%.

To stabilize the suspension 0.01% of tetra sodium pyrophosphate was added. The final solution appeared clean and almost transparent, but after use for a period of about 6 weeks, it turned cloudy and showed tendencies to flocculate when left undisturbed for some time, although it still maintained birefringent properties. For a more extensive research on the physical and

optical properties of bentonite solutions of different solid concentration the reader is referred to E. R. Lindgren (1957).

The method used to determine the solution viscosity is described in Appendix A. The solution density was approximately 0.99 g/cc at room temperature. Photographs were taken of the flow patterns over a wide range of flow rate for various area ratios and test section diameters. The optical components were carefully aligned to obtain the best dark background possible. Flow rate and temperature were recorded for each photograph taken. Illumination was provided by a sodium vapor lamp and the results recorded on ASA 400 film, using a 35mm Mamiya Sekor DSX-1000 camera with close-up attachments.

To freeze the fluid motion in time and observe the turbulent eddies it was necessary to reduce the exposure time to 1/250 or 1/500 of a second depending on the flow conditions, with an aperture setting corresponding to f/2.

Even with the lens wide open the amount of light was insufficient and the film had to be overdeveloped and printed on high contrast paper. For future experiments it is recommended that either a more intense light source or a more sensitive film be used so the lens aperture can be smaller, thereby improving the depth of field.

Pressure Drop Measurements

The pressure drop measurements were performed only on flow through the 1.27 cm test section, using pressure taps located at different positions upstream and downstream from the constricted region. A Robinson-Halpern low pressure transducer P20 series connected to a Hewlett-Packard D.C. Vacuum Tube Voltmeter Model 412A were used as shown in Figure 2.2b to detect and record the pressure drop across the constricted region in the cylindrical section.

To cover the pressure drop range encountered during the experiment two pressure transducers were needed, one of range 0-0.15 psig and the other from 0-1.0 psig both calibrated with distilled water.

The Robinson-Halpern P20 series low pressure transducers are electromechanical devices used to measure gas, liquid or vapor pressures. The principle of operation is a pressure sensing element (capsule). The motion of the capsule is transmitted to the core of a linear position transducer by means of a stainless steel support rod. A change in the pressure of the medium being measured moves the core and produces an AC electrical output that is directly proportional to the pressure change. This AC signal output is demodulated filtered, and then fed into an output network that is matched to the specific load impedance to be used.

Both pressure transducers were calibrated by adding distilled water to two vertical manometers tubes connected to the low and high pressure ports of the transducer. The distance (cm of water) between the meniscuses formed on each pressure side was measured with a travelling microscope. A photographic wetting agent was added to the water to reduce the surface tension variations. The calibration curve (pressure in cm of water versus output voltage) showed a good linear behavior in both cases.

It was of extreme importance to eliminate all the air trapped in the tubing between the pressure port and the capsule in order to obtain accuracy and repeatability in the measurements. This occurred because the output of the transducer changed due to surface tension of any air bubbles in the transducer ports. The pressure transducer and voltmeter were allowed to warm-up for about 30 minutes before taking any readings.

CHAPTER III
EXPERIMENTAL OBSERVATIONS

Flow Visualization Experiments

The flow visualization experiments were conducted
with the dual purpose of obtaining experimental informa-
tion on the flow characteristics close to the transition
region, and, determining the peculiarities and location
of the stationary turbulent region as a function of the
flow rate for different area ratios and pipe diameters.

It should be emphasized that the stream double-
refraction technique does not provide streamline visual-
ization but rather visualizes shear stresses present
at the various locations. Regions of no shearing forces
appear black under crossed polarizers, while increasing
rates of shear cause increase of the illumination in
that flow region, until saturation effects appear.

Flow Patterns Downstream of the Constriction

The fluid patterns downstream of the constricted
region according to experimental observations can be des-
cribed in general terms as follows. Undisturbed laminar
flow when viewed through the analyzer (crossed at right
angles with the polarizer) appears as an illumination of
the outer regions with a smooth transition to a darker

region at the center of the test section, where the shearing forces are smaller. For purely laminar flow this dark region remains steady (see Figure 3.1a) with a width depending on the dimensionless area ratio; smaller area ratios having very narrow dark regions, and with a tendency to contract with increasing flow rate, when the flow is still laminar.

As the needle valve was adjusted increasing the flow velocity, the dark region was observed to perform some oscillatory motion (see Figure 3.1b). This oscillatory motion was interpreted as indicating the initial propagation of instabilities in the disturbed laminar flow. These distortions or undulations in the flow which appeared periodically, were not stationary but propagated downstream, tending to decay rapidly. This behavior signifies the onset of a different flow regime where shear-layer waves and their stability play the dominant role.

A very small increase in the flow rate caused the disturbance waves to occur more frequently and with a higher intensity. Increasing the flow velocity, these undulations began to lose definition and to form eddies of more random behavior. It is important to indicate at this point that this disturbance appeared, to the naked eye, to start propagating not immediately downstream from the constriction but a few pipe diameters

away, and that the flow variations necessary to change the flow behavior were extremely small, indicating a very high flow sensitivity close to the onset of undulations.

A still further increase in the flow velocity caused a stationary disturbed region (localized eddies) to develop downstream in the test section (see Figure 3.1d). This region appeared to move closer to the constriction as the flow velocity was increased, until turbulence appeared to develop right at the jet exit location. The extension of this stationary turbulent region was relatively small, with all turbulent activity decaying gradually to laminar flow as the fluid moved downstream the test section. Figure 3.1a through Figure 3.6 represent this sequence of events as the flow rate was increased for the specified area ratio and pipe diameter.

Quantitative Observations

The Onset of Disturbances

The first quantitative observations were to determine the flow rates at the onset of disturbances, for the various area ratios and test sections. Starting with a purely laminar flow, the flow rate was increased in the smallest incremental steps allowed by the needle valve, until the oscillations appeared almost continuously. The flow rate was then measured. By closing the needle valve the disturbances were almost made to disappear, indicating again

a laminar flow condition, the flow rate was then measured and averaged with the first reading. This determined the flow rate at the onset of disturbances, or the critical flow rate.

The definition of this critical point in the fluid presents some uncertainty since there is a small flow rate range over which the flow shows similar behavior, and only the frequency and intensity of the disturbances seems to change gradually, always increasing with increasing flow rate. The onset of disturbances was defined when disturbances appeared almost continuously to insure that they were produced by the jet instability mechanism and not by any external mechanical vibrations.

Next step was to introduce different constriction models to determine the dependency of the onset parameters on the dimensionless area ratio, and to experiment with different test section diameter. The results of these experiments are shown in Figures 3.7, 3.8, and 3.9. The magnitude of the critical flow rate was found to increase progressively as the area ratio was increased as shown in Figure 3.7. The critical Reynolds number based on the test tube diameter Do, is plotted against the ratio between Do and the constriction diameter D_1 in Figure 3.8. This relation seems to scale the phenomenon of onset of flow undulations.

Increments in the area ratio from small numbers to almost unity produced three distinguishable flow regions, each one possessing its own characteristic behavior. A first region corresponding to the smaller area ratios was highly unstable, with oscillations of high frequency and intensity and with very precise boundaries between the laminar region and the region of localized turbulence. Figures 3.3a, b, c are representative examples of this region which extended to approximately an area ratio of 0.065.

Similar flow phenomena occurred in all test sections as observed visually. However, as the diameter ratio, D_1/Do became larger, the disturbances appeared less violent, of lower frequency and intensity. The boundaries of the locally disturbed region were not as precise as in the first region, especially the downstream boundary for the larger area ratio. In this range the critical Reynolds number showed a linear dependency on the area ratio A_1/Ao, and the linear relation still existed when the test tube diameter was varied. This linear region extended approximately between an area ratio of 0.065 and 0.30. For area ratios larger than 0.30 the slope of the critical Reynolds number versus area ratio curve began to gradually change, indicating a trend to a more stable configuration. Flow sensitivity to changes in flow rate decreased, and the stationary turbulent region as perceived by the eye composed of larger eddies, which
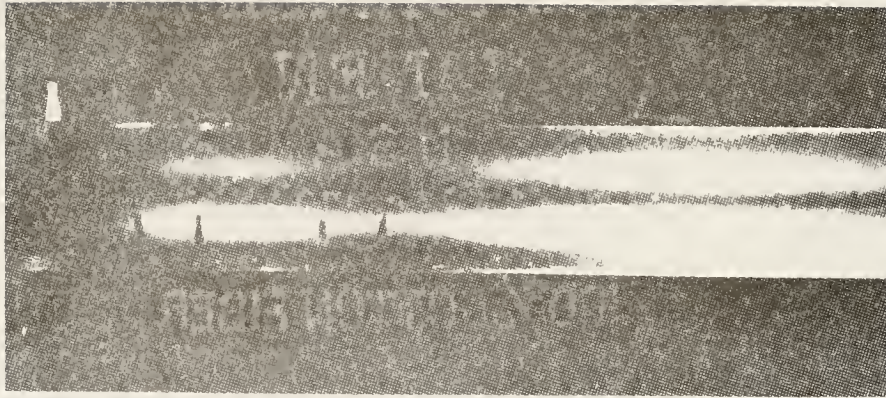
(a) Re = 311

(b) Re = 507
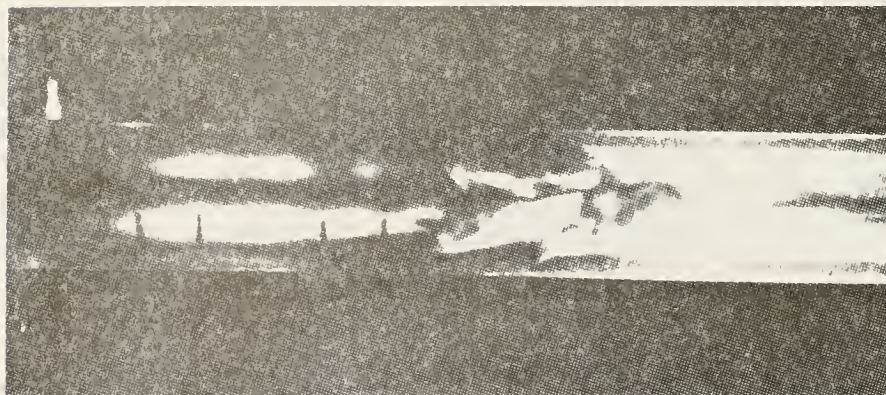
(c) Re = 570

Figure 3.1 Development of Jet Instability
(Do =1.90 cm, D₁/Do = 1/2)

36
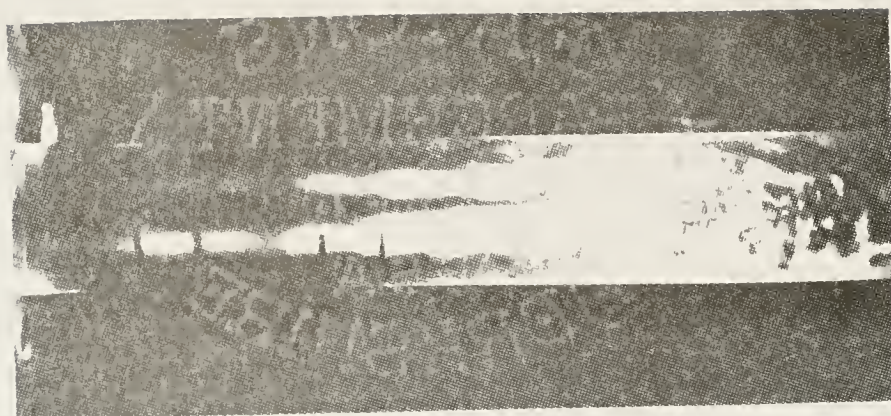
(d)   Re=685

(e) Re=980
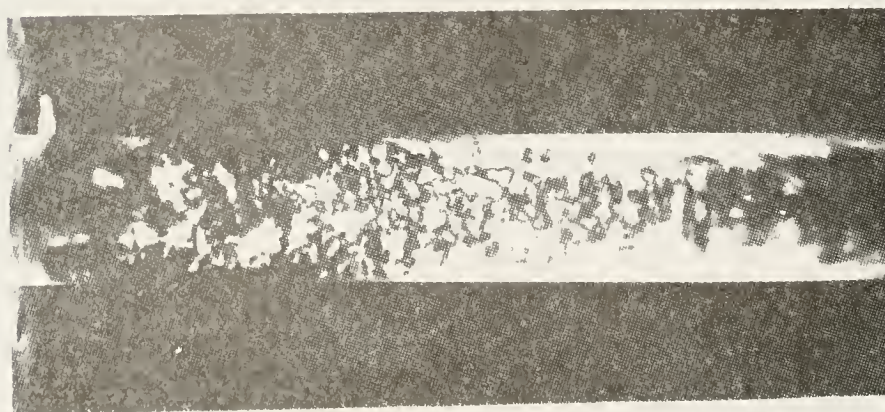
(f)   Re=1418

Figure 3.1 Continued
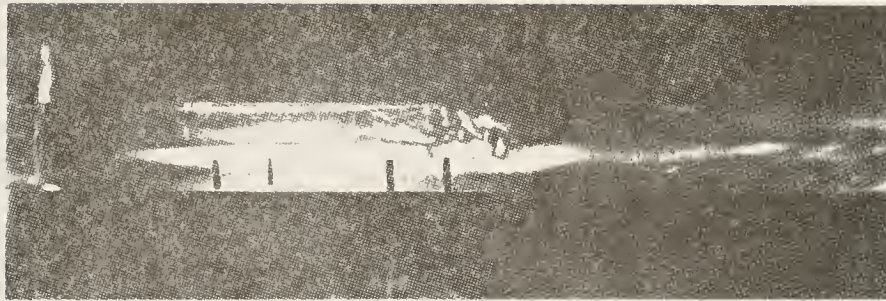
(a) Re = 187
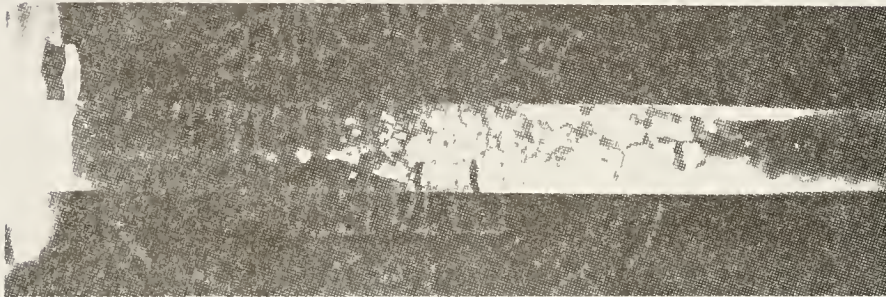
(b) Re = 301
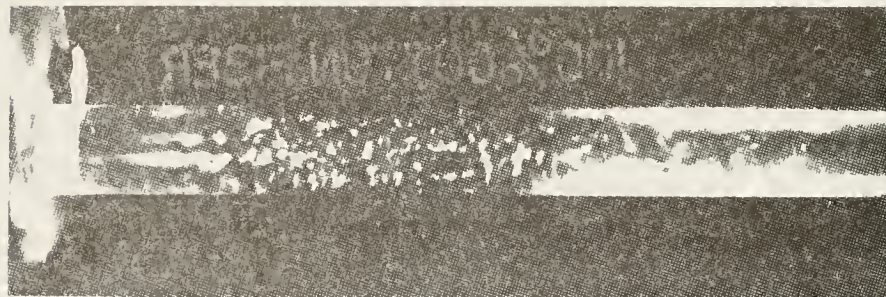
(c) Re = 426
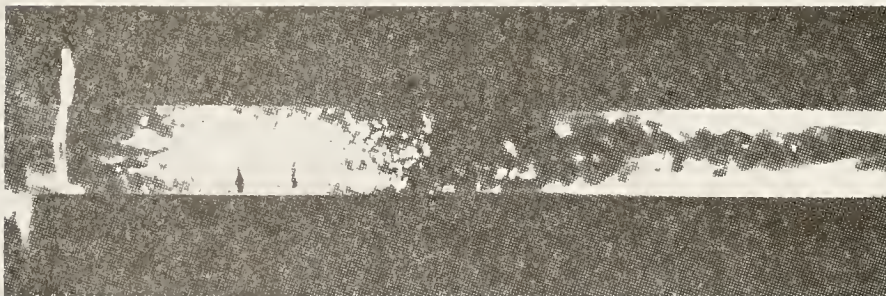
(d) Re = 605

Figure 3.2   Development of Jet Instability
$(D_0 = 1.27$ cm, $D_1/D_0 = 1/4)$

(a) Re = 108

(b) Re = 185

(c) Re = 323

Figure 3.3   Development of Jet Instability

(Do = 1.90 cm, D₁/Do = 1/6)
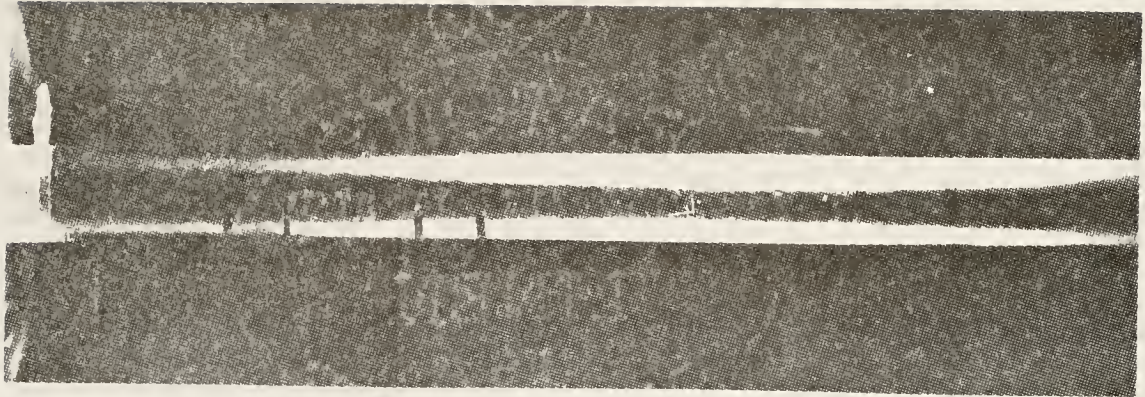
(a) Re = 1678
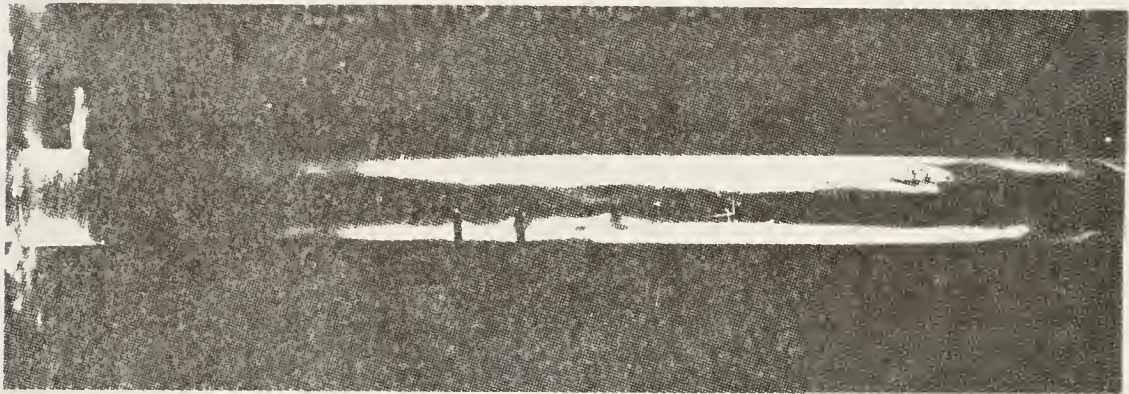
(b) Re = 1920

(c) Re = 2335

Figure 3.4 Development of Jet Instability

$(D_o = 1.27$ cm, $D_1/D_o = 13/16)$
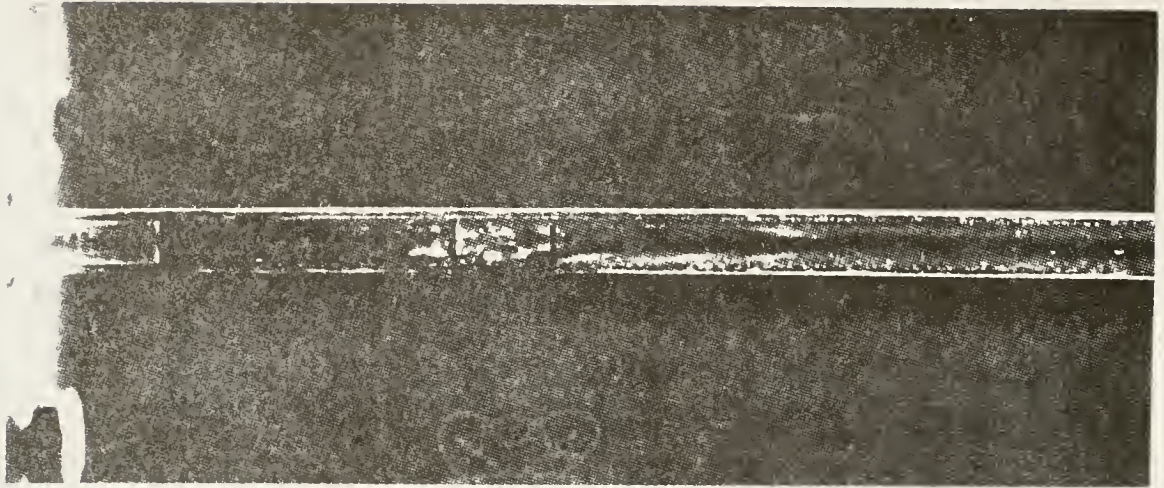
Figure 3.5   Stationary Turbulent Region
(D_1/D_0 = 1/2, Re = 692)
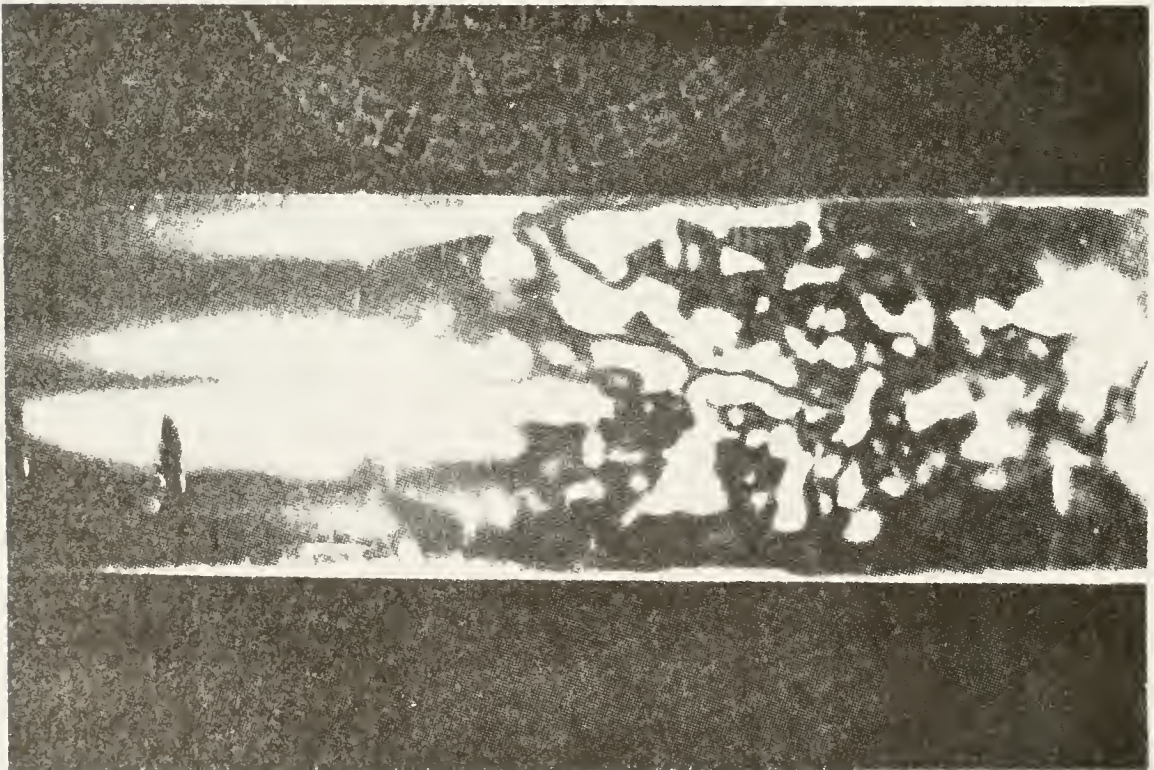
Figure 3.6   Breakdown of Disturbances Into
Turbulence   (D_1/D_0 = 1/6, Re = 150)

diffused slowly into the laminar region making the down-
stream boundary of this region hard to determine.

Near an area ratio of 0.60 the slope of the curve
increased even more toward stability and what appeared to
be disturbances of a different origin began to propagate.

As the area ratio approached unity the curve leveled
off, showing a different type of breakdown mechanism
which overlapped with the one described before, but taking
priority as the area ratio increased. The onset of dis-
turbances in this region was characterized first by large
wavelength undulations of the dark region in the middle
of the flow, moving occasionally to an unsymmetric posi-
tion in the tube. Disturbances then appeared over large
sections of the tube (see Figure 3.4) and propagated
downstream more in the form of slugs. It was not possi-
ble for these large area ratio to obtain a stationary
disturbed region with laminar flow on both sides, but
rather large sections of disturbed flow which overlapped
as the flow rate was increased, filling the test section
totally.

Due to the high degree of difficulties in making
constrictions models of large area ratio, only a few
experimental observations were made in this range, mostly
in the 1.27 cm pipe diameter. Observations made on the
flow in the upstream side of the constriction showed this
region to be laminar and free of disturbances over most
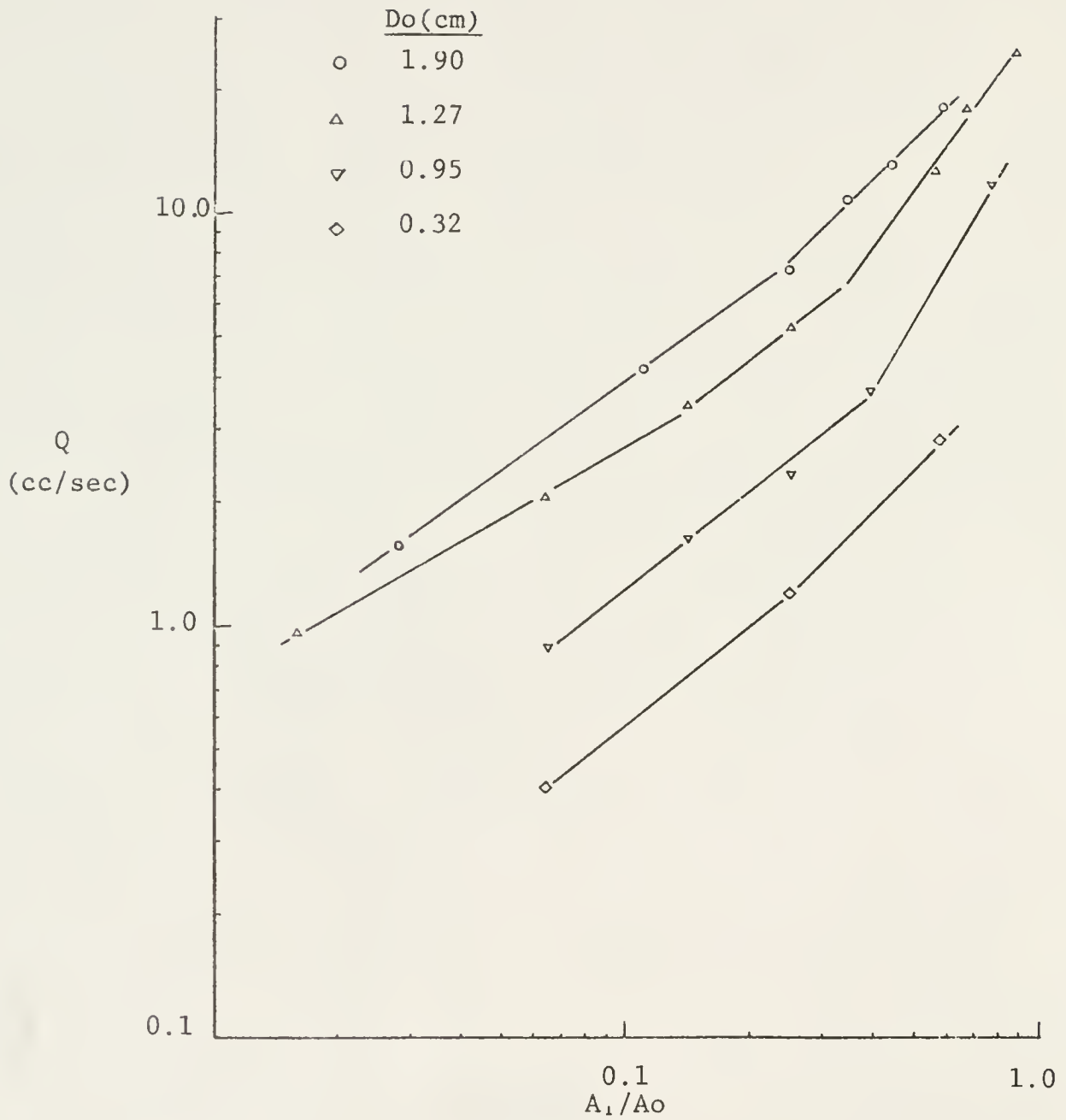
Figure 3.7   Critical flow rate
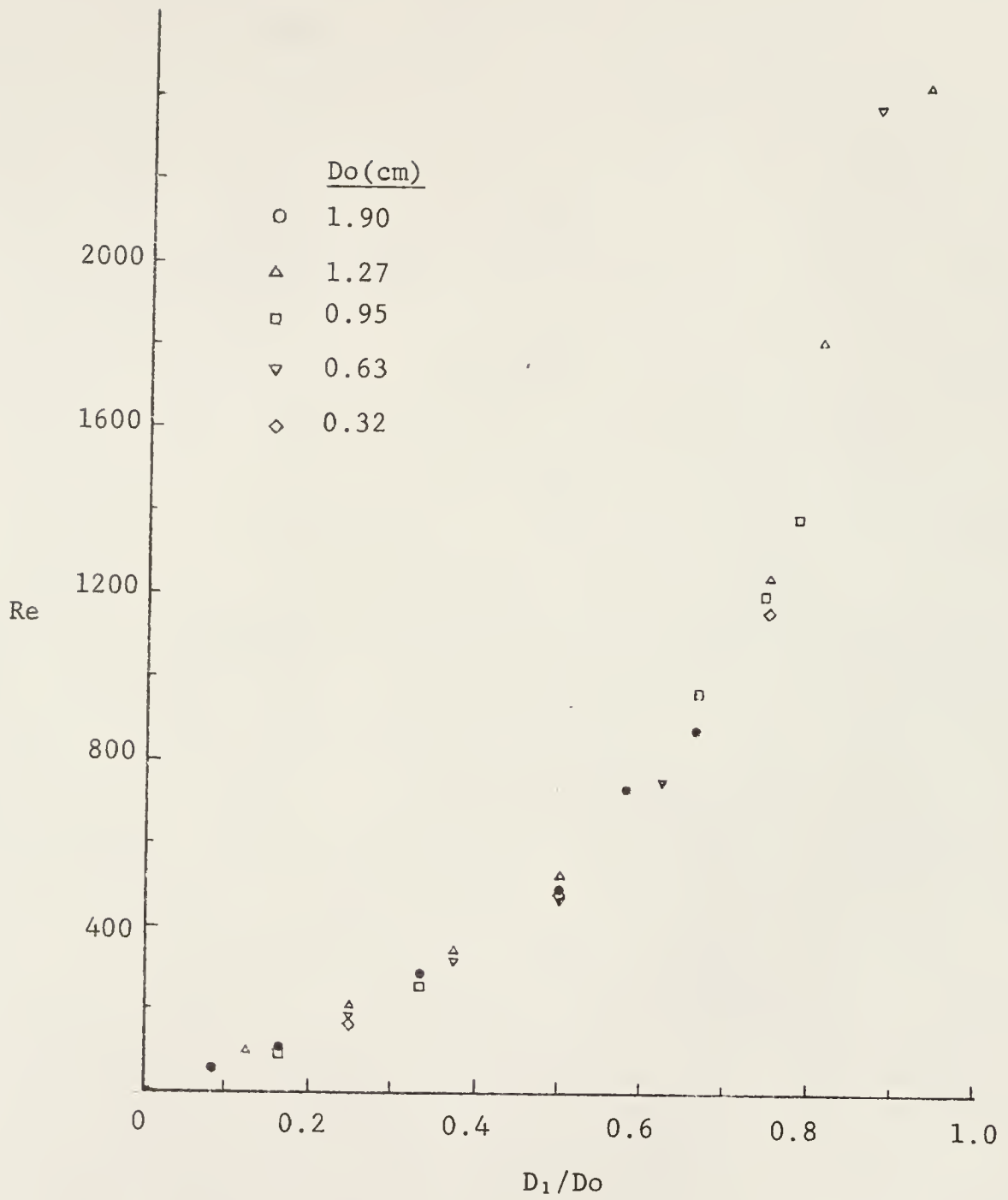
Figure 3.8   Critical Reynolds number
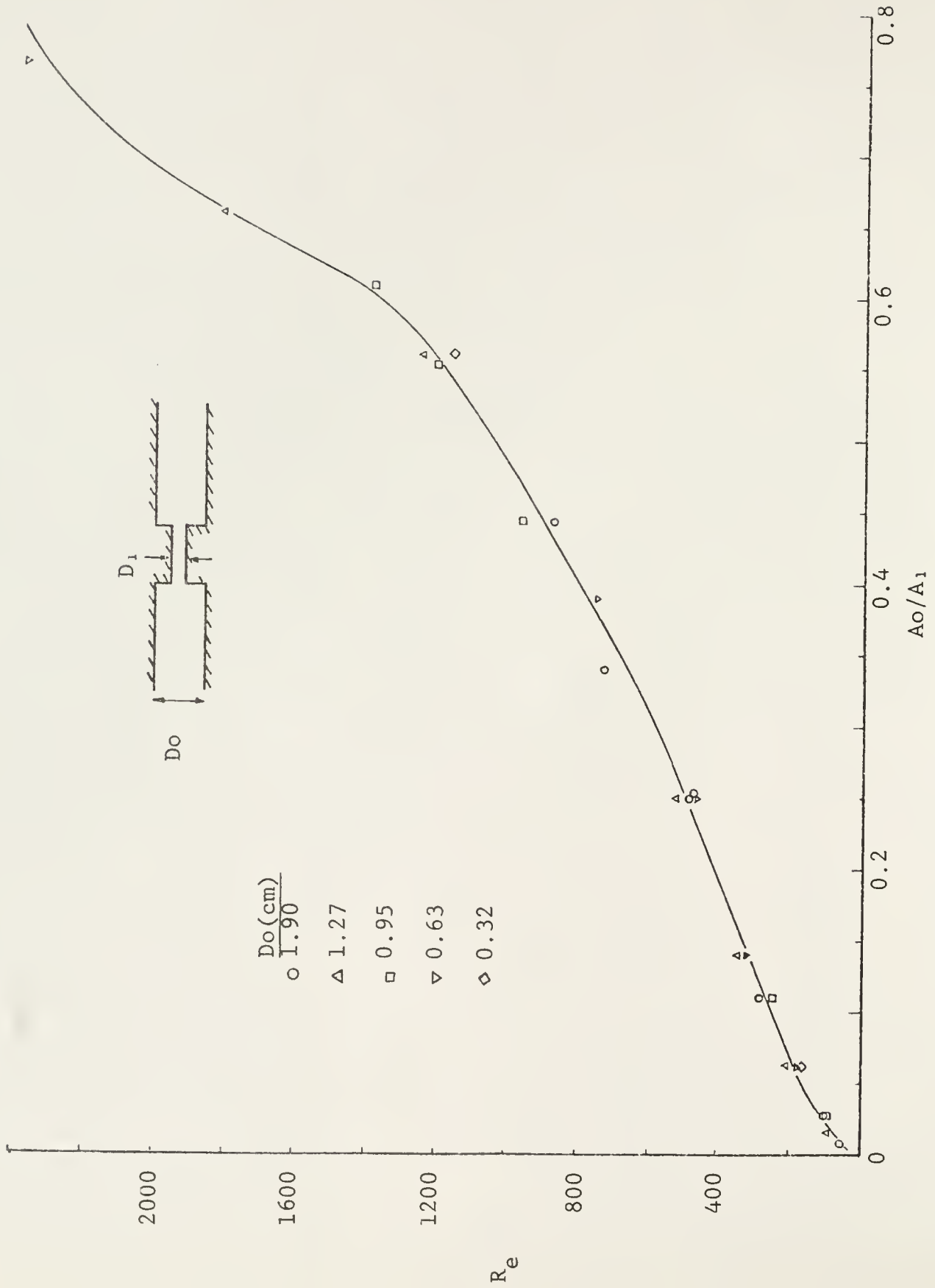
Figure 3.9 Critical Reynolds number versus area ratio

of the experiment Reynolds number range, even when the downstream portion was highly disturbed and a localized turbulent region had developed. As the transition Reynolds number approached 1700-1900 disturbances were also present in the upstream side. These oscillations were probably produced by entrance disturbances propagating in the entrance section that had not decayed (due to the high flow velocity) before entering the tube constriction.

The Position of the Stationary Turbulent Region

As described in previous sections, increasing the flow rate beyond the onset of disturbances produced an unstable stationary region of highly irregular motion. The transition phenomenon from a steady laminar jet to the appearance of disturbances and then to the final breakdown into turbulence was not instantaneous but occurred over a small range of Reynolds number. The transition region as a function of the geometrical diameter ratio is shown in Figure 3.10. This region is bounded by the onset of disturbances curve and the approximated boundary at which the stationary turbulent region first appeared. Flow corresponding to the area to the right of these boundaries was considered stable, while flow corresponding to the area to the left showed signs of instability.

It is important to notice that the turbulence

generated was of very weak nature, promptly decaying through viscous dissipation to laminar flow.

The next set of experiments were directed to measure the location of the stationary turbulent region with respect to the jet orifice for various test section diameters as a function of the area ratio. The characteristics of the flow and the position of the disturbed region have strong physiological implications during the formation of a post-stenotic dilatation in arteries. Fluid pressure fluctuations generated by turbulence are transmitted to the bounding walls and seem to affect the tissue elastic properties in localized areas downstream of the stenosis.

The boundaries of the disturbed region were defined at the point of attachment and detachment from the walls. These boundaries were easier to evaluate in the large diameter test sections when conducting experiments with the small areas ratio models. As the area ratio increased the position of the downstream boundary was progressively more difficult to locate. In general these boundaries oscillated slightly around a mean position, which was determined by taking several readings at a constant flow rate. As an area ratio close to one was approached, the turbulent stationary region ceased to exist, and the fluid started showing characteristics common to the flow of fluids in uniform cylindrical test sections in the transition region.

The position of complete recovery to laminar undisturbed flow was not measured since it usually occurred outside the test section dimensions. The measured location of the stationary turbulent region for a pipe diameter of 1.90 cm is shown in Figures 3.11a, b, c, d, for several diameter ratios. The upstream and downstream boundaries are described as a function of the average jet velocity at the orifice. The tail shown in the right-hand side corresponds to the transition region where the flow showed extreme sensitivity to flow rate. Increasing the flow rate caused the disturbed region to move upstream (i.e., closer to the orifice). Once in close proximity to the orifice an increase in flow rate produced a small increase in the region dimensions. Further increasing the flow velocity produced violent turbulent motion, filling large portions of the test section. Under these circumstances the downstream boundary was not clearly defined.

The location of the stationary turbulent region for the 0.95 and the 0.32 cm ID test sections are shown in Figures 3,12a, b, and 3.13a, b. The general characteristics were the same. Of especial interest was the smallest test section of 1.32 cm ID, since this dimension is representative of some arteries in humans and animals. The maximum length of the disturbed region for this test section was approximately 1.0 to 1.5 cm,

depending on the area ratio. The most common types of
PSD seem to be developed immediately distal to the
stenosis and of dimensions comparable to our experimental
observations.

An attempt was made to non-dimensionalize the prob-
lem by plotting the Reynolds number versus the dimension-
less axial position for a constant area ratio and differ-
ent pipe diameters. The results were only fair, showing
some spread in the data, probably caused by the diffi-
culties in determining the boundaries of the turbulent
region. The dimensionless length of the turbulent region
when it extended to the orifice is shown in Figure 3.14 as
a function of the diameter ratio, for various test
sections. By examining these results, three regions were
again noticed, depending on the diameter ratio. Up to a
ratio of approximate 0.20 the length increased, between
0.20 and approximately 0.40, it remained fairly constant,
increasing again for a diameter ratio above 0.40. The
smallest test section of 0.32 cm ID consistently produced
smaller values for the length (L_D) of the turbulent
region.
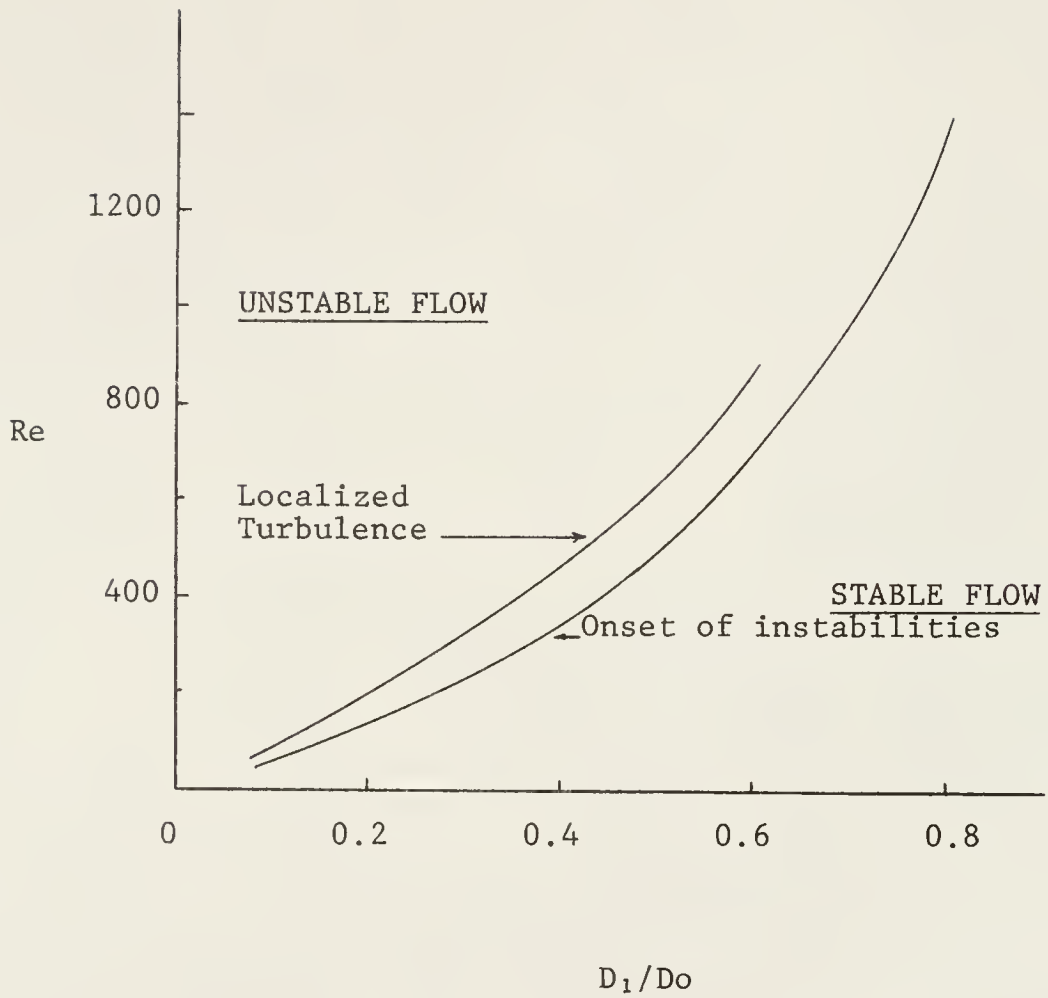
Figure 3.10   Transition Region
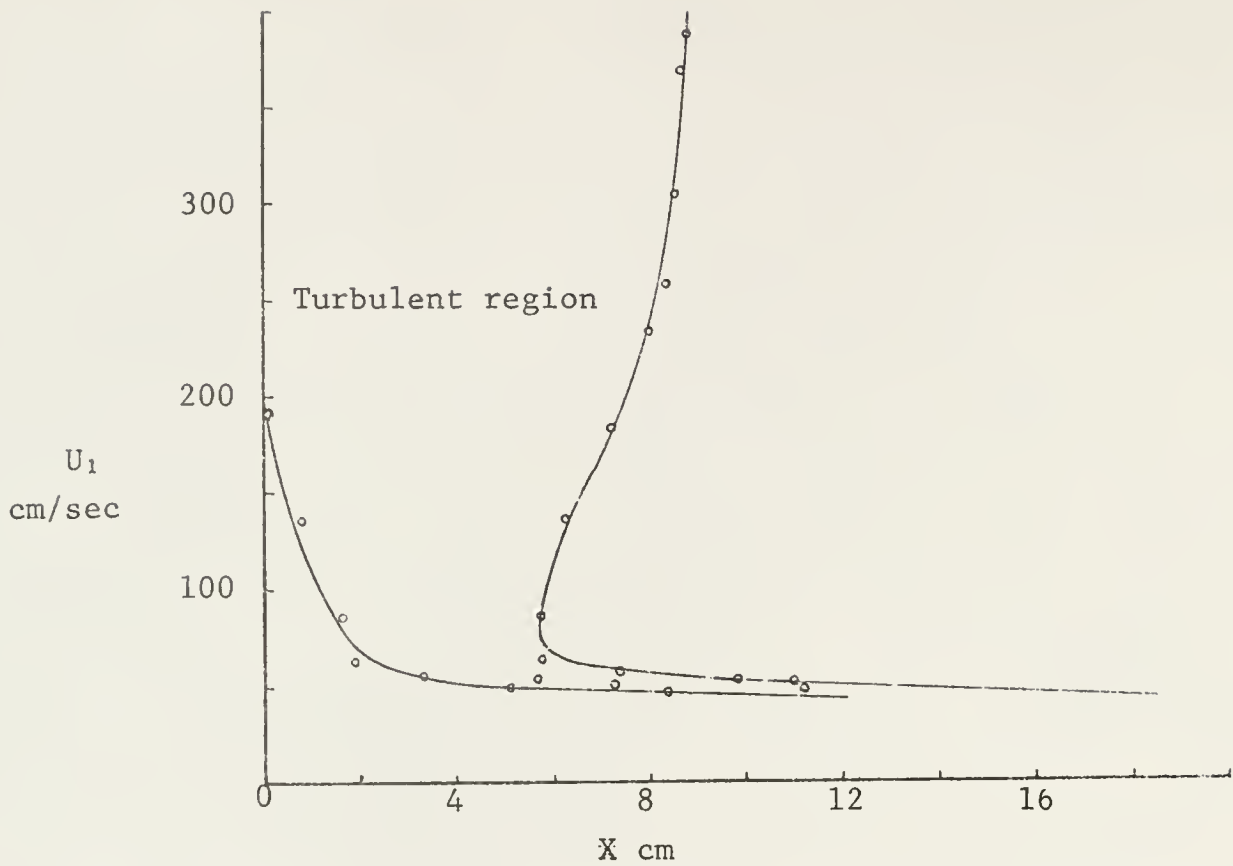
Figure 3.11a   Turbulent region DO=1.90cm, $D_1/_{Do} = 1/12$
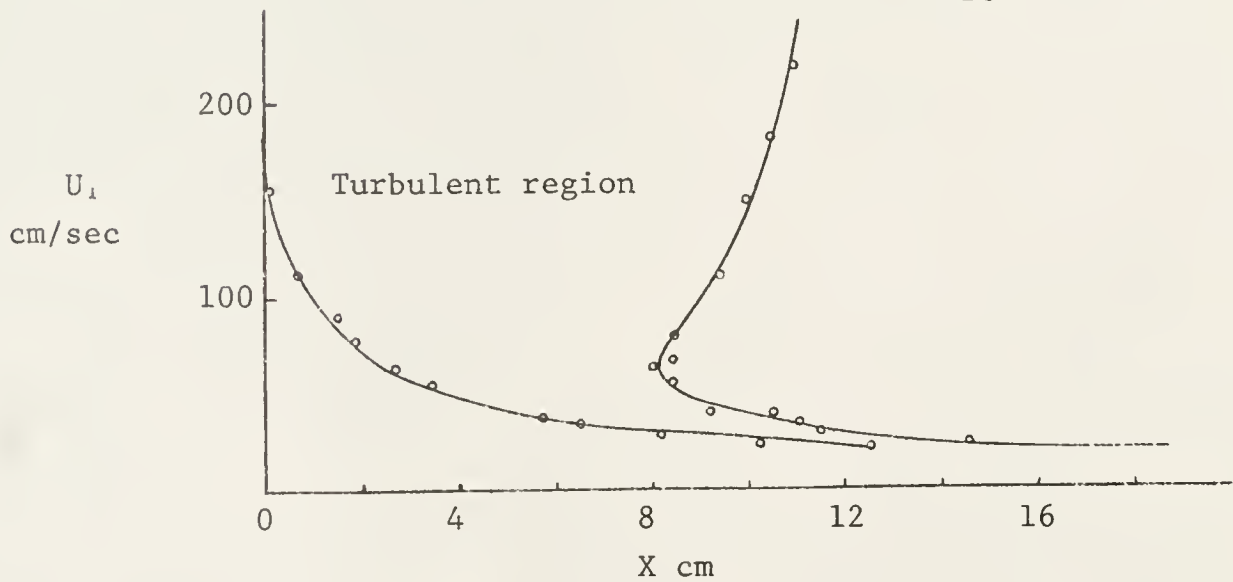
Figure 3.11b   Turbulent region Do=1.90cm, $D_1/_{DO} = 1/6$

Figure 3.11c   Turbulent Region. Do=1.90cm, $D_1/_{Do} = 1/3$
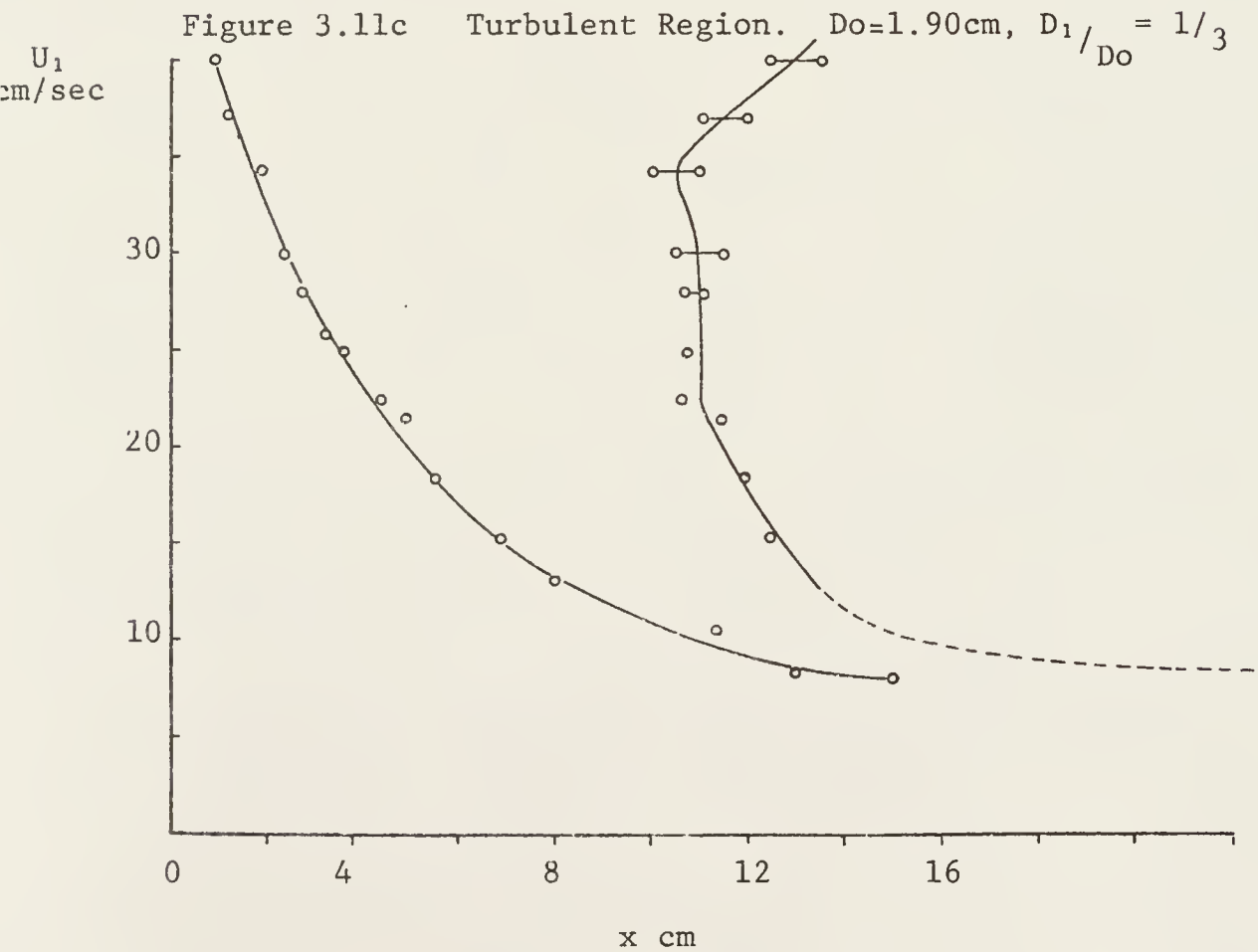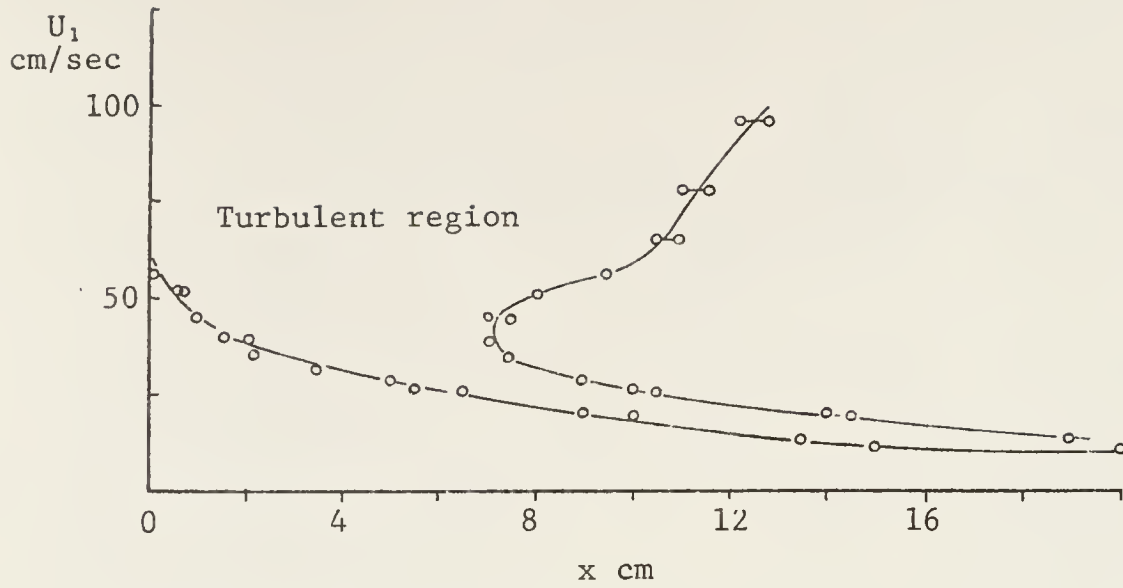
Figure 3.11d   Turbulent Region.   Do=1.90cm, $D_1/_{Do} = 1/2$
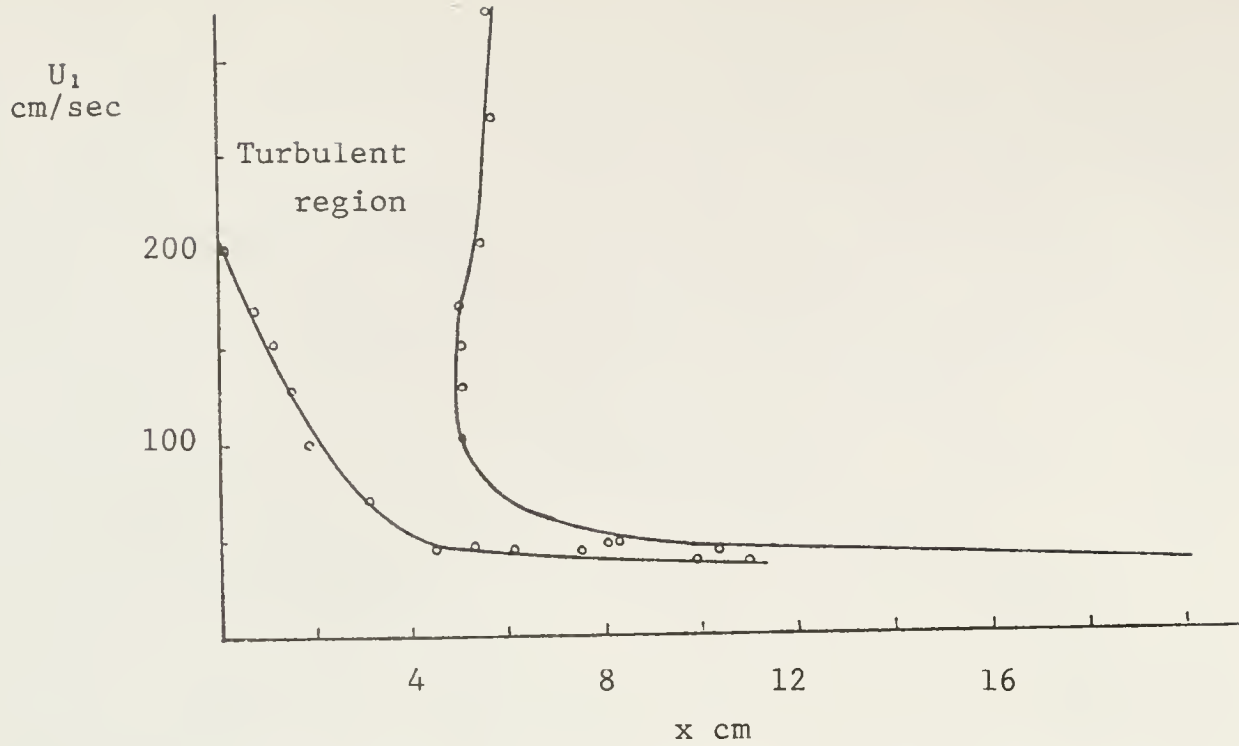
Figure 3.12a   Turbulent Region.   Do=0.95cm, $D_1/Do=1/6$
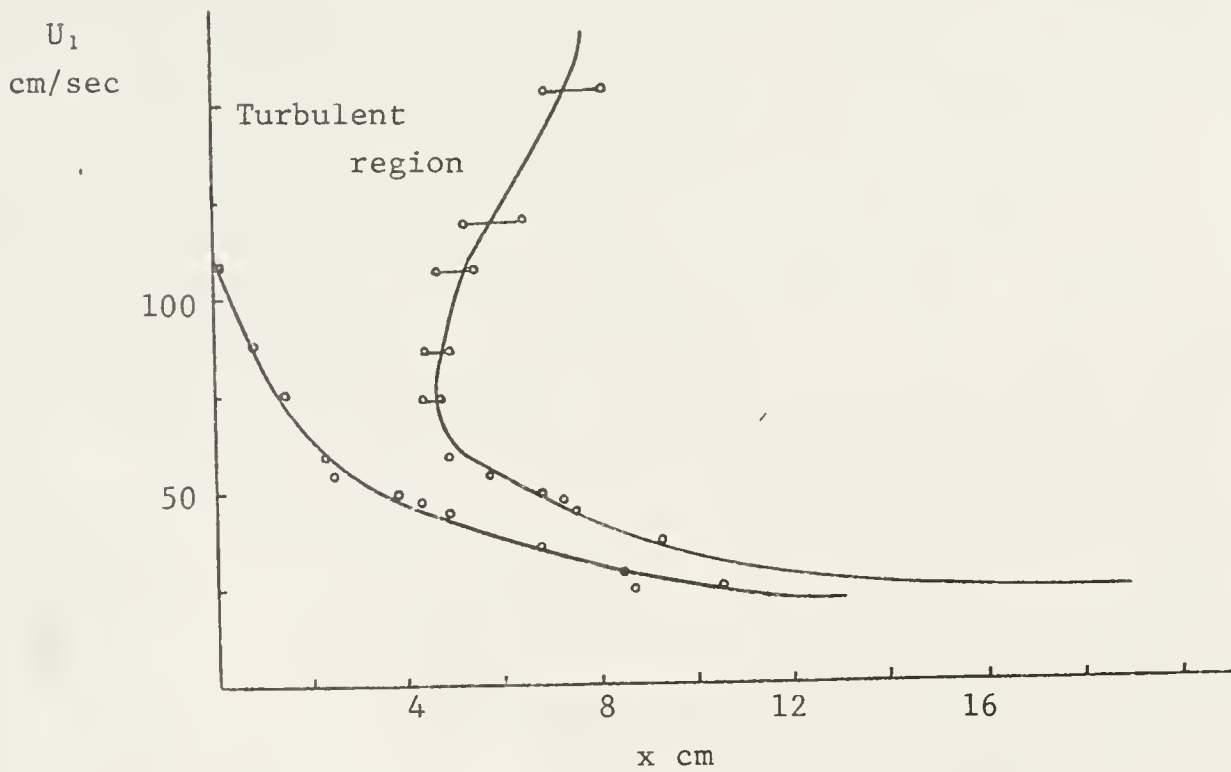
Figure 3.12b   Turbulent Region.   Do=0.95cm, $D_1/Do=1/3$
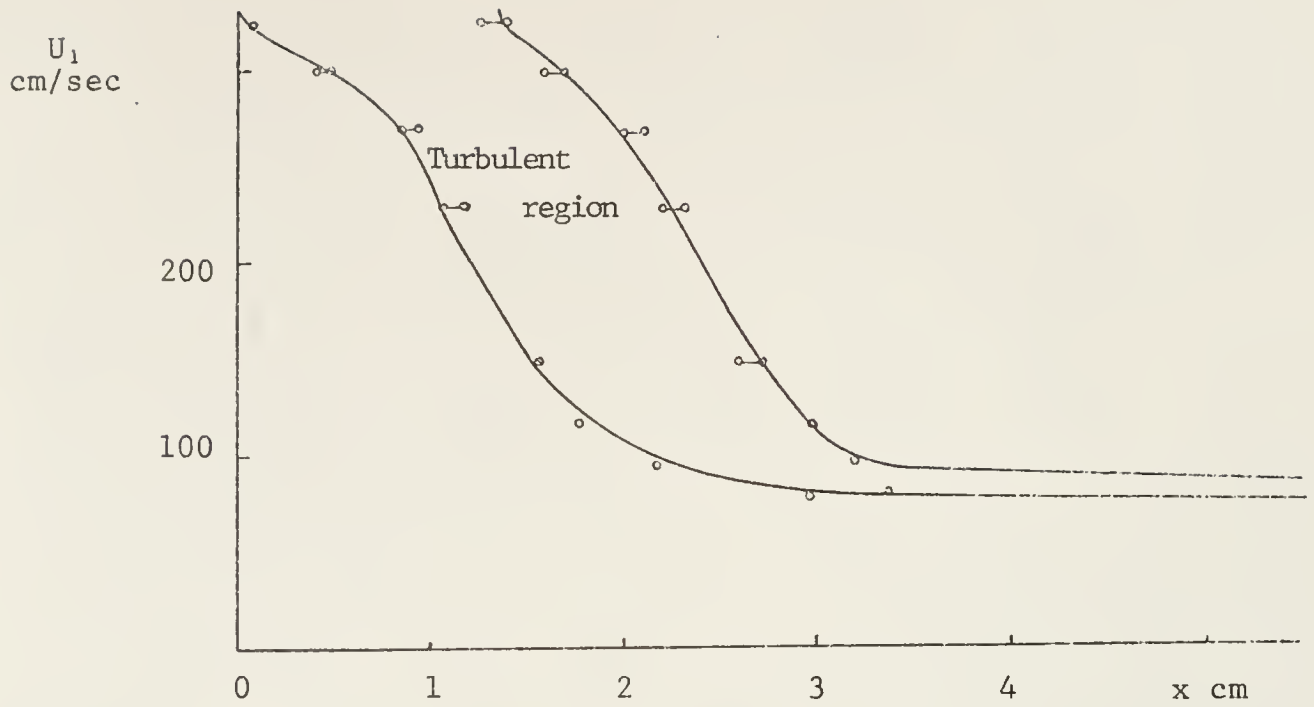
Figure 3.13a   Turbulent Region. Do=0.32cm, $D_1/Do=1/6$
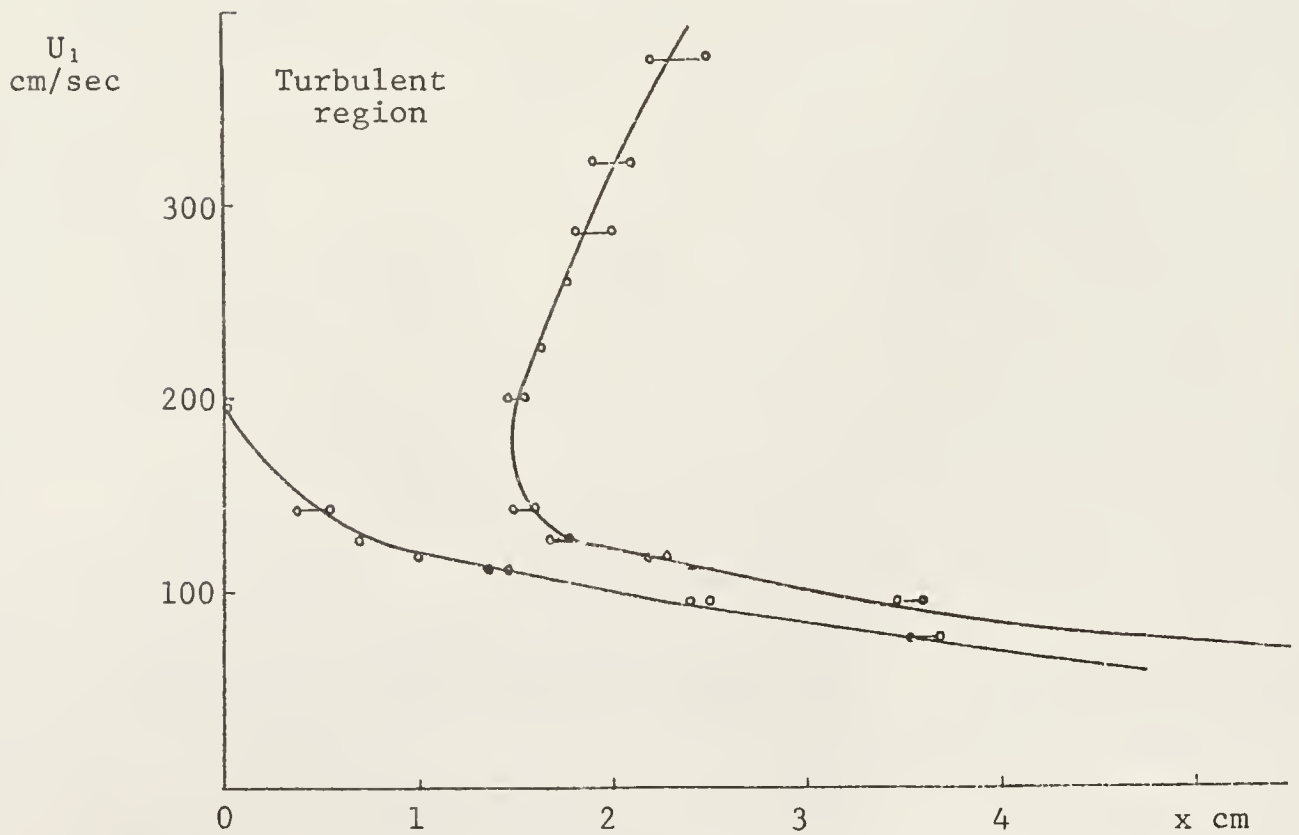
Figure 3.13b   Turbulent Region. Do=0.32cm, $D_1/Do=1/2$
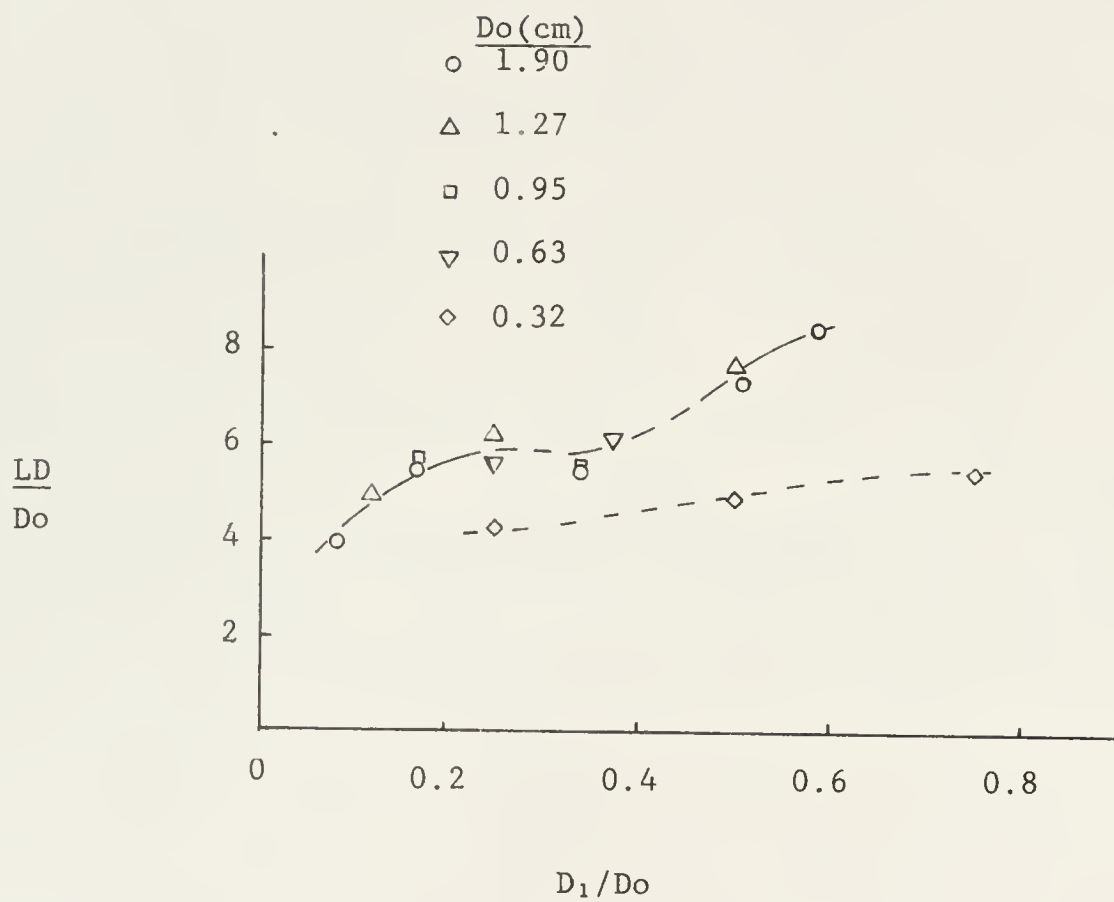
Figure 3.14   Length of turbulent region when close to orifice

Effects of Changes in Constriction Geometry on the Onset
of Disturbances

The purpose of the following experiments was to
determine if changes in the geometry of the constriction
were an important factor with regard to the critical flow
rate for the onset of disturbances and for the flow top-
ology downstream of the constricted region. Several
models were constructed similar to the square edge models
but with beveled or rounded edges as shown in Figure 2.3b.
The dimensions of all models were 3 cm long and made to
fit in the 1.27 cm pipe. The location of the turbulent
region was determined and critical flow rates for various
orifice sizes. The fluid flow conditions for the differ-
ent geometries at the onset of instabilities are described
in Table II. In all models tested the effects produced
by a geometry change were not significant and the onset
of disturbances appeared to be determined primarily by a
critical jet velocity and the shear stress layer associ-
ated with it. Figures 3.15a, b show the location of the
turbulent region as a function of the average jet velocity
for a diameter ratio of 1/8 and 1/4. The position of the
turbulent region is closer to the constriction for the
rounded geometry than for the straight one, at the same
flow velocity. It seems to be shifted in position by a
distance which is very close to half the constriction
length. This is an indication that the disturbances will

break down into random turbulent motion at a certain distance from some location at which they originate (in this case 1.5 cm), depending on their growth rate. For the sharp edge geometry (90° corners) the high shear stress layer originates at the end of the constriction, while for the rounded geometry it is closer to the constriction throat.

TABLE II

Geometry Effects on the Critical Reynolds Number

Model No.	$\frac{D_1}{Do}$	Edges Geometry	Qcrit	Re	Re_1
7	1/8	Sharp	0.81	81	648
		Rounded	0.89	89	712
Model No.	$\frac{D_1}{Do}$	Sharp	2.05	203	812
8	1/4	Beveled	2.16	217	867
		Rounded	2.25	226	905
Model No.	$\frac{D_1}{Do}$	Sharp	5.22	523	1026
10	1/2	Beveled	5.35	537	1074
		Rounded	5.75	576	1152
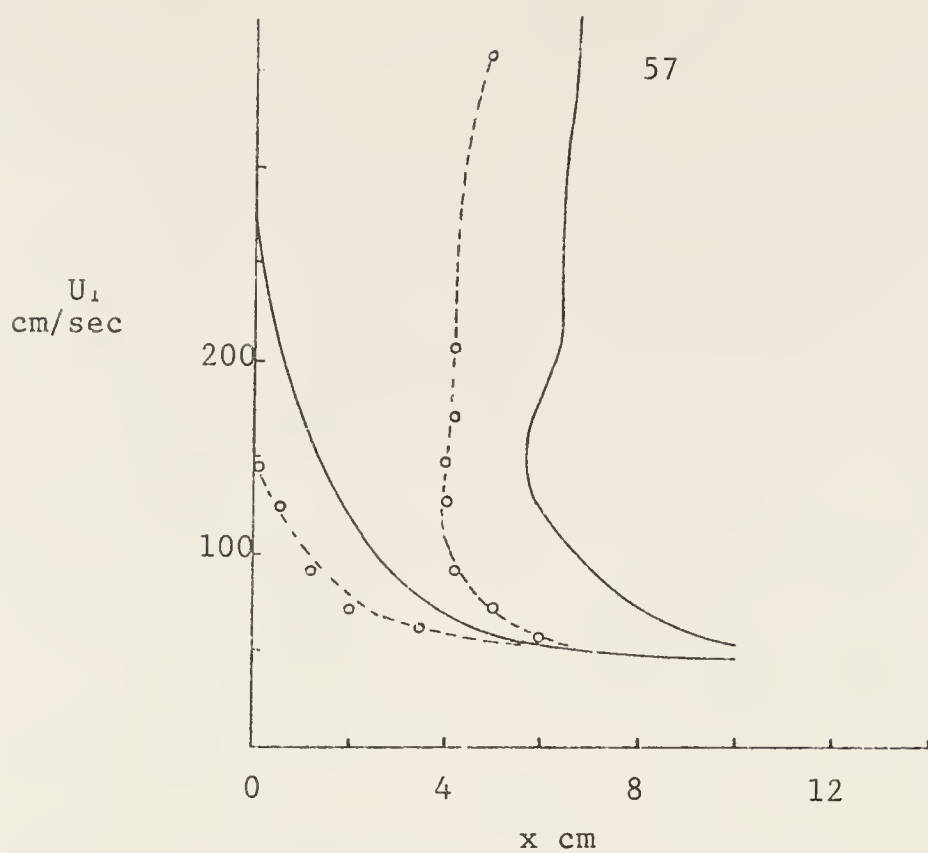
Figure 3.15a   Turbulent region for different geometries. $D_1/D_0 = 1/8$

○ Rounded edges
▲ Beveled edges
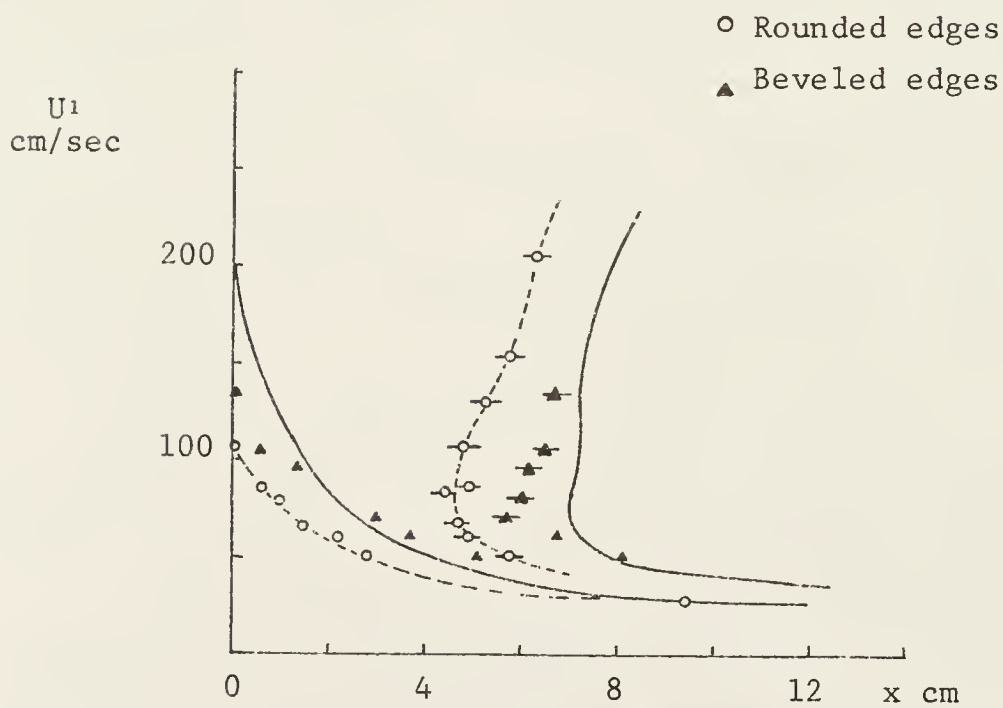
Figure 3.15b   Turbulent region. $D_1/D_0 = 1/4$

Correlation with Previous Experiments

Introduction

In this section attempt is made to correlate the experimental observations with some of the previous investigations on the properties of cylindrical jets in bounded regions, and, to explain these results in the light of present observations.

Experiments on fluid flow across locally constricted test sections can be found in the literature since the beginning of the century, such as the Johansen's experiments (1929) on orifice plates. Since then, a large number of experiments have been conducted on orifices and venturi shape constrictions for a variety of engineering applications, such as the rate of flow meter. More recently the problem has been studied from the physiological point of view in order to associate hydrodynamic factors to the development and progression of arterial stenoses.

The results on the onset of disturbances as determined from our experiments are correlated with Johansen's observations and Young and Tsai's (1973) measurements on the transition Reynolds number. Sound onset as measured by Sacks et al., (1971) (in vivo) and by Gonzalez (1974) (in vitro) are related to the onset of disturbances and turbulence to determine the relation between these phenomena.

Johansen's Experiments with Pipe Orifices

The characteristics of the flow through pipe orifices at low Reynolds number were investigated by Johansen in 1929. Using a dye (methylene blue), Johansen made observations on the flow pattern downstream from a diaphragm orifice of 1.34 cm diameter in a cylindrical tube of diameter 2.68 cm ($\frac{D_1}{D_0} = 1/2$). These observations were mainly concerned with jet transition charactersitics from laminar to turbulent, and the relation between the discharge coefficient and the differential pressure head across the orifice.

According to his observations, at a pipe Reynolds number of about 300 (orifice Reynolds number of 600) vortex ripples appreared close to the orifice and moved downstream, losing translational velocity and definition. Close to a Reynolds number of 500, transition of the jet occurred, resulting in the formation of a train of vortex rings which gradually loose identity downstream.

Comparing Johansen's flow photographs (Figures 7 and 8 in Johansen's report) at pipe Reynolds numbers of 300 and 500 with our experimental results using the Bentonite Solution, it appears that the onset of disturbances in the present experiments corresponds to Johansen's description of the flow behavior close to or above a Reynolds number of 300.

As shown earlier in Figure 3.8, for a diameter ratio
of 1/2, onset of undulations occurred at a Reynolds number
of about 470, which is higher than Johansen's value for
flows through an orifice.

At this point it is appropriate to mention a possi-
ble source of disagreement between experimental data
taken for orifice flows as compared with similar data on
extended constricted region. The flow velocity profile
coming out of an orifice is probably almost flat, while
the velocity profile at the jet exit position of an
extended constricted region should be curved. Another
source of discrepancies in the correlation of similar
experiments is the technique used to obtain the informa-
tion. The flow visualization technique based on the
optical properties of Bentonite Solutions is a non-
disturbing method while techniques using velocity probes,
dye injections, etc., are likely to induce flow disturb-
ances. More important still is that the dye follows the
fluid motion, while, streaming birefringence does not.

Transition in Models of Arterial Stenoses

The critical Reynolds number and flow characteristics
in a cylindrical tube with rounded axisymmetric and non-
symmetric constrictions, were partially investigated by
Young and Tsai (1973), using the hot-film probe technique.
By connecting the anemometer to an oscilloscope or strip-

chart recorder, critical flow conditions were determined for different probe locations. The initiation of the transition regime was identified by the relative low frequency oscillations in the hot-film signal. The nature of the fluctuations varied considerably with the position of the probe along the axis of the test section.

The experimental critical Reynolds numbers obtained for a probe position of 15.2 cm with respect to the constriction center are shown in Table III, for two models with different diameter ratio, but with the same length to diameter ratio ($Zo/Do = 2.0$). Also included in the Table are the present experimental results at the onset of disturbances for models with 90° edges and a ratio Zo/Do equal to 1.57. Both sets of experiments were conducted on the 1.90 cm pipe.

TABLE III

Correlation with Young's Experiment

Model Geometry	Model Length Zo/Do	Diameter ratio D_1/Do	Critical Re	Experimental Technique
Rounded Axisymmetric (Young's)	2.0	1/3	325±20	Hot-film Probes
90° Edges Axisymmetric	2.0	2/3	800+50	
	1.57	1/3	28̄2	Flow Visualization (birefringence)
Present Investigation)	1.57	2/3	872	

The correlation of these data appear to be good considering that the models dimension and geometry are different. These results validate our previous conclusion that the length and geometry of the model play a secondary role in the transition phenomenon.

In Vivo Experiments on the Onset of Sound in Arteries

Sacks, Tickner and MacDonald (1971) in their investigations on the onset of vascular murmurs conducted a series of in vivo experiments to determine the minimum flow Reynolds number necessary to generate sounds in artifically produced stenosis in the descending aorta of anesthetized dogs.

The experimental procedure performed on forty-nine adult mongrel dogs was to expose the aorta; after applying tourniquets above and below, the aorta was severed to allow insertion and fixations of a brass cylinder into which machined orifice plates could subsequently be placed. The orifice plate was located at the distal end of the brass cylinder, thus allowing the vascular wall to participate normally in the production of sound associated with the flow instabilities generated downstream from the constricted region. Blood flow rate was measured by an untrasonic flowmeter mounted proximal to the brass cylinder, and just distal to the aortic arch. A catheter-tip microphone pressure transducer with a frequency response of 0 to

1000 Hz was threaded into the femoral (thigh) artery up to various locations relative to the orifice in the thoracic aorta, and its output recorded simultaneously with the flow rate and pressure.

Critical flow rate at the onset of sound was calculated from the oscillograph record of the flow rate during occlusion. The Reynolds number at the instantaneous value was based on the internal vessel diameter and flow velocity proximal to the orifice. The blood viscosity was calculated from the non-newtonian viscous parameters described by Hershey and Smolin (1967) using the rectal temperature.

Using the described experimental apparatus Sacks and collaborators generated a general sound boundary curve which established the critical flow Reynolds number at onset of sound as a function of the constriction to artery diameter ratio.

The experimental results were approximated by a least square parabola fitted to the experimental data. The spread in the experimental data points for the tethered and untethered artery at a constant diameter ratio were significant, especially for the large diameter ratios. According to Sacks the Reynolds number limit curve for the onset of sound is given by

$$Re_o = 2384 \; \frac{D_1}{D_o}^2 \tag{3.1}$$

and illustrated in Figure 3.16. Flow conditions specified

by Reynolds number and diameter ratio to the left of the curve in Figure 3.16, representing Sacks data, will produce sound, whereas those below and to the right will not. Sacks and collaborators also concluded that this sound has a broad frequency band, with intensity dropping off as frequency increases, and is strongly suggestive of free turbulence or jet instability rather than periodic vortex shedding.

In Figure 2.16, equation (3.1) representing the "in vivo" experimental results on sound onset in arteries are compared with visual observations of this study on the onset of disturbances in circular pipes of different diameters. We must keep in mind that the in vivo experiments were conducted on arteries probably of variable internal diameter, and distensible walls, under pulsating flow conditions through an orifice plate, while the "in vitro" investigations were performed on rigid tubes and steady flow conditions through a constricted region 3.0 cm long.

At a diameter ratio larger than 0.45 the data representing equation (3.1) deviates considerably from our visual observations which indicate less stable flow conditions. Near a diameter ratio close to unity the critical Reynolds number in both experiments is close to 2400.

The parabolic curve described by (3.1) falls mostly in between the curves in Figure 3.16, representing the onset of disturbances, and the appearance of a locally

disturbed flow region. This result seems to indicate that sound may be generated at the very early stages of flow instabilities, at least for severely constricted arteries. Whether or not the pressure fluctuations produced by these initial instabilities are strong enough to make the walls vibrate, so that sound can be detected by an external microphone, is something still to be discussed.
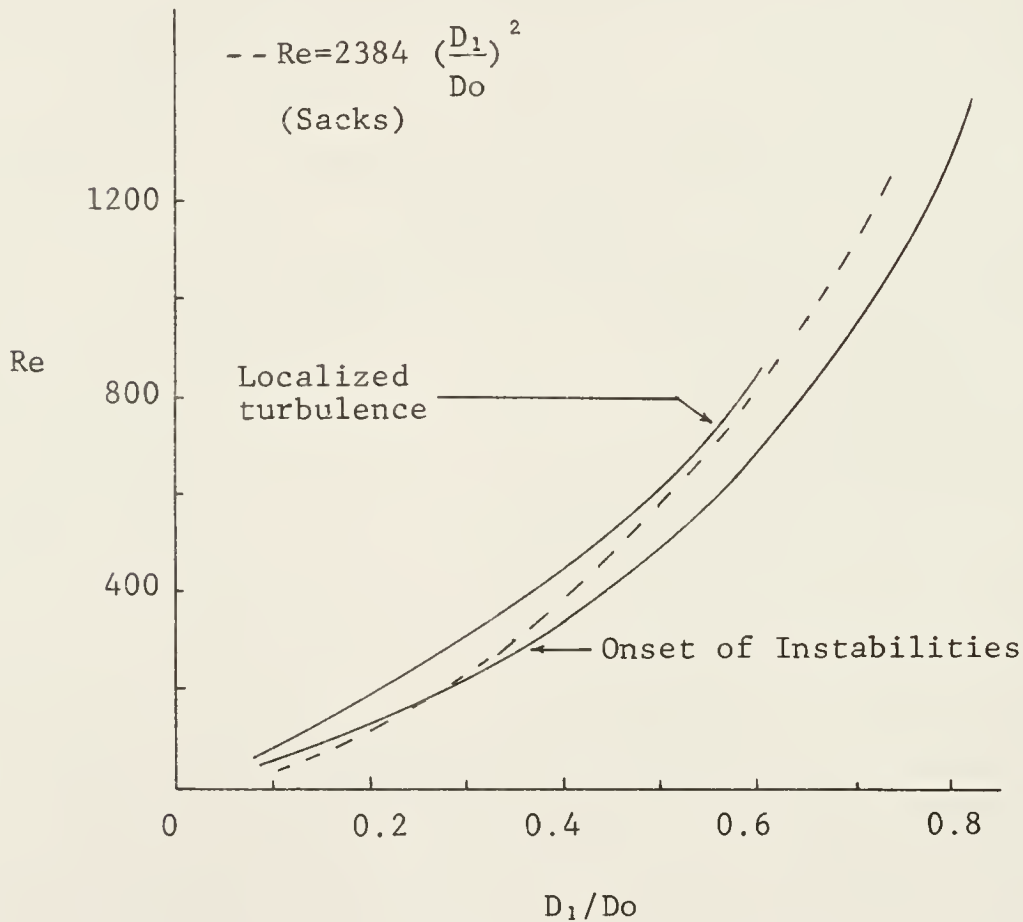
Figure 3.16   Correlation with Sacks experiments

Turbulence Spectra

Turbulence spectra downstream from a constricted region in a cylindrical test section were measured by Kim and Corcoran (1974). The inside diameter of the tube was 0.95 cm and the constriction models made of plastic cylinders with various orifice sizes. Measurements were made for water with flow rates giving upstream Reynolds numbers in the range of 800 to 2000. Turbulence spectra were determined for various orifice sizes at several axial positions, using a spectrum analyzer with the probe located at the center of the tube. Signals were then processed with a digital computer which utilized the fast Fourier processor. The comparison of turbulence spectra for different orifice diameters is shown in Figures 3.17a, b, c, d, for upstream Reynolds numbers of 800, 1200, 1600, and 2000 for measurements taken 2.54 cm downstream from the orifice. According to Kim and Corcoran no flow disturbances were observed for a Reynolds number of 800 when the orifice diameter was 0.79 cm ($\frac{D_1}{D_0} = 5/6$). The "onset of disturbance" curve in Figure 3.8 shows that onset of disturbances for this diameter ratio does not occur until a Reynolds number of approximately 1800. Figures 3.17c, d show that turbulent velocity fluctuations for a 0.79 cm orifice diameter appeared somewhere between a Reynolds number of 1600 and 2000.

Sinusoidal fluctuations of low intensity with a frequency of 14 Hz (see square in Figure 3.17a) was observed

at a Reynolds number of 800 for an orifice diameter of
0.635 cm ($\frac{D_1}{D_0}$ = 2/3). For this diameter ratio our obser-
vation showed that onset of disturbance occurred at a
Reynolds number close to 840. The correlation between
some of Kim and Corcoran measurements and our visual
observation appears to be good. For smaller orifice
diameter vigorous fluctuations occurred with increasing
turbulence intensity and frequency range, as observed
during the present investigation.

It is apparent by looking at Figures 3.17a, b, c,
and d that the turbulence spectra are different for diff-
erent orifice diameters for small upstream Reynolds
numbers, and somehow this must be related to the differ-
ent distinguishable regions for the onset of disturabances
curve. For large orifices the flow is either laminar or
laminar-disturbed showing low intensity fluctuations and
a low frequency range. As the diameter of the orifice
becomes smaller the flow becomes fully turbulent, with an
increase in turbulence intensity and range of frequency
as interpreted previously from the visual observations.
An increase in flow rate maintaining the same orifice
diameter indicates an increase in turbulence intensity
and the frequency range.

The comparison of the turbulence spectra for the ori-
fice diameter of 3/16 ($\frac{D_1}{D_0}$= 1/2) at different probe locations
is shown in Figure 3.18 for a Reynolds number of 1600. In order

to show the difference in the shape of the spectra clearly,
the spectra were nomalized by dividing by the area under
the curve.   It is shown that as the flow moves down-
stream, the eddies with high frequencies disappear, while
there is large drop in turbulence intensity, indicating that
laminar flow is gradually developing.

The turbulence spectra as described in Figure 3.18 for
different axial positions of the probe can be correlated
with Figure 3.11 d describing the position of the highly
disturbed region for a constriction diameter ratio of 1/2
in the 1.90 cm pipe diameter. At a Reynolds number of
1600 the turbulent region begins at about 1.8 cm from the
constriction edge and its length is about 8.5 to 9 cm. In
this case the probe located 2.54 cm from the constriction
is inside the highly active region, and turbulence inten-
sity and range of frequency are high. The probe located
at 10.2 cm from the constriction edge is closer to the
downstream boundary of the locally turbulent region where
turbulent activity begins to decay. The probe located at
about 20 cm is outside the turbulent region, where the flow
is laminar-disturbed and laminar flow is gradually developing.

Kim and Corcoran also conducted experiments trying to
understand the contribution of flow turbulence and the wall
to the spectrum of sound. Preliminary experiments on a
simulated constriction in a latex tube using a contact type
microphone demonstrated that the sound spectra and the

69
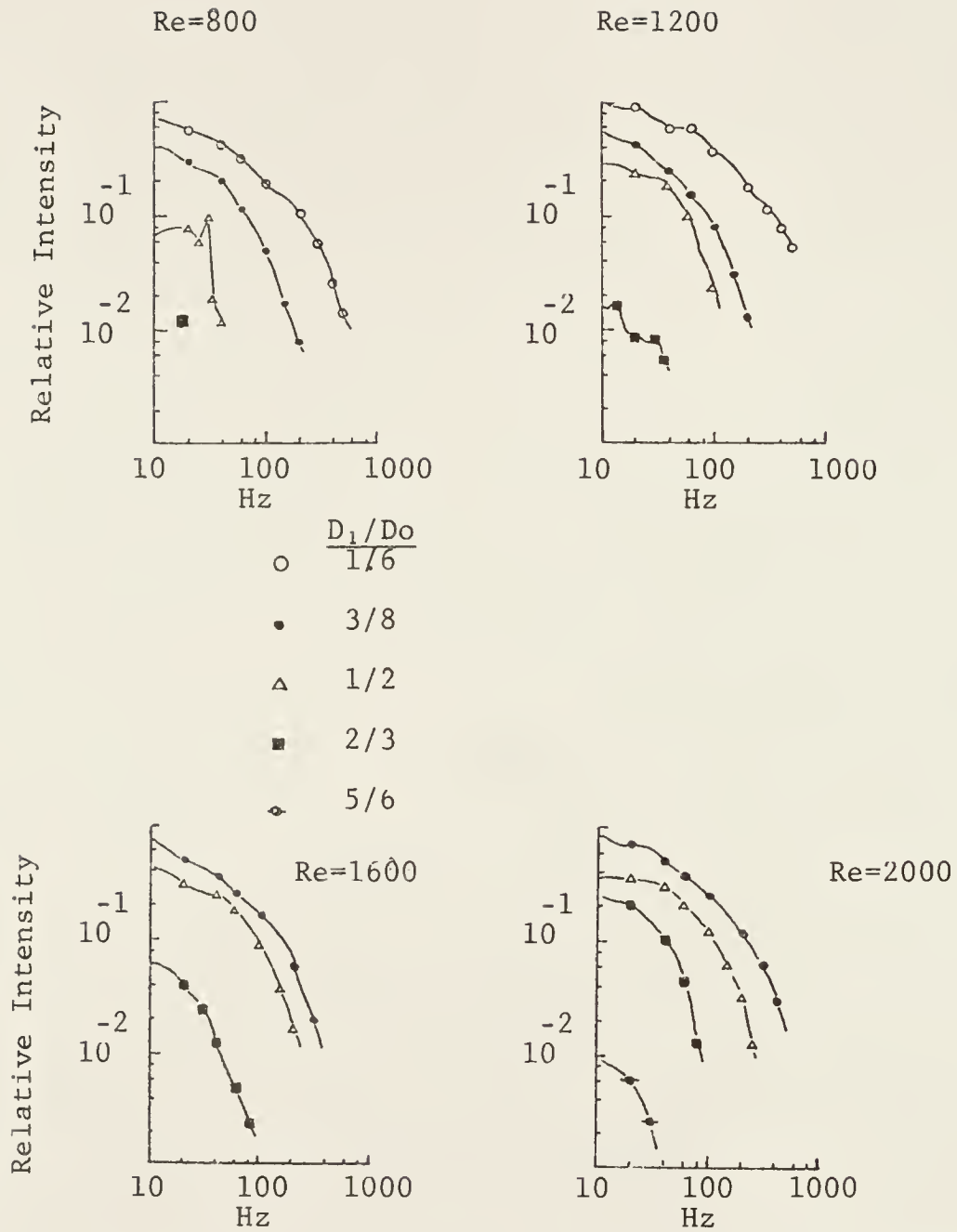
Figure 3.17   Comparison of Turbulence Spectra
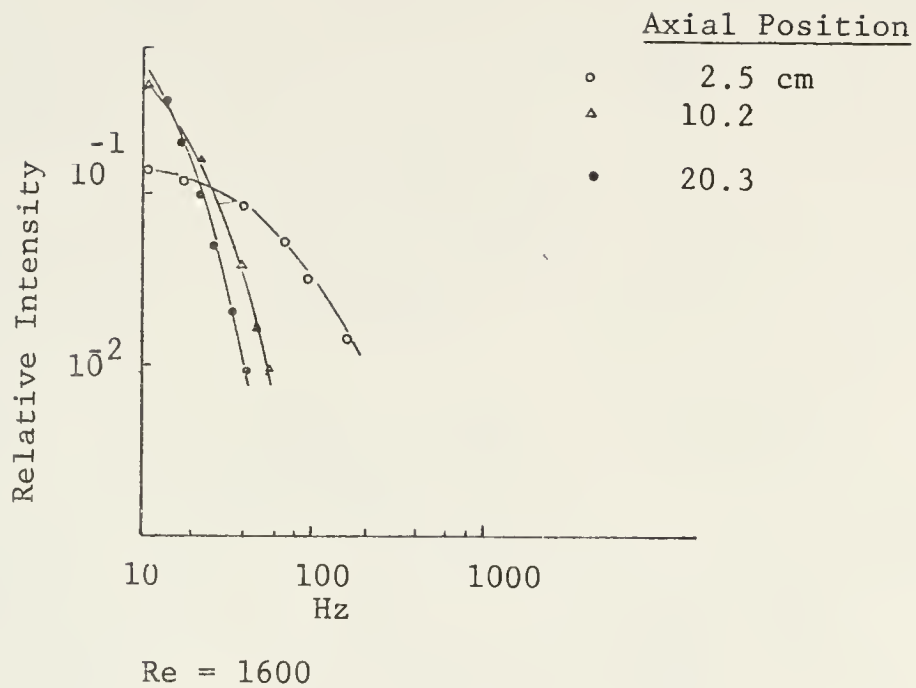
Figure 3.18 Turbulence spectra at various
probe locations

turbulence spectra were quite different for the same flow
rate and orifice diameter. Peak frequencies appeared in
the sound spectra which were not detected in the turbulence
spectra, indicating a strong dependency of the sound spectra
on the vibrations mode of the test section determined by the
geometry and physical properties of the tube.

Onset of Sound in Flexible Tubes

Gonzalez (1974), in his investigations on the origin of
Kortkoff sounds, studied the onset of sound in flexible
tubes locally constricted to simulate a pressure cuff applied
to an artery. The experimental test sections were made of
clear vinyl tubing constricted at the midpoint by squeezing
the sections between two square plexiglass plates held
together by screws at the corners. The edges of the plates
pressing against the tubing were rounded off so that the
contour of the ends of the constriction was smooth and
rounded.

Steady flow of water at constant pressure head was pro-
vided by an elevated reservoir tank. Flow rate was regulated
by adjusting the exit height, in relation to the reservoir
tank, and measured by collecting the flow in a graduated
cylinder during a known time interval.

Sounds were detected externally via a stethoscope rest-
ing against the tube walls downstream of the constricted
region. The length of the constriction was 4.0 cm and test

sections of various diameters. The method of pressing
flat plates against a round tube produced a non-circular
constriction in a circular tube, and the cross-sectional
area had to be calculated prior to each experiment from
measurement of the vertical clearance under the constric-
tion.

According to Gonzalez, resting the stethescope on
the tube walls just distal to the constriction, flow
noise having a murmur-like character could be heard
only under certain flow conditions. The sound intensity
could be increased by increasing the flow rate or by
decreasing the constriction cross section at different
positions along the tube, and it always decreased in
intensity as the distance from the constriction was
increased. Onset of sound was determined by adjusting
the constriction size and increasing the flow rate until
sound was noticed downstream. Then starting with the
maximum flow, the rate was decreased until the sound dis-
appeared. The average of the two measured flow rates was
recorded as the critical flow rate for the onset of sound.
A linear relationship between critical flow rate and area
ratio was obtained for all tests with sound disappearing
at area ratios between 0.6 and 0.70.

In Figure 3.16 the onset of flow disturbances, as
obtained by our study, was compared with Sacks' sound
onset curve in arteries using an internally placed micro-

phone pressure transducer. In Figure 3.19 the critical flow rate at the onset of disturbances is compared with the critical flow rate for the onset of sound (Gonzalez's experiment) as detected by a stethoscope resting against the tube walls. Also shown in the same figure are the approximated magnitude of the Reynolds number when turbulence appeared to be generated right after the constriction exit.

The measurements taken on the 0.67 cm ID tube and the measurements taken on the 1.27 cm ID pipe are both shown. Both presented the same general behavior, showing that the onset of sound as detected by the stethoscope is well above the critical flow rate at the onset of disturbances as obtained from visual observations.

For the small area ratios (high degres of contraction) the flow rate at the appearance of localized turbulence is close to the critical flow rate at the onset of sound, indicating that for the highly constricted tubes the turbulence pressure fluctuations are of sufficient initial intensity and frequency range to produce wall vibrations that can be detected by the stethoscope. This was previously confirmed by our visual observations and Kim's experiments on rigid tubes. As the area ratio increases maintaining the same flow rate, turbulence intensity and frequency decreases (see Figure 3.17) and no sound can be detected any longer.

As expected, when the area ratio was increased higher flow rates were needed to produce sound that could be detected by the stethoscope, but the sound boundary curve shows a steeper slope and for an area ratio larger than 0.20 the flow rate was above the curve describing the flow rate when the turbulent region developed right at the jet exit location. Similar behavior was observed in the larger diameter pipe as shown in Figure 3.19.

The critical flow rate at the onset of sound, determined by means of an internal probe in arteries, showed fair correlation with the critical flow rate at the onset of disturbances in this study, while the critical flow rate at the onset of sound determined externally with a contact microphone in vinyl test sections deviated considerably, always occurring at relative large flow rates.

The external contact microphone actually detects the walls vibrations produced by pressure oscillations in the jet turbulence. Thus, the sound spectrum in this case will depend strongly on the vibration mode of the test section, determined by the geometry and the wall elastic properties, as observed previously by Kim and Corcoran.

The absence of sound (as detected by a contact microphone) for large area ratios could be explained by looking at Figures 3.17c, d. For large area ratios the sound intensity and frequency range is greatly reudced even at the large Reynolds numbers. In some cases the sound intensity is not only very small but also the frequency range is below the audible threshold (about 20 Hertz).
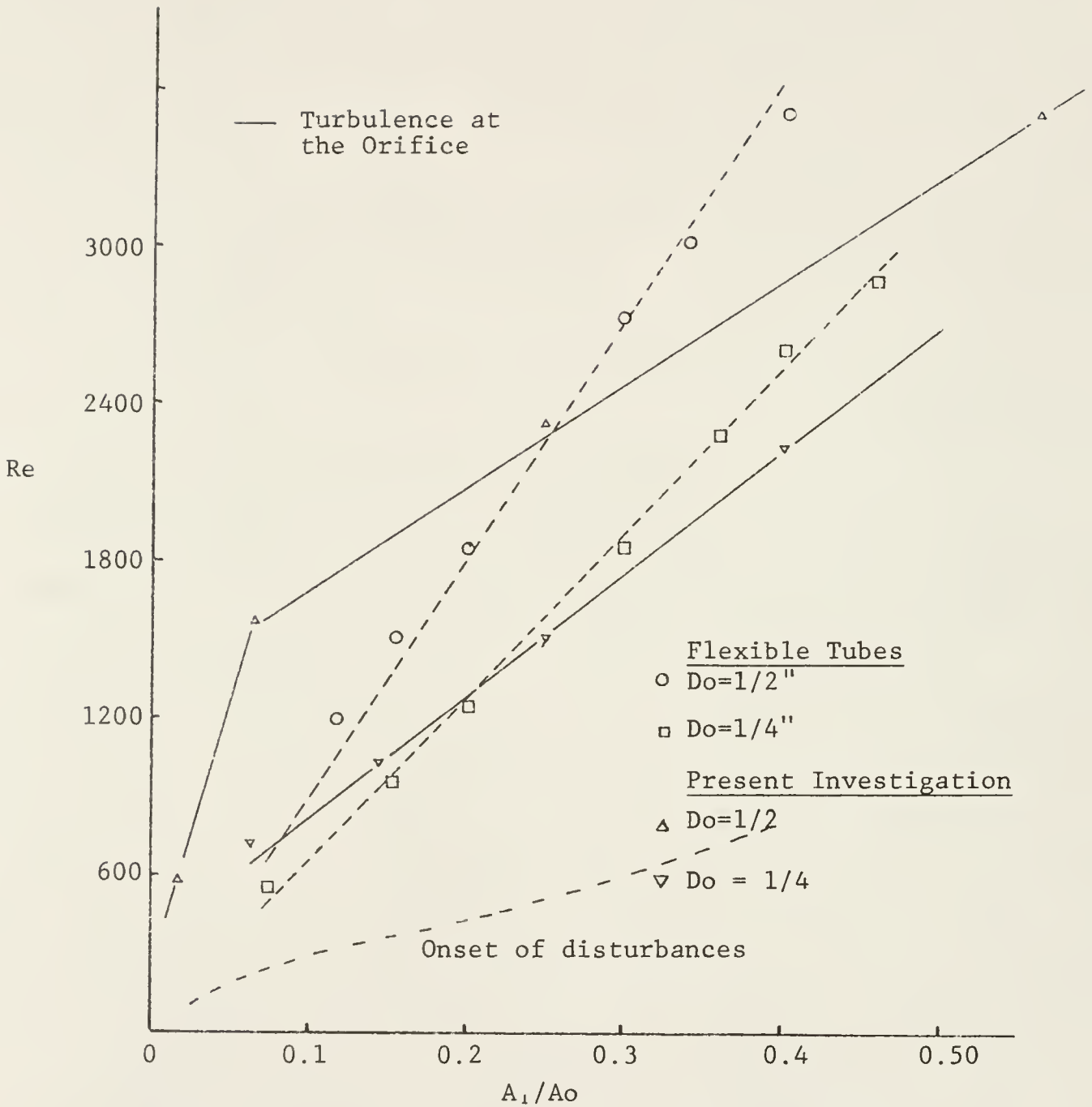
Figure 3.19 Comparison with the onset of sounds in
flexible tubes.

Pressure Drop Measurements

Introduction

These experiments were performed as a direct continuation of the flow visualization experiments. The main purpose of these investigations was to determine (a) the pressure drop along a locally constricted region within a tube of circular cross section, and the dependency of the pressure drop on the constriction geometry and the Reynolds number, (b) the pressure recovery region downstream from the constricted region, and (c) the correlation (if any) of pressure drop characteristics with features of the flow pattern observed visually. The experiments were carried out using the same apparatus used in the flow visualization experiments. The fluid used in all tests was distilled water.

Investigations on the flow behavior and the pressure drop across locally constricted cylindrical test sections is an old problem in fluid dynamics, mostly directly to the establishment of the orifice as a flow meter. The present investigation is more oriented towards physiology, so the flow Reynolds number has been maintained inside the arterial blood rate of flow range. Thus, the range of Reynolds number considered was approximately 200-2500.

Since the flow of blood in arteries is unsteady, arterial walls are distensible, and blood is a suspension,

studies based in the steady flow of a Newtonian fluids (water) in rigid tubes must be considered, at best, a first approximation to the biological problem.

The pressure drop across a constricted region in a circular section has strong physiological implications. One of the most serious consequences of an arterial stenosis is the large pressure loss which may develop across a severe stenosis. The reduced pressure distal to the stenosis significantly alters the blood flow to the peripheral beds supplied by the artery. The pressure loss is primarily dependent on the flow rate and the geometry of the stenosis since the fluid properties of density and apparent viscosity are relatively constant. Geometrical factors like the area ratio (degree of stenosis); the length of the stenosis; and some measure of the eccentricity could drastically change the pressure drop across the region.

Although arterial blood flow is unsteady, the effect of the unsteadiness on pressure drop seems to be small for a severe stenosis, i.e. one for which the reduction in area is greater than ca, 80% (Young, 1973). It is well established that under normal physiologic conditions the effect of the stenosis on flow and pressure is small unless the stenosis is severe. Thus the pressure drop experiments with models 8 and 9 (Table I) represent essentially observations on the moderate to severe stenosis.

The influence of the geometric characteristics upon the pressure drop, along the constricted region were

studied by a series of experiments on the flow of water through the 1.27 cm test section. A dimensional analysis shows that the pressure drop due to a single constriction in a conduit can be studied in terms of the dimensionless variables.

$$\Delta p / \rho U^2 = f \left[Re, \frac{Ao}{A_1}, \frac{L}{Do}, \frac{Zo}{Do}, \frac{2e}{Do} \right] \tag{3.2}$$

Where Δp is the pressure drop over the length L

    ρ fluid density

    U mean velocity in the unobstructed tube

    Re Reynolds number, DoU/ν where ν is the fluid kinematic viscosity

    Ao the unobstructed area

    A_1 constriction flow cross section

    Zo length of the constriction

    e eccentricity

The length of all the models used was constant and equal to 3 cm, and the hole drilled along the plub center-line (zero eccentricity). The pressure drop was measured over a constant pipe length of 28.4 cm. This reduced the number of non-dimensional variables to two, the Reynolds number and the non-dimensional area ratio. The area ratio was changed by trying different models on the 1.27 cm pipe. Reynolds number was varied by adjusting the needle valve controlling the rate of flow.

Pressure readings were taken at different positions located upstream and downstream of the constricted region by means of pressure taps separated at a distance in multiples of the pipe diameter from the constriction edges. The pressure tap locations are shown in Figure 3.20. Pressure taps were also made of acrylic glass and machined to fit the pipe circumference. The top holes in the tube walls were approximately 0.5 mm in diameter.

TAP LOCATION (Do)
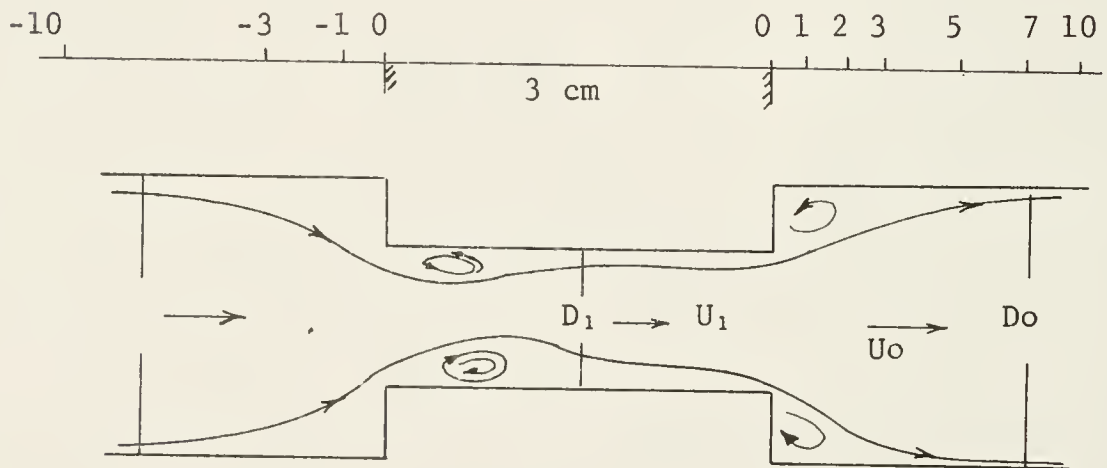
Figure 3.20   Constriction geometry

Experimental Results

The pressure drop across the constricted region was measured using the pressure taps located at ± 10 Do from the constriction edges. Since the diameter of the pipe was 1.27 cm ID and the length of the constriction 3 cm this resulted in a magnitude for $\frac{L}{D_o}$ of approximate 22.3. This insured that the pressure drop was measured over a sufficient length for pressure recovery downstream from the constriction.

For a given constriction, the dimensionless pressure drop is a function only of the Reynolds number. The experimental results obtained using models 8, 9, and 10 are shown in Figure 3.21. The general behavior of the dimensionless pressure drop curves was found to be the same for all models. At low Reynolds number the pressure drop is due primarily to viscous effects and the dimensionless pressure drop decreases with increasing Reynolds number. Laminar separation may take place at low Reynolds numbers. With an increase in Reynolds number the flow becomes locally unstable, and disturbances begin to propagate in the flow.

At higher Reynolds number turbulence develops and the dimensionless pressure loss along the constriction is due primarily to turbulence. Thus at high Reynolds numbers, turbulent losses are dominant and the dimensionless pressure drop coefficient becomes independent of the

Reynolds number. The pressure drop coefficient illus-
trated in Figure 3.21 includes also the measured pressure
loss in the unobstructed section (Poiseuille pressure
loss).

Assuming laminar flow up to a Reynolds number of
2000, the flow rate Q is given by

$$Q = \frac{\pi Ro^4}{8} (\Delta p/L) \tag{3.3}$$

Where Ro is the radius of the unobstructed pipe.

Expressing the pressure drop in dimensionless form
and replacing the flow rate by the equivalent Reynolds
number in the experimental pipe, we obtain

$$\xi_\ell = 32 \quad (\frac{L}{Do}) \quad (\frac{1}{Re}) \tag{3.4}$$

for this case (L/Do) is 22.3 and the dimensionless laminar
pressure drop coefficient given by

$$\xi_\ell = 713.6 \quad (\frac{1}{Re}) \tag{3.5}$$

The strong influence of the area ratio upon the
pressure drop is clearly shown through a comparison of
the data for different constrictions in Figure 3.21. For
example at a Reynolds number of 1000 the dimensionless

pressure drop for the heavily constricted model (8) is
approximately 20 times the corresponding value for the
moderately constricted model (10).

No information about the effects of the constriction
length upon the pressure loss can be obtained from these
set of experiments, since this length was the same for all
constrictions. Experiments conducted by Young and Tsai
(1973) on cylindrical test sections demonstrated that the
effect of this parameter is small in the range of Reynold
number studies (100 -5000), for rather constricted tubes
having the same area ratios (89%) but different length
to pipe diameter ratio, $(Z_0/D_0 = 1,2)$.

However, experiments conducted by Robbins and Bentov
(1967) on the effect of length of stenosis on flow volume
(using cylindrical models in a 3.3 mm pipe diameter) in-
dicated that the length of the constricted region has a
rapidly increasing influence with increasing severity of
stenosis (small area ratios). When severe levels of
stenosis were reached, such as 90 per cent, increasing
the length of the stenosis from 0.5 to 2.0 cm results in
a decrease of the flow rate by 50%.

The dimensionless axial pressure distributions down-
stream of the constricted region are shown in Figures
3.22a, b, for different area ratios and Reynolds numbers.
Pressure readings were taken at several locations along
the tube as shown in Figure 3.20. The closest pressure

taps were located at a distance of ± 1 pipe diameter from the constriction edges; no readings were taken inside the constriction models. It is noted that as the fluid approaches the contraction, it accelerates which results in a rapid pressure drop.

In the downstream side the pressure variations are smoother and recovery takes place over a greater tube length. The minimum pressure occurs inside the constricted flow region. An important point is, that most of the pressure loss occurs downstream from the abrupt change in corss-sectional area, where the jet formed by the sudden contraction attains a minimum area.

The minimum jet cross section area, the so-called "vena contracta," is located about one constriction diameter downstream of the constriction entrance (Whitaker, 1968).
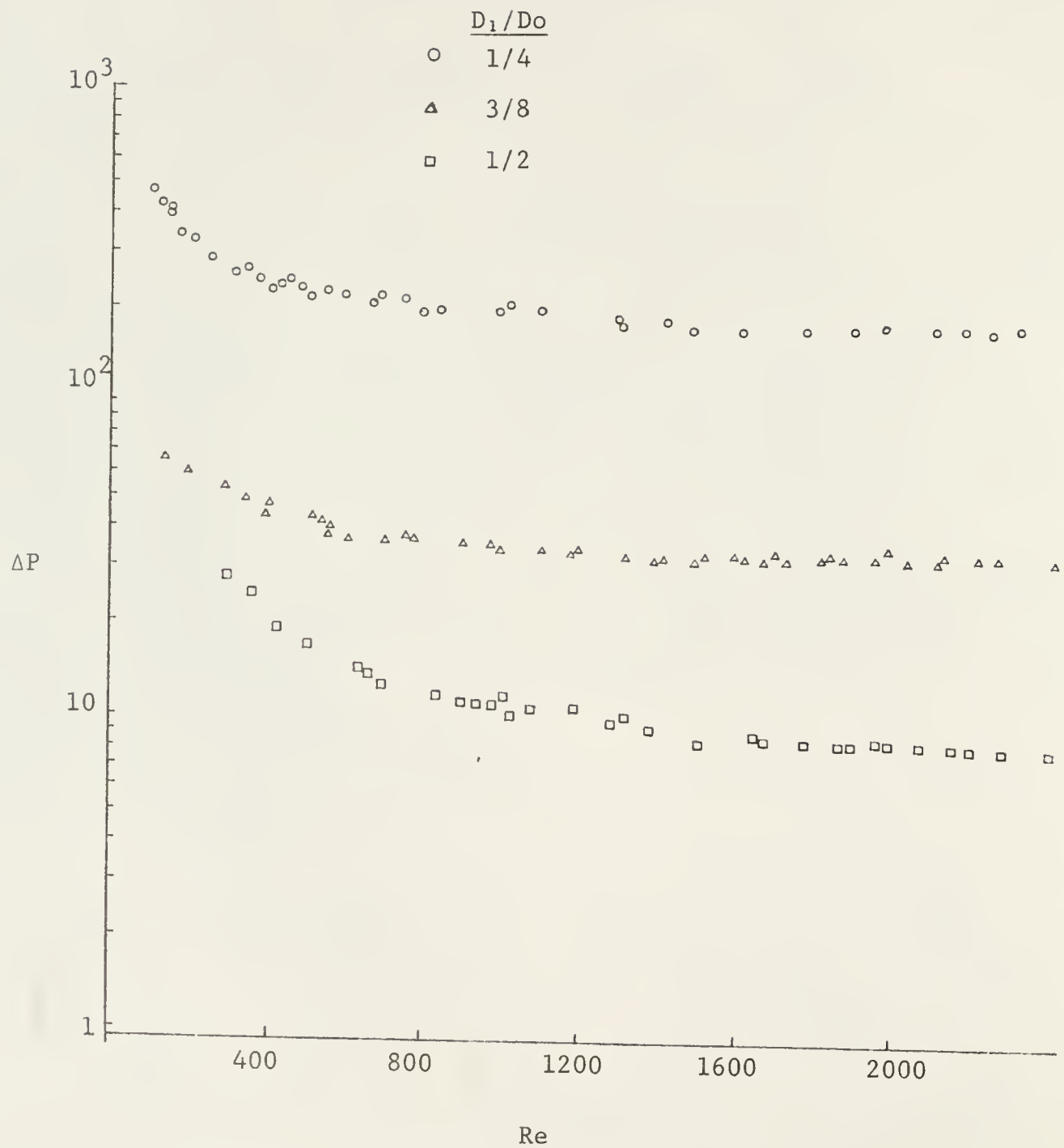
Figure 3.21   Dimensionless pressure drop
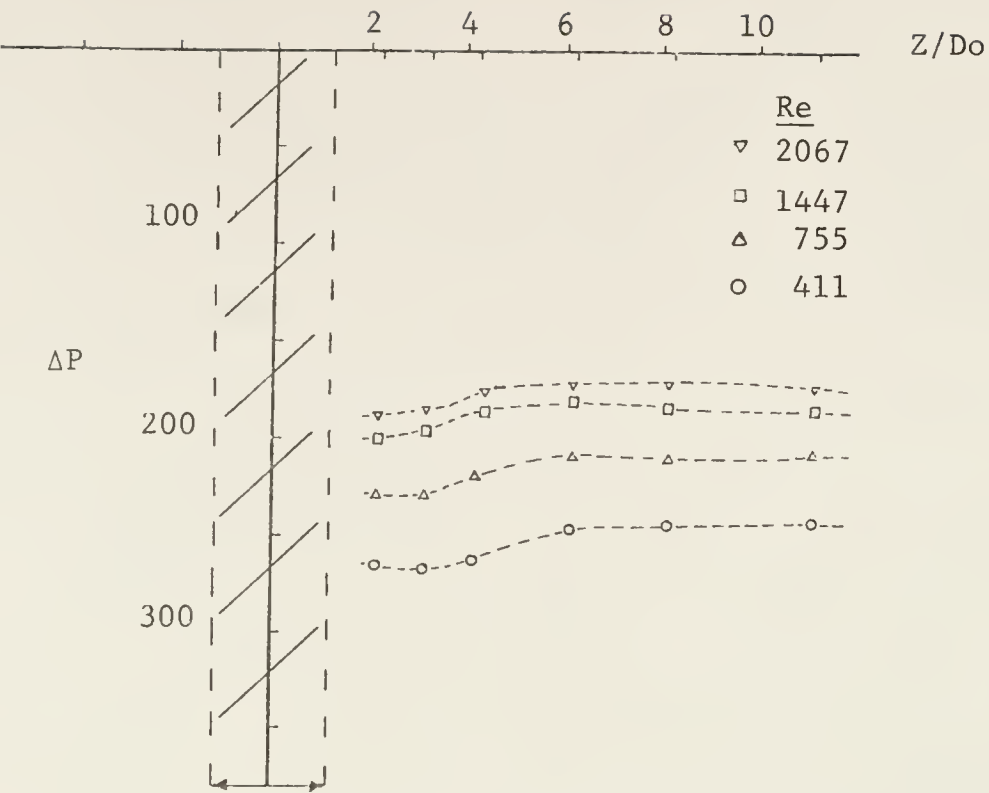
Figure 3.22a   Pressure distribution. $D_1/D_o = 1/4$
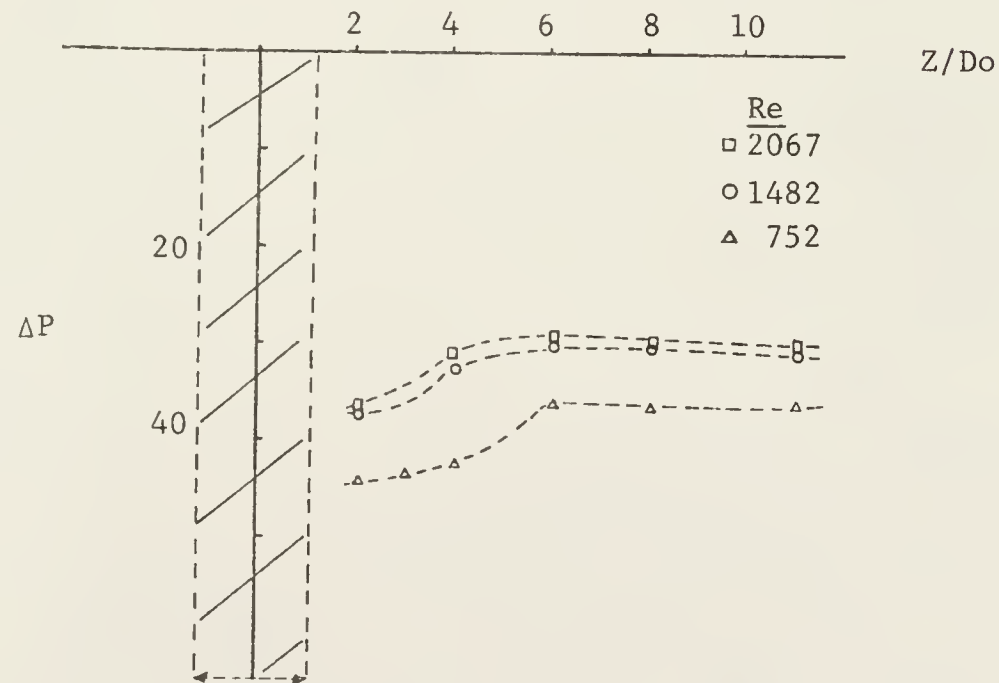
Figure 3.22b   Pressure distribution. $D_1/D_o = 3/8$

Effects Produced by Changes in Geometry

In Figure 3.23 the total dimensionless pressure drop coefficient for model 8 is compared with model 8R. For this case the area ratio of the two models is the same but model 8 was constructed with square corners and model 8R with rounded corners, both axisymmetric models. The purpose was to determine the variation in pressure coefficients due to the shape of the constriction. Constrictions with rounded edges provide a smoother entrance flow and probably provides a more realistic representation of an arterial stenosis. In general the development of stenosis does not follow any well-defined geometrical pattern and the geometry of the growth is quite variable. According to Figure 3.23 the dimensionless pressure drop in the square-edged model is about 100% higher than the round entrance model for the range of Reynolds number tested.

Obviously the pressure loss in the contraction is considerably influenced by the geometry of the constriction. It seems the geometry of the model controls the degree of vortex formation and hence energy dissipation. It would appear that the well-rounded model, by streamlining the flow, prevents the occurrence of the vena contracta and accompanying vortex formation.

All the experimental results described during this investigation apply only to axisymmetric models. Young

and Tsai studied experimentally the effects of asymmetric constrictions upon the dimensionless pressure drop coefficient, and concluded that the pressure losses in non-symmetric cases were considerably higher than losses in the corresponding axisymmetric constrictions.

Experiments conducted by Seeley and Young (1976) demonstrated that the constriction eccentricity had little effect on the pressure drop for small diameters constrictions (greater than approximately 90%). As the constriction diameter ratio increases, the effect of eccentricity may increase but the overall pressure drop decreases so that mild or moderate constrictions are of less practical importance. A series of experiments performed by Robbins and Bentov (1967) determined the effect of shape on stenosis flow. In all cases the venturi shape provided the maximum rate of flow, presumably because laminar flow was set up at an earlier downstream distance.

Figure 3.24 illustrates a comarison between the dimensionless pressure distribution obtained with the sharp edged constriction, and the pressure distribution obtained for flows through the constriction with rounded edges. These measurements correspond to a Reynold's number of 760, for a diameter ratio of 1/4. The axial pressure recovery in constriction 8R looks smoother than the one measured for constriction 8.

Figure 3.23   Effects produced by geometry change on pressure drop
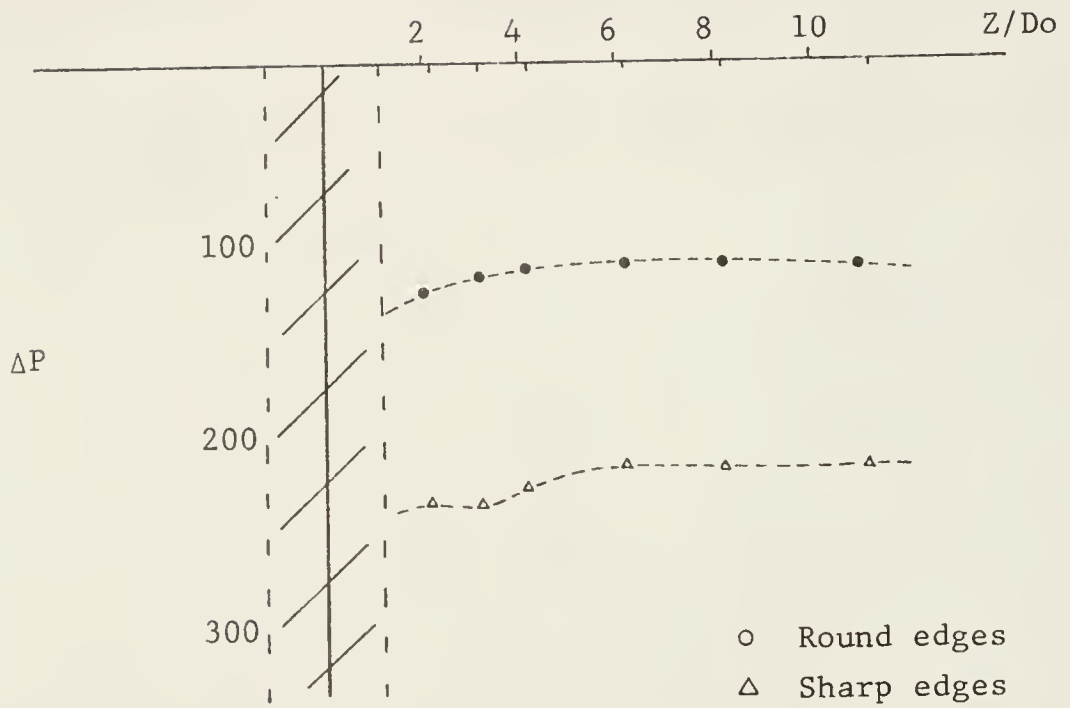
Figure 3.24   Effects produced by geometry change
on pressure distribution

Correlation with Momentum Balance Approach

The momentum and mass balance in a control volume in space can be used to approximate the dimensionless pressure drop in a cylindrical section as described by Whitaker (1968). The dimensionless pressure drop across a sudden contraction can be approximated by

$$\Delta P_c = \frac{Ao}{A_1} \left[\frac{Ao}{A_1} - 1 \right] \tag{3.6}$$

Where Ao is the cross-sectional area of the pipe and A is the cross-sectional area of the obstructed section, and the dimensional pressure drop is defined as follows

$$\Delta P = \Delta p / \rho U^2 \tag{3.7}$$

depending only on the area ratio when the viscous effects are neglected (large Reynolds numbers).

The pressure recovery in a sudden expansion can be obtained similarly and it is described by

$$\Delta P_e = \left[1 - \frac{Ao}{A_1} \right] \tag{3.8}$$

The pressure drop across a sudden contraction is always larger than the pressure recovery across the sudden expansion. The net pressure drop is given by

$$\Delta P_t = \left[\frac{Ao}{A_1} - 1 \right]^2 \tag{3.9}$$

These results, obtained using the momentum and mass balance equation, are valid for an incompressible fluid.

where viscous surface forces were considered negligible and the velocity profiles were assumed to be flat at the entrance and exit of the fixed control volume. Under those assumptions the dimensionless pressure drop depends only on the geometrical area ratio of the problem.

Due to difficulties in constructing pressure taps inside the constricted region with the existing models, no pressure readings were taken inside the constriction where the lowest pressure is most likely to occur. In this case the approximated pressure drop as calculated from equation (3.6) can only be correlated with the experimental pressure reading using the closest pressure tap located at 2.77 cm from the center of the constriction model.

The total pressure drop approximated by (3.9) can be correlated with the experimental total pressure drop measured between tap No. 1 and No. 9. Pressure recovery is obtained by subtracting the two readings.

These results are given in Table IV for models number 8, 9, and 10 using the 1.27 cm ID test section at Reynolds number of 750 and 2000. Pressure drop along each model was found by subtracting the computed Poiseueille loss (equation 3.5) from the total pressure drop across the test section. The discrepancies between the analytical approximation and the experimental data are less than 20%, with the higher Reynolds number showing larger discrepancies.

The experimental value seems to be lower than the predicted by the momentum balance approach. The unexpected result that the deviation increases as the Reynolds number increases is probably a consequence of the assumption that the pressure on the annular surface was taken to be equal to the average pressure in the surrounding area.

At very low Reynolds number viscous effects cannot be neglected. A dimensional analysis will show that the dimensionless pressure drop will depend on the Reynolds number. Seeley and Young (1976) in their investigations on the effect of geometry on pressure losses along models of arterial stenoses, assumed that at low Reynolds numbers viscous losses are dominant and the pressure drop is linearly dependent on the velocity. Similarly at high Reynolds number inertia and turbulence will control the pressure drop. The total pressure drop including both effects over the entire range of Reynolds number can be predicted by the equation

$$\Delta P_t = \frac{Cv}{Re} + C_t \left[\frac{Ao}{A_1} - 1 \right]^2 \qquad (3.10)$$

Where Cv is only a function of the dimensionless geometric variables of equation (3.2) and C_t a coefficient that should not depend strongly on geometry.

Using an iterative weighted residual least-squares curve fitting based on equation (3.10) Seeley and Young

found experimentally that for blunt plugs (square-edges) forming axisymmetric constrictions the constants were given by the relations

$$Cv = 32 \ \left(\frac{Za}{Do}\right) \left(\frac{Ao}{A_1}\right)^2 \tag{3.11}$$

with

$$\frac{Za}{Do} = 0.83 \ \left(\frac{Zo}{Do}\right) \ + 1.64 \ \left(\frac{D_1}{Do}\right)$$

and

$$C_t = 1.52$$

showing the dependence of the pressure drop on constriction length Z_0, diameters Do and D_1, and Reynolds number.

The correlation of our experiments with the empirical-analytical approximation described by equations (3.10) and (3.11) is very good as shown in Table IV.

Seeley and Young also studied the effects of two constrictions in series, finding that if the distance separating the two was sufficiently large, the pressure drop could be obtained by adding both individual effects. However as the distance between the two decreased, there was an interaction and the overall pressure drop was less than the sum of the two, with magnitude between the sum of the two pressure drops and that for a single constriction having the combined length of the two.

TABLE IV

Comparison of Measured Pressure Drop with the Momentum
Balance Approach

Re	Model No	$\frac{Ao}{A_1}$	ΔPc	ΔPc (Exp.)	ΔPe	ΔPe (Exp.)	ΔP_t	ΔP_t (Exp.)
750	8	16	240.0	226.7	-15.0	-20.7	225.0	206.0
2000				189.9		-15.3		174.6
750	9	64/9	43.5	44.1	-6.1	-8.9	37.3	35.2
2000				36.1		-6.6		29.7
750	10	4	12.0	12.8	-3.0	-3.9	9.0	8.9
2000				10.7		-3.3		7.4

TABLE V

Comparison of Measured Pressure Drop with Seeley and Young
Approach

Re	Model No	$\frac{Ao}{A_1}$	$\frac{Cv}{Re}$	$C_t \left(\frac{Ao}{A_1} - 1\right)^2$	ΔPt Eqn. (3.10)	ΔPt (Exp)
750	8	16	25.87	171.0	196.9	195.9
2000			9.70		180.7	174.6
750	9	64/9	5.55	28.38	33.9	33.0
2000			2.08		30.5	29.7
750	10	4	1.90	6.84	8.7	8.9
2000			0.71		7.5	7.4

Experiments Using Polymer Solutions

Introduction

It has been known for some time that certain high
molecular weight additives reduce turbulence appreciably.
In 1948 Toms reported that very dilute solutions of poly-
methyl methacrylate in monochlorobenzene could cause
large reductions in the turbulent pipe flow pressure
drop, relative to that obtained with the pure solvent
at the same flow rate (typically a 50% reduction for 0.05%
solution). This phenomenon, which has been observed to
occur for different polymers and solvents, is commonly
referred to as 'drag reduction with dilute polymer solu-
tions' or 'Toms phenemenon.' Polymer solutions, while
appreciably altering the turbulent flow behavior, cause
very small effects on laminar flow and hence very small
effects on density and viscosity relative to that of
the pure solvent.

The polymer concentration needed is very small: Virk
et al. (1966) reported a large effect on pressure drop on a
pipe at polymer concentration as low as 5ppm. Exploratory
test with blood transfusion fluids (dextran, saline, and
plasma) by Hoyt and White (1966) indicated the turbulent
flow friction to be greatly reduced. The polymer effects
on the development of transition were investigated by
Castro and Squire (1967) showing a reduction in the turbu-

lent slugs at a given Reynolds number.

After looking at the large amount of experimental data on polymers effects on pipe flow at relatively large Reynolds number, (a good review is given by Hoyt, 1972) we decided to study the effects (if any) of friction reducing polymers on the flow downstream of the constricted region and to determine the variations in pressure drop along the constriction relative to that of the pure solvent.

Polyox Solution Characteristics and Preparation Technique

The additive used in this experiment was Polythylene Oxide (Polyox WSR-301) supplied by Union Carbide Corporation. Polyox resins are polymers with the common structure $\{O\text{-}CH_2CH_2\}_n$. The degree of polymerization, n, varies from about 2,000 to about 100,000, depending upon the viscosity grade of resin. The corresponding molecular weights are said to vary from 100,000 to 5 million, with an approximate molecular weight of 4 million. Polyox resins are soluble in water, forming hydrogen bonds with water molecules. They are also soluble in many common organic solvents. Polyox resins are supplied as white granular powders.

Many of the polyox properties are dependent upon polymer degradation which can bring about significant changes in their drag reducing ability. High shears produced during preparation and circulation of the solution

through the new apparatus are common causes of degradation. Polymer solutions can also be degraded by chemical and thermal effects, and these must also be taken into account when handling and carrying out measurements. As determined by Paterson and Abernathy (1970) in the case of polyethylene oxide in distilled water at room temperature the chemical and thermal degradation is negligibly small.

The procedure was to first prepare a highly viscous stock solution of 1% polymer concentration in distilled water, and then dilute the stock solution when necessary to the desired working solution concentration, usually 0.01% (100 PPM).

To prepare a 1% resin solution 10g of polyox were dispersed in 40g of anhydrous isopropanol, and this slurry added to 950g of distilled water. Instead of using a variable speed stirrer as recommended by the manufacturer, the solutions were slowly stirred by hand, to minimize shear degradation. The isopropanol according to Union Carbide brochure F-42933 serves a dual purpose, not only prevents agglomerate formation but also inhibits the oxidation of the polymer solution. It usually took a few days for the polymer to completely dissolve in water and

the final solution appeared very clear and transparent and pulled out into a long thread when falling from a stirring rod.

Solutions prepared without the isopropanol were more difficult to disperse in the water solvent forming large agglomerates, but showed after complete dissolution the same properties of the solutions prepared using the iso-propanol

Pressure Drop Measurements

The idea behind the experiment was to determine if there was any additives effects on the onset of disturbances or in the characteristics and position of the stationary decaying turbulent region, at these low Reynolds number well below the transition Reynolds number in pipe flow. An attempt to make direct vidual observations by mixing the bentonite and polymer solution failed. Probably due to the good flocculating properties of the polyox solution, bridging the bentonite colloidal material. No optical activity was observed after mixing the two solutions. It was decided then to proceed with the pressure drop measurements and this way determine if there was any significant change in the flow behavior as compared with the measurements taken with the pure solvent.

The method used to measure the pressure drop across the constriction was identical to the one described before,

but a few modifications had to be made in the experimental apparatus to minimize the degradation effect produced by shear forces.

Fluid coming out of the test section was not recirculated, but drained into a sink. Flowmeter was taken out of the loop and the flow rate measured by weighting the amount of fluid in a certain period of time during the experiment. The standard impeller type pump was replaced by a relative low shear peristaltic pump, and the working solution (100 ppm) slowly pumped from a storage tank to the pressure tank.

A pressure drop reduction across a partially occluded tube by a drag reducing polymer has important applications in industry and medicine. The power required to pump a fluid at a given flow rate, Q, across a pressure drop, Δp, is given by $Q\Delta p$. If the pressure drop can be reduced to Δp^1 by a drag-reducing agent, the power saved is $Q (\Delta p - \Delta p')$. In the circulatory system, for example, the pressure drop across an occlusion could be reduced by a non-toxic drag-reducing polymer, causing the heart to work less in order to maintain a constant blood supply to the body. With this idea in mind pressure drop measurements were taken in the 1.27 cm ID pipe constriction model No. 9, in the Reynolds number range 0 to 2000.

The experimental results are described in Figure 3.25 where the pressure drops across the constriction produced

by the flow of the pure solvent (distilled water) are
compared with the pressure drops obtained with a Polyox
solution of 50 PPM concentration. The reduction in
pressure drop is very small, about 8 or 9% at an up-
stream Reynolds number close to 1800. Experiments
using Polyox solutions of 100 PPM concentration pro-
duced similar results.

The absence of drag reducing effects appears to be
related to the "threshold" shear stress which must be
exceeded in order for the polymer effect to manifest
itself. At the moderate Reynolds number in question,
the shear produced in the 1.27 cm ID test section is
below this minimum. The existence of a threshold is
consistent with the requirement that the turbulence
scales must be small enough to be affected by the addi-
tive polymer molecule. Virk, et al (1966) hypothesized
that the onset of drag reduction would occur at a wall
shear stress approximated by

$$R_G{}^2 \tau_w{}^* \approx 45 \times 10^{-10} \text{ dynes} \qquad (3.12)$$

where τ_w is the onset wall shear stress.
For Polyox WSR-301 the radius of gyration (R_G) is approx-
imately 1977 $\overset{o}{A}$ and we would expect the threshold value
for the shear stress to be around 11.8 dynes/cm^2. Fabula
et al., (1966), using polymer theory, suggested the onset
to be about 2.1 dynes/cm^2. In any case, the maximum flow

rate tested during the present investigation yielded approximated shear stress well below this threshold. Future experiments should be carried out in smaller pipe diameters such as the 0.3 cm ID test section.

Similar experiments under pulsating flow conditions using high molecular weight polyacrylamide polymers (Separan AP-30 and AP-273) solution in water and calf blood were conducted by Greene, Nokes and Thomas (1974), obtaining pressure drop reduction on the order of 10-15% at an upstream Reynolds number above 400 in a glass test section of 0.33 cm ID, locally constricted. They also found that the effects of the polymer on pressure change was dependent on the constriction geometry, showing a small increase in pressure loss for some geometries.
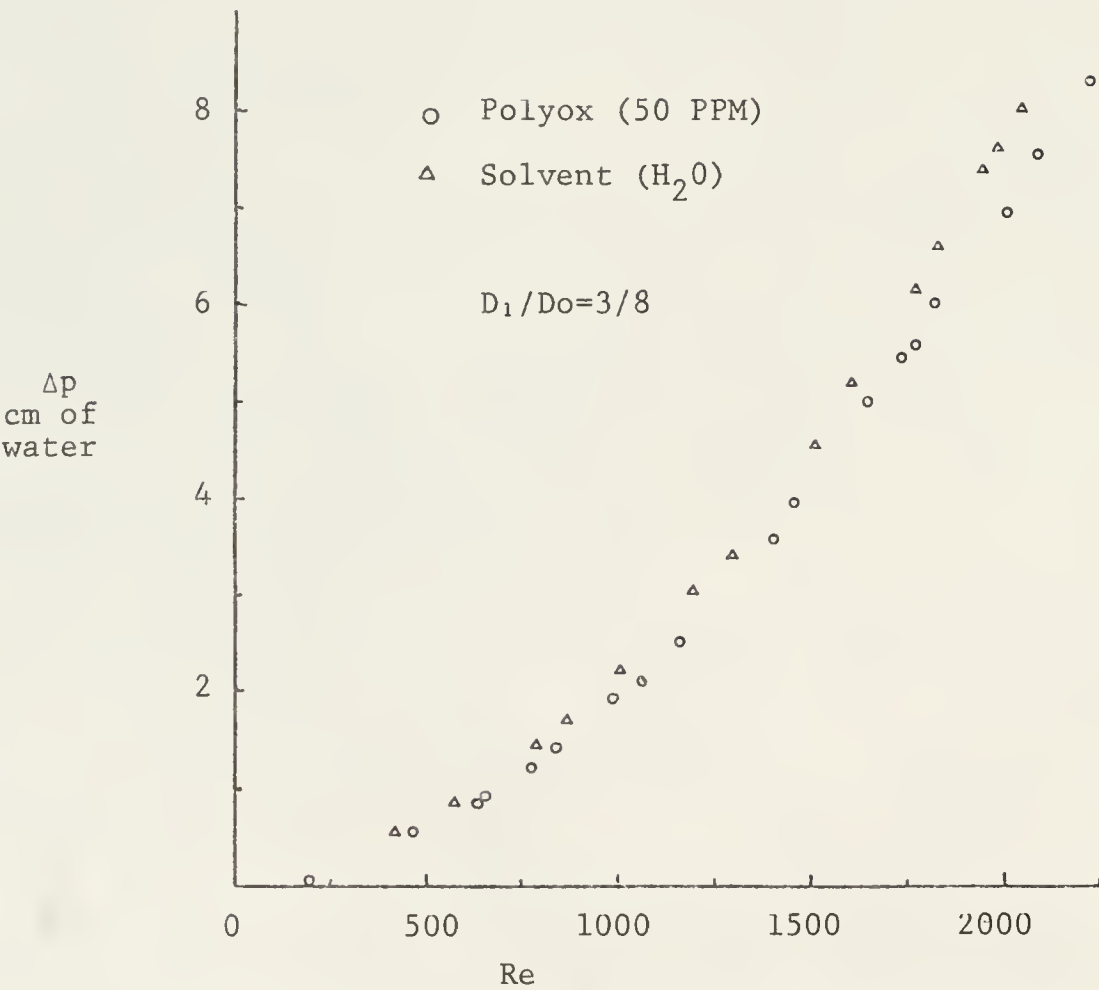
Figure 3.25   Pressure drop using Polymer solution.

CHAPTER 4
STABILITY ANALYSIS

Introduction

It was determined by the experiments on the critical
conditions at the onset of instabilities that the fluid
behavior was characterized by the appearance of wave-like
disturbances that eventually propagated downstream,
breaking down into a random turbulent motion after travel-
ling a short distance. The wavy motion can be observed
in figure 3.1b and 3.6, when the flow was close to the
critical value. In this section an attempt is made to
correlate the observed disturbance wavelength as measured
from the flow visualization experiments with the predicted
results of the linear inviscid analysis. If the analysis
indicates an instability only the early stages can be
studied because, as the disturbance amplitude increases,
the non-linear terms in the equations of motion are no
longer negligible and the linearized form is no longer
valid.

To accomplish this task we start from the Orr-
Somerfeld stability equation, and introduce two further
simplifications. The first is to assume that instabili-
ties will only propagate when the Reynolds number is

large, so the viscous forces can be neglected in relation
to the inertial forces. This yields a simplified version
called the frictionless stability equation, first derived
by Rayleigh (1880). We further assume that for rectangu-
lar coordinates the velocity distribution in the vicinity
of the inflection point can be approximated by straight
line profiles, with constant velocity gradient in each
separated region. This approximation procedure had been
used earlier by Michalde and Schade (1963) in their studies
of free boundary layer stability. The resultant stability
equation is greatly simplified with solutions in the form
of exponential or hyperbolic functions, and subject to
the boundary conditions of the problem. Approximate
values for the complex eigenvalue $\omega = \omega_r + i\omega_i$ can be found
after matching the kinematic and dynamic interface condi-
tions. The inviscid analysis is not able to predict the
critical Reynolds number but does provide information
regarding the stability of a given velocity profile and
its sensitivity to the wavelength disturbance. The
assumption of partially linear profile to represent the
velocity distribution is a good approximation especially
in the case of very inflected profiles developed close to
the jet orifice. The development of the almost flat
velocity profile into a parabolic distribution is approxi-
mated by moving the interface position away from the

center line, and the corresponding instability growth
rate determined by the linear inviscid analysis. The
computations are carried out for symmetric and anti-
symmetric disturbances in rectangular and cylindrical
coordinate systems.

Mathematical Formulation in Rectangular Coordinates

We would like to discuss the inviscid stability to
small disturbances of steady two-dimensional, incompress-
ible flow. It is assumed that the flow velocity is
composed of a mean flow which is regarded as steady and
described by its Cartesian components U, V, and its
pressure P, with superimposed non-steady perturbations
components, $\hat{u}$, $\hat{v}$, and $\hat{p}$ respectively. Hence in the result-
ant motion the flow velocity components are described by

$$u = U + \hat{u} \qquad v = V + \hat{v} \qquad (4.1)$$

and the pressure is $\quad p = Po + \hat{p}$.

The problem is then to determine the stability of the
mean flow to the small disturbances. In all cases it is
assumed that the perturbation components are very small
compared with the corresponding quantities of the mean
flow.

The stability equation describing a two dimensional
incompressible flow in the x, y plane can be derived from
the Navier-Stokes equations of motion (neglecting the body
forces)

$$\frac{\partial \vec{q}}{\partial t} + \vec{q}\cdot\vec{\nabla}\vec{q} = \frac{-1}{\rho}\vec{\nabla}p + \nu\vec{\nabla}^2\vec{q} \tag{4.2}$$

and the continuity equation

$$\vec{\nabla}\cdot\vec{q} = 0 \tag{4.3}$$

where the total velocity vector

$$\vec{q} = u(x,y,t)\ i + v(x,y,t)\ \hat{j} \tag{4.4}$$

We further assume that the mean velocity U depends only on the transverse coordinate y and that the transverse component of the mean flow is negligible (parallel flow). In this case

$$U = U(y),\ V = 0,\ P = P(x,y) \tag{4.5}$$

Hence the resultant motion is

$$u = U + \hat{u},\ v + \hat{v},\ p = p_o + \hat{p} \tag{4.6}$$

It is required that the mean flow satisfies the equation of motion, and it is also required that the resultant motion, equation (4.6), must also satisfy the equations of motion.

Substituting equation (4.6) into the Navier-Stokes equation of motion, and linearizing the resultant equations by neglecting the effects of a perturbation on another perturbation and considering that the mean flow satisfies the equation of motion, we obtain a simplified set of equations in the disturbance components, which can be expressed in the form

$$\frac{\partial\hat{u}}{\partial t} + U\frac{\partial\hat{u}}{\partial y} + \hat{v}\frac{dU}{dy} + \frac{1}{\rho}\frac{\partial\hat{p}}{\partial x} = \nu\nabla^2\hat{u} \tag{4.7a}$$

$$\frac{\partial\hat{v}}{\partial t} + U\frac{\partial\hat{v}}{\partial x} + \frac{1}{\rho}\frac{\partial\hat{p}}{\partial y} = \nu\nabla^2\hat{v} \tag{4.7b}$$

$$\frac{\partial\hat{u}}{\partial x} + \frac{\partial\hat{v}}{\partial y} = 0 \tag{4.7c}$$

These three equations describe the behavior of the flow disturbances $\hat{u}$, $\hat{v}$ and $\hat{p}$ subject to the boundary conditions of the problem.

Mathematical Form of the Disturbance

The stream function satisfying (4.3) and representing a single oscillation of the disturbance is assumed to be of the form

$$\Psi(x,y,t) = \phi(y)\, e^{i(kx - \omega t)} \qquad (4.8)$$

where $\phi(y)$ represents the amplitude of the fluctuation, which depends only on y because the mean flow depends only on y, k is the axial wavenumber and ω is the complex oscillation-amplification factor. We shall be concerned with temporal instabilities, for which the wavenumber will be real while ω is complex.

$$\omega = \omega_r + i\,\omega_i \qquad (4.9)$$

The disturbance will be damped if $\omega_i < 0$ and the laminar flow will be stable, whereas for $\omega_i > 0$ the oscillatory disturbances will grow and the mean flow will be unstable.

The wave velocity is given by the ratio

$$c = {}^{\omega}/_k = c_r + ic_i \qquad (4.10)$$

where c_r denotes the velocity of propagation of the wave in the x-direction (phase velocity) and c_i determines the stability of the mean flow. For $c_i < o$ the disturbances are damped and the mean flow will be stable, and for $c_i > 0$ the flow will be unstable to small disturbances.

From equation (4.8) the perturbation velocity components can be obtained as follows

$$\hat{u} = \frac{\partial \Psi}{\partial y} = \phi'(y) \, e^{i(kx - \omega t)}$$

$$\hat{v} = -\frac{\partial \Psi}{\partial x} = -ik\phi(y) \, e^{i \, (kx - \omega t)}$$

(4.11)

where the prime indicates a derivative with respect to the y coordinate.

Introducing these expressions into the equation of motions and eliminating the pressure term we obtain the familiar Orr-Somerfeld stability equation (Schlichting, 1968).

(4.12)

$$(U-c)(\phi''-k^2\phi) - U''\phi = -\frac{i}{kRe} (\phi''''-2k^2\phi''+k^4\phi)$$

where Re is the Reynolds number and the derivatives are taken with respect to the y coordinate. This ordinary fourth-order differential equation for the amplitude of the disturbance determines the stability of the laminar mean flow.

Inviscid Analysis

Since we expect instabilities to be amplified only at relative large Reynolds number, the viscous term in the right hand side of equation (4.12) can be neglected as compared with the inertial terms on the left-hand side. The resultant second-order differential equation is known as the frictionless stability equation or Rayleigh's equation (1880) and constitutes the point of departure for the inviscid analysis.

$$(U-c)(\phi'' - k^2\phi) - U''\phi = 0 \qquad (4.13)$$

with the amplitude ϕ vanishing at infinity or at a boundary. The omission of the viscous term reduced the order of the differential equation from four to two. This implies that only two boundary conditions of the original four can be satisfied. Equation (4.13) does not contain any information regarding the critical Reynolds number at which the shear layer becomes unstable, but it answers the question of whether a given flow is stable or not and to which disturbance wavenumber the flow will be more sensitive.

We now proceed to study the inviscid stability of disturbances generated at the high shear region separating the high velocity flow entering the test section and the almost stationary flow. Since an analytical solution for equation (4.13) for the general velocity profile is not readily obtainable, (assuming $U(y)$ is a known function) a solution for a steadily curving profile in general has to be determined numerically. Following Rayleigh (1895) we assume that the vorticity of the steady motion is constant throughout any layer, $U''(y) = 0$ and whenever $(U-c)$ does not also vanish the stability equation can be written in the form

$$\phi'' - k^2\phi = 0 \qquad (4.14)$$

with exponential or hyperbolic solutions of the form

$$\phi(y) = A \cosh(ky) + B \sinh(ky)$$

or $\qquad \phi(y) = C\, e^{ky} + D\, e^{-ky}$ $\qquad (4.15)$

where A, and B, or C and D are constants satisfying the
boundary and the interface conditions.

The equation of motion for the amplitude of the
disturbance had been reduced to a simple linear second-
order differential equation with constant coefficients
by approximately the velocity profile by a partially
linear profile, as shown in Figures 4.1a, b. The linear
velocity segments are joined together at the interface
positions d_1 and d_2, where the velocity gradient is
discontinuous. Michalke and Shade (1903) showed a con-
vergence proof that for steadily increasing approxima-
tion the solution for the approach profile converges
toward the solution of the exact profile.

Experimental Velocity Profiles

The experimental velocity distribution for low Reynolds
number flow in a symmetric sudden expansion were measured
by Durst, Melling and Whitelaw (1974) using laser anemom-
eter techniques. The results obtained in rectangular
test section with a diameter ratio of 1/3 at a downstream
Reynolds number of 170 are shown in Figures 4.2a and 4.2b
at different axial positions. The velocity distribution
approached the parabolic distribution at a downstream
position close to 10 times the step height (H) of the
expansion. Also shown in those figures are the approx-
imated velocity profiles using straight line segments

(U''(y) = O).

The experimental observations reported by Durst,
Melling and Whitelaw were applied to the flow in a sudden
expansion, and not to the flow out of a small constricted
region, but we believe they provide a good representation
of the velocity distribution downstream from the constricted
region. It was also observed by Durst that symmetric pro-
files existed from the expansion to a fully developed
parabolic profile far downstream, although there were
substantial 3-dimensional effects in the vicinity of the
separation regions. As the Reynolds number increased
stability problems appeared producing a non-symmetric
velocity distribution. Similar phenomena were observed
in our observations in rectangular test sections using
the Milling Yellow solution.
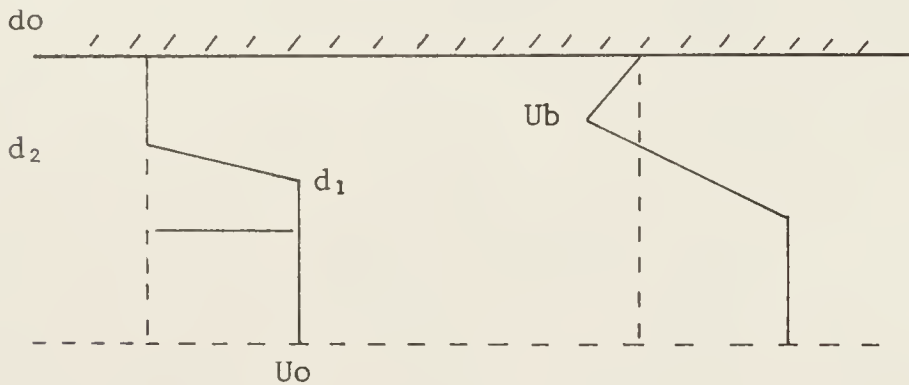
Figure 4.1   Analytical profiles in rectangular
              coordinates

1.0   U/Uo

-- Experimental profile

— Approximated profile

H = Do/3

.8

.6

.4

d_1 = 0.15

d_2 = 0.65

ℓ = 0.15

x/H = 1.5

d_1 = 0.15

d_2 = 0.30

^{x}/H = -0.25

.2

0.4   1.0   y/Do

0

d_1 = 0.12

d_2 = 0.75

ℓ = 0.10

^{x}/H = 2.5

0.6

0.40

d_1 = 0.20

d_2 = 0./5

^{x}/H = 3.5

0.20

0   0.40   1.0   y/Do
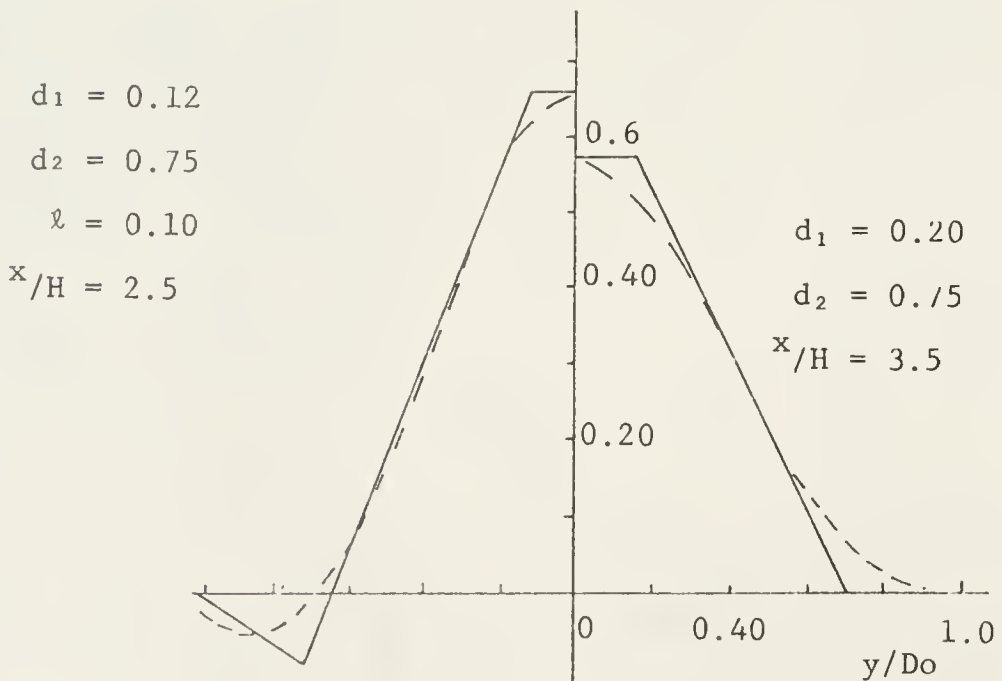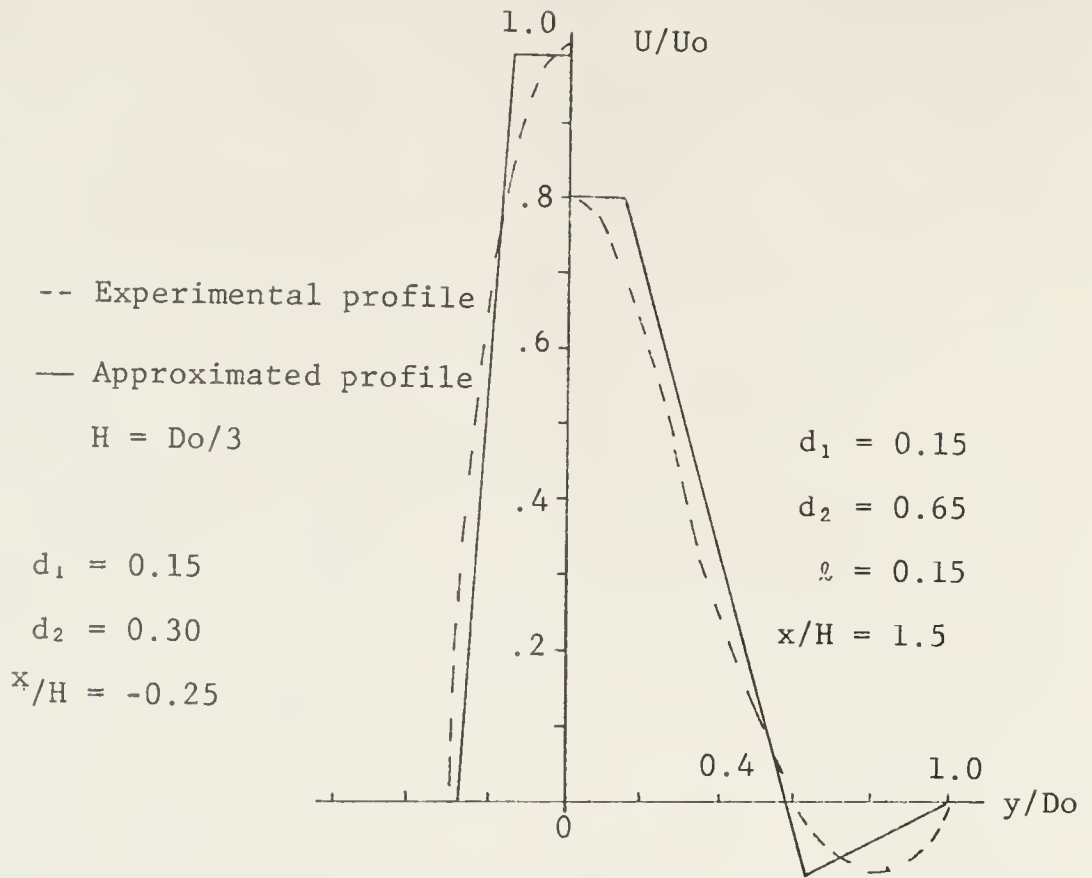
Figure 4.2   Approximated experimental velocity profiles.

Instability Modes of Propagation

The eigenfunctions describing the amplitude of velocity fluctuations could be symmetric or antisymmetric with respect to the centerline, yielding two different modes of jet oscillations. We will call the oscillation mode produced by symmetric disturbances, the symmetric mode of propagation and the corresponding mode originated by antisymmetric disturbances, the anti-symmetric mode of propagation.

Symmetric Disturbances

For the symmetric mode of propagation the boundary conditions on the transverse disturbance are

$$\hat{v} \ (y=\pm do) = 0 \tag{4.16}$$

and $\qquad \hat{v} \ (y=o) = 0 \tag{4.17}$

where do is the position of the wall in the unobstructed section. To simplify the algebra of the problem, we assumed that since the mean flow is symmetric the analysis can be conducted only in the range $0 \overset{<}{=} y \overset{<}{=} do$. The flow region between the centerline and the wall is then separated in three areas, as shown in Figure 4.1a, with straight line segments representing the velocity distribution in each region. The solutions to the stability equation in the different fluid layers satisfying the boundary conditions (4.16) and (4.17) are

$$\phi_1(y) = A_1 \ \sinh(ky) \qquad\qquad \text{for } o \leq y < d_1$$

$$\phi_2(y) = A_2 \ \sinh(ky) + B_2 \ \cosh(ky) \qquad d_1 \leq y < d_2 \quad (4.18)$$

$$\phi_3(y) = A_3 \ \sinh k(do-y) \qquad\qquad d_2 \leq y \leq do$$

then mean flow velocity profile as shown in Figure 4.1a
is given by

$$U(y) = \begin{cases} Uo & \text{for } o \leq y < d_1 \\ Uo \quad \dfrac{d_2 - y}{d_2 - d_1} & d_1 \leq y < d_2 \quad (4.19) \\ 0 & d_2 \leq y \leq do \end{cases}$$

and the velocity gradient given by

$$U'(y) = \begin{cases} 0 & \text{for } o \leq y < d_1 \\ \dfrac{-\ Uo}{d_2 - d_1} & d_1 \leq y < d_2 \quad (4.20) \\ 0 & d_2 \leq y \leq do \end{cases}$$

In the three layers in each of which the vorticity is
constant, the various solutions of the form (4.18) are to be
fitted together, the arbitrary constants are then chosen as
to satisfy the interface conditions. The first of the inter-
face conditions is that the normal component of the perturba-
tion displacement must be continuous across the fluid inter-
face (Chandrasekhar, 1961). For a continuous velocity
profile this corresponds to the continuity of $\hat{v}$ across an
interface or that the function ϕ is continuous. This
yields the perturbation displacement or kinematic inter-
facial condition

$$\Delta\phi = 0 \qquad\qquad\qquad (4.21)$$

where the symbol Δ means the difference in the function ϕ
evaluated across an interface of infinitesimal thickness ξ.

The second interface condition may be obtained by inte-
trating equation (4.13) across the boundary between $y=dj-\xi$
to $y=dj+\xi$. After performing the integration and making
use of the first condition and the continuity of the
velocity profile, we obtain the pressure condition as
obtained by Rayleigh (1887), and also Michalde and Schade
(1963).

$$(U-c).\Delta\phi' - \Delta U'.\phi = 0 \tag{4.22}$$

Applying the two conditions (4.21) and (4.22) at the in-
terface position, $y=d_1$, we obtain

$$\phi_1(d_1) = \phi_2(d_1) \tag{4.23}$$

and

$$(Uo-c)\ \phi_1'(d_1) = (Uo-c)\phi_2'(d_1) - U'\phi_2(d_1) \tag{4.24}$$

and the position $y = d_2$

$$\phi_2(d_2) = \phi_3(d_2) \tag{4.25a}$$

$$-c\phi_2'(d_2)-U'\phi_2(d_2) = c\phi_3'(d_2) \tag{4.25b}$$

substituting (4.18) to (4.20) into (4.23) to (4.25b) leads
to a secular relation. For a nontrivial solution to exists
the determinant must be qual to zero.

$$\begin{vmatrix} -\tanh kd_1 & \tan kd_1 & 1 & 0 \\ -1 & 1+L\tanh kd_1 & L+\tanh(kd_1) & 0 \\ 0 & -\sinh kd_2 & -\cosh kd_2 & \sinh k(do-d_2) \\ 0 & \cosh kd_2-M\sinh kd_2 & \sinh kd_2-M\cosh kd_2 & \cosh k(do-d_2) \end{vmatrix} = 0 \tag{4.26}$$

where $L = \dfrac{Uo}{k(d_2-d_1)(Uo-c)}$ and $M = \dfrac{Uo}{ck(d_2-d_1)}$ (4.27)

Solving the determinant described by (4.26) we obtain a
quadratic equation in the non-dimensional complex eigen-
wave velocity

$$\bar{c} = \frac{c}{U_0} \tag{4.28}$$

of the form $\bar{c}^2 + B\bar{c} + C = 0$ (4.29)

where the coefficients are only functions of the disturb-
ance wavenumber and the geometry of the problem

$$B = \left[\frac{1}{k\,(d_2-d_1)}\right]\left[\frac{1}{2}(\sinh 2dk_1 - \sinh 2kd_2) + \coth kd_0 \right.$$
and
$$\left. (\sinh kd_2{}^2 - \sinh{}^2 kd_1)\right] - 1 \tag{4.30}$$

$$C = \left[\frac{1}{k\,(d_2-d_1)}\right]^2 \frac{\sinh k(d_0-d_2)}{\sinh kd_0}\left[\sinh kd_2\,(k(d_2-d_1) - \frac{1}{2}\sinh{}_2 kd_1) + \right.$$
$$\left. \sinh kd_1 \cosh kd_2\right]$$

The solution to the quadratic equation (4.29) is given by

$$\bar{c} = \frac{-B}{2} \pm \frac{1}{2}\sqrt{B^2 - 4C} \tag{4.31}$$

Instabilities will be expected to grow whenever the quan-
tity inside the radical in (4.31) is negative ($B^2 < 4C$).   In
those cases equation (4.29) will have complex roots and
the perturbation will develop in time according to

$$\Psi(x,y,t) = \phi(y)\,e^{\omega_i t}\,e^{i(kx-\omega_r t)}$$

with a growth rate given by $e^{\omega_i t}$, where $\omega_i = k\,c_i$.   If the
roots of equation (4.29) are real the oscillation will
maintain its sinusoidal motion with zero growth rate and
the fluid motion will be stable.   Since the equations are
invariant under complex conjugation, any non-zero value of

ωi will produce instabilities, with the amplitude of the disturbance increasing with time.

The wave speed and the amplification factor for a growing disturbance are given by

$$\bar{c}_r = \frac{c_r}{Uo} = \frac{-B}{2} \quad , \quad \bar{c}_i = \frac{c_i}{Uo} = 1/2\sqrt{4C-B^2} \qquad (4.32)$$

and they are shown in Figures 4.3 and 4.7 for different interface positions, holding the first interface position at 0.30do. The dimensionless parameter $\delta = d_1/(d_2-d_1)$ is an indication of the sharpness of the transition region between the mean flow Uo and the stationary flow, and consequently a measure of the shear between the two layers at a specified position d_1. A large δ will then indicate a sharper transition region of high shear. This is representative of the velocity distribution measured near the jet orifice. We will expect these profiles to be highly unstable since they produce very high shear layers, where disturbances can be generated with large growth rates. The spreading of the jet profile is approximated by increasing the relative interface distance (d_2-d_1). A decrease in the dimensionless factor δ thus indicate the type of velocity distributions normally found further away from the orifice. These profiles will eventually approach the parabolic velocity distributions. We will expect velocity profiles characterized by a small δ to

be less unstable to small periodic pertubations, with
smaller growth rates, as indicated by Figure 4.4 where
the instability amplification or growth rate $\sigma = e^{\omega_i t}$ had
been defined following Michalde and Schade (1963) using
(4.10), and defining the unit of time as the ratio of
the larger thickness d to the perturbation phase velocity.
In this case the growth rate is

$$\sigma = kd \left({c_i} / {c_r} \right) \tag{4.33}$$

as observed by an observer travelling with the wave phase
velocity.

The growth rates as defined by expression (4.33) are
shown in Figure 4.4 for symmetrical disturbances, main-
taining the first interface position at $d_1 = 0.30$ and the
wall position at $d_0 = 1.0$. Numerical calculations were
carried out using the standard scientific subroutines in
the IBM-360 digital computer at the University of Florida.
The symmetrical velocity profiles were stable under
symmetric disturbances of wavenumber kd larger than approx-
imate 1.29. For sharp transition profiles (large δ's) the
maximum growth rate approached the magnitude of 0.4 at a
non-dimensional wavenumber of approximate 0.8.

A decrease in the interface parameter δ produced a
considerable stabilizing effect on the stability of
symmetrical disturbances. The wave phase velocity for
different profiles is shown in Figure 4.7, where they
are compared with the results obtained for antisymmetrical

perturbations. At large wavenumbers (kd) the wave phase velocity approached half of the mean flow velocity, whereas those at low wavenumbers corresponding to slow variations of the perturbation travelled above that speed.

Antisymmetric Disturbances

The case of $\phi(y)$ an even function corresponds to the antisymmetrical mode of propagation. This mode of propagation is of physical interest, since it is found to occur frequently during an experiment. The eigenfunction in the first region is then

$$\phi_1(y) = A_1 \cosh ky \qquad \text{for } o \leq y < d_1 \qquad (4.34)$$

satisfying the boundary condition

$$\hat{u}(y=o) = 0 \qquad (4.35)$$

Proceeding as in the case of symmetric disturbances we derived a similar determinant whose solution yielded a quadratic equation in the complex velocity similar to equation (4.29) with the coefficients B and C given for this case by the following expressions

$$B = \left[\frac{1}{(k(d_2-d_1))}\right]\left[\tanh kdo \ (\cosh^2 kd_1 - \cosh^2 kd_2) + \frac{1}{2}(\sinh_2 kd_2 - \sinh_2 kd_1)\right] - 1 \quad (4.36)$$

$$C = \left[\frac{1}{k(d_2-d_1)}\right]^2\left[\frac{\sin k(do-d_2)}{\cosh kdo} \ (\cosh kd_2 \ k(d_2-d_1) + \frac{1}{2}\sinh 2kd_1 - \sinh kd_2 \ \cosh^2 kd_1)\right] \quad (4.38)$$
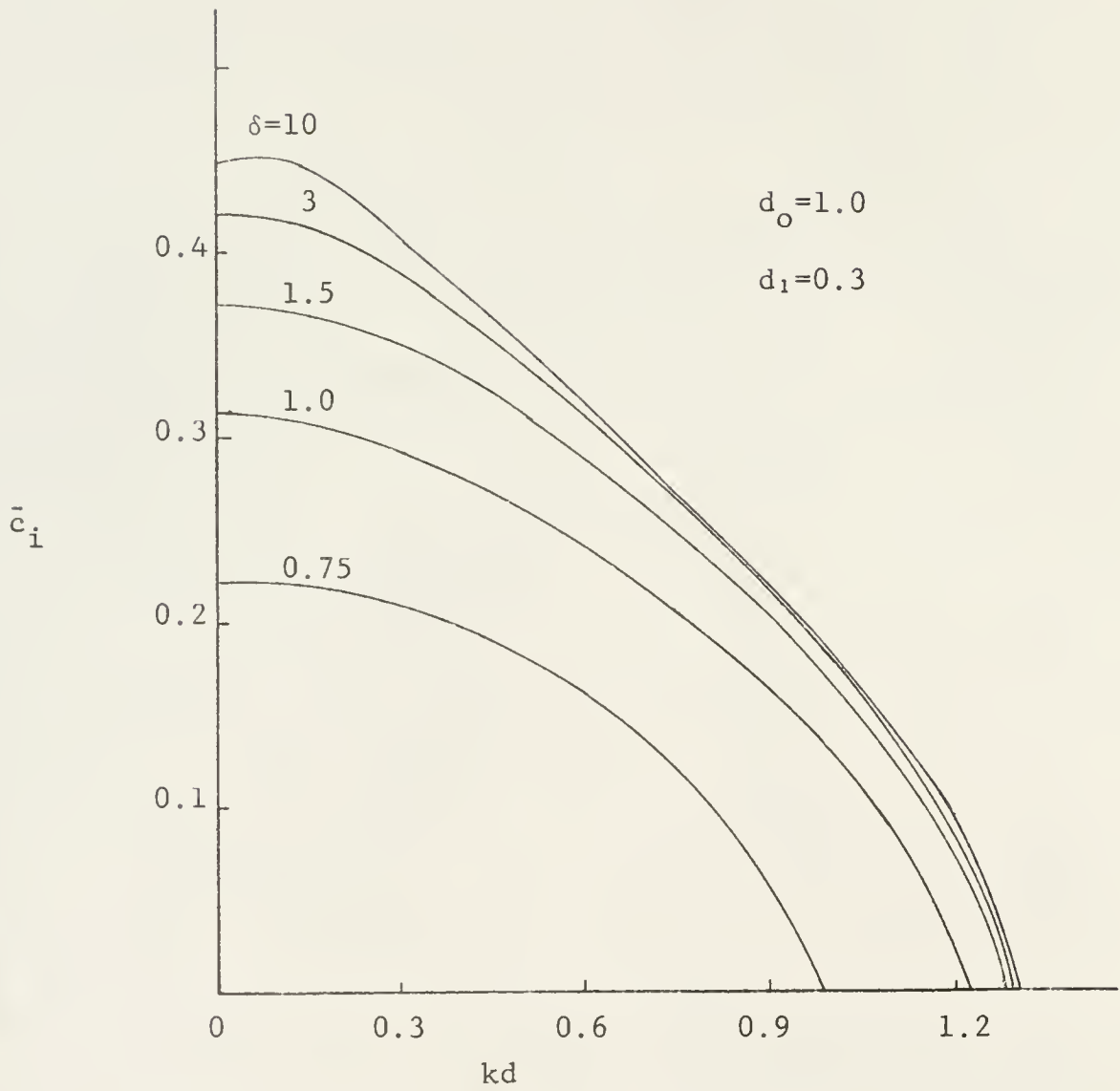
Figure 4.3 Growth factor curves for symmetrical
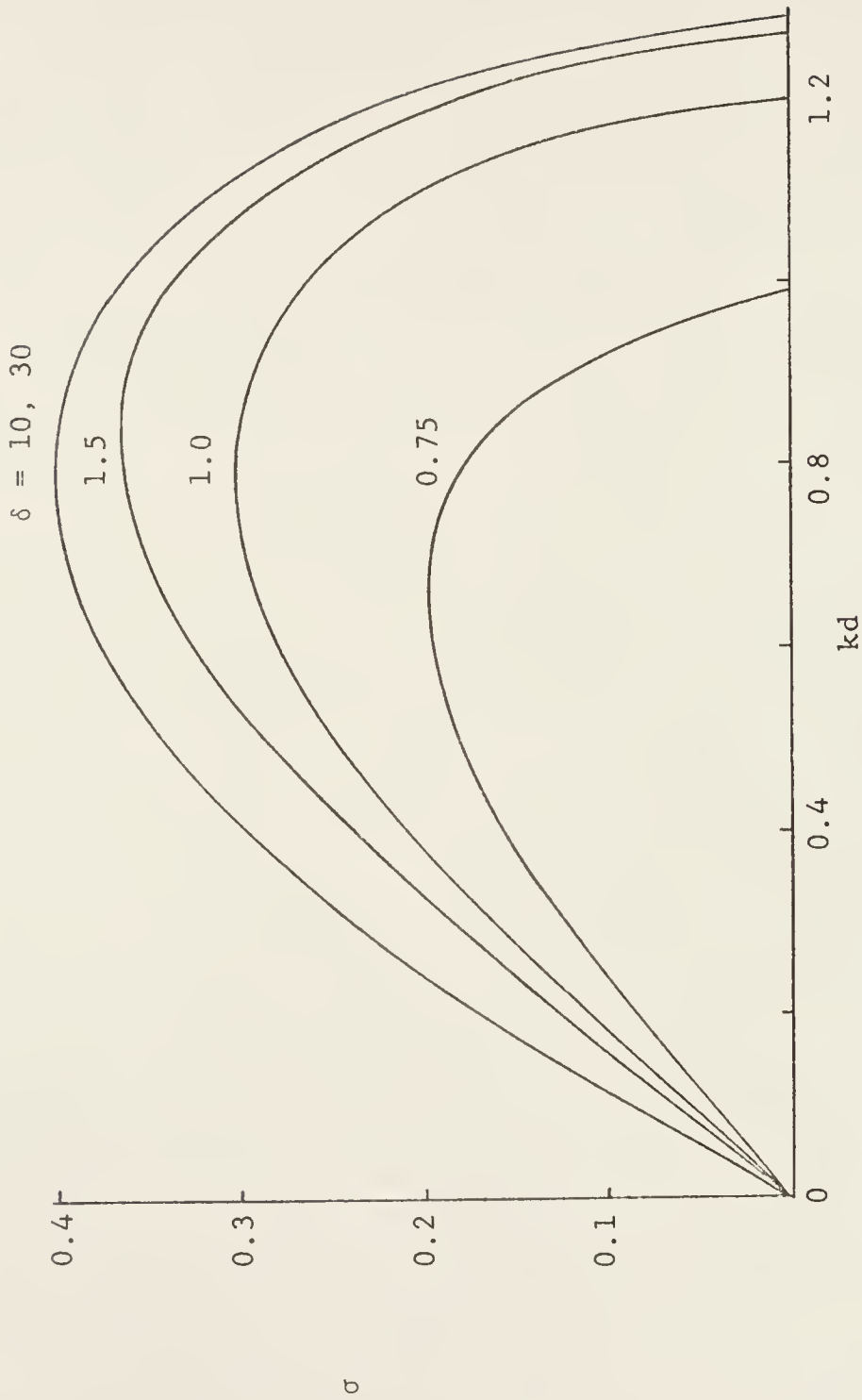disturbances

Figure 4.4   Growth rate curves for symmetrical disturbances

As described previously in the symmetric case, instabil-
ities will grow if the roots of the quadratic equation
are complex ($B^2 < 4C$). The wave phase velocity, growth
factor and growth rate as defined in expressions (4.32)
and (4.33) are shown in Figures 4.5, 4.6 and 4.7, for
different values of the parameter δ. The location of d_1
and do was maintained at 0.30 and 1.0 respectively, as
in the case of symmetrical disturbances.

In the case of non-symmetrical disturbances a decrease
in the dimensionless parameter S produces a destabilizing
effect on the flow characteristics. The smallest δ com-
puted was 0.50, producing a maximum growth rate of ap-
proximate 0.6 at small wavenumbers within the instability
range $o < kd < 0.78$. For large δ's the non-symmetrical per-
turbations growth rate approached that ones correspond-
ing to symmetrical disturbances at large δ's. This can
be observed by comparing Figures 4.4 and 4.6. Another
noticeable characteristic is a non-vanishing growth rate
at low wavenumbers. As the wavenumber increases inside
the instability range, the disturbances travel at about
half the mean flow velocity as in the case of symmetrical
disturbances. The phase velocity decreases toward zero
as the dimensionless disturbance wavenumber decreases,
indicating a slow propagation velocity for long wave-
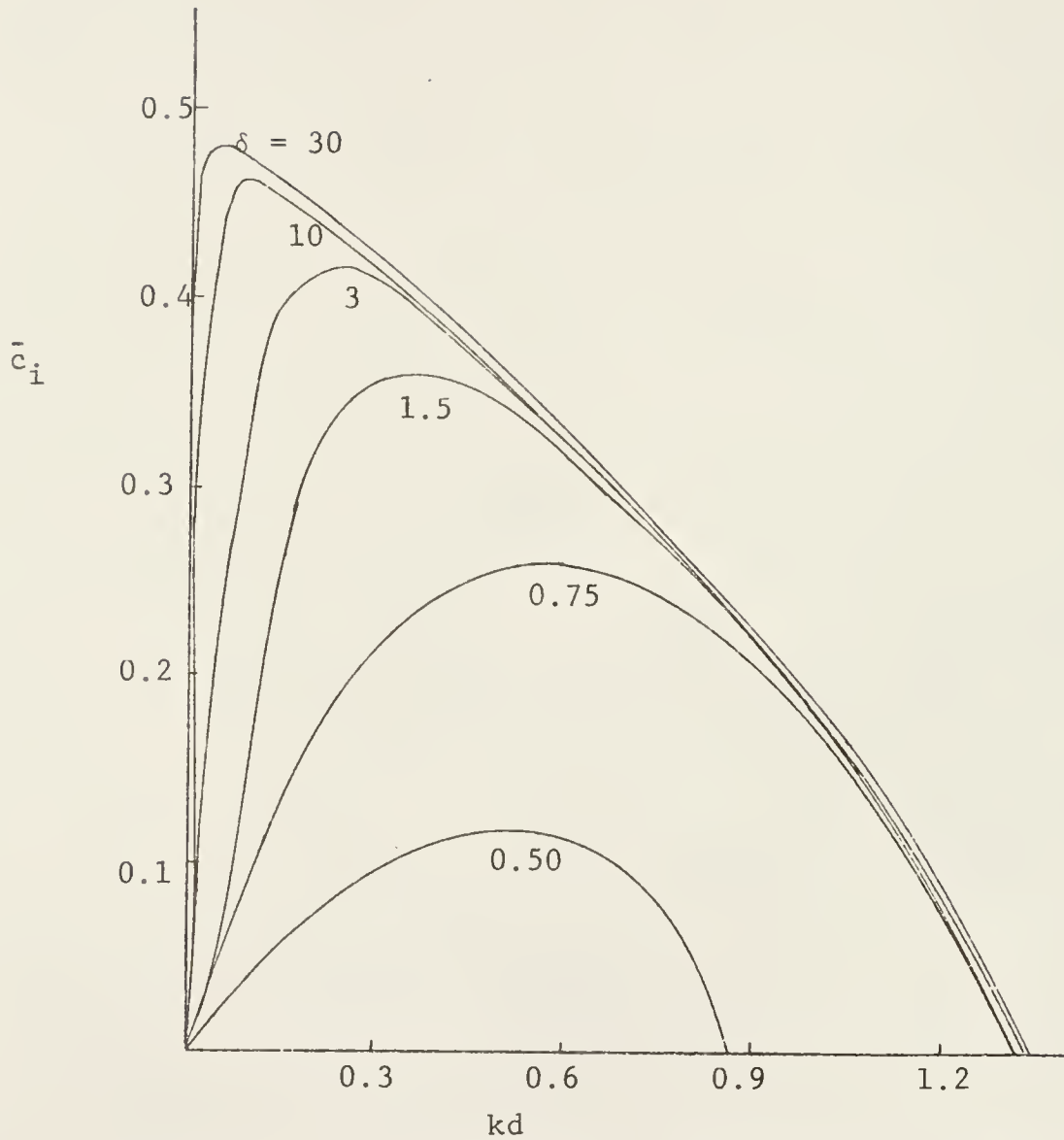length disturbances.

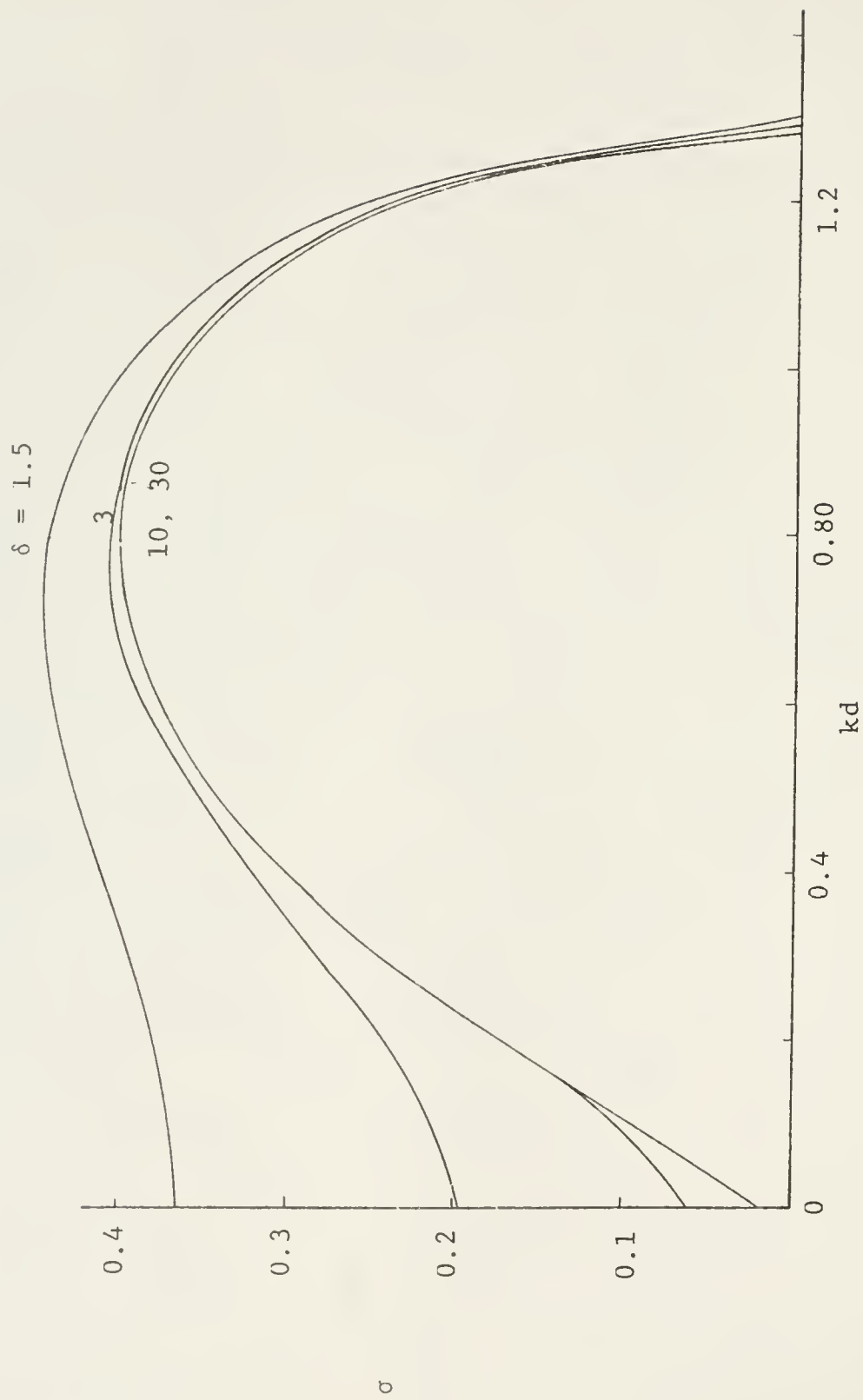Figure 4.5   Growth factor curves for antisymmetrical
disturbances

Figure 4.6   Growth rate curves for antisymmetrical disturbances
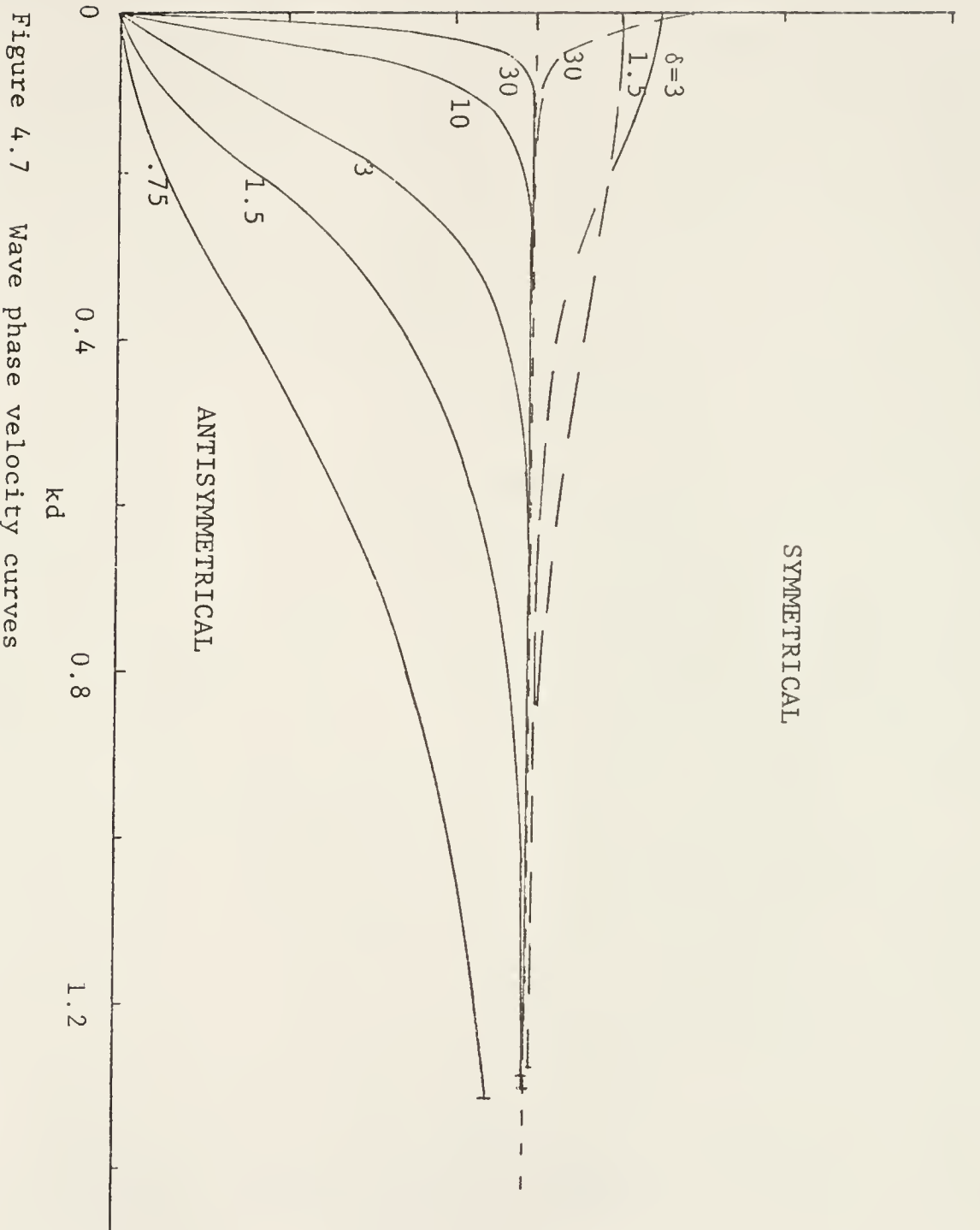
Figure 4.7 Wave phase velocity curves

125

Antisymmetric Disturbances in the Presence of a Back-Flow Region

As the jet profile develops a back-flow region is formed between the main flow and the bounding walls. To investigate the effects of this phenomenon on the inviscid stability of jets, let us assume again that the velocity profiles can be approximated by straight line segments that extend into the back-flow region, as indicated in Figure 4.16. According to Durts et al., 1974, experimental measurements using laser anemometer techniques, the magnitude of the back-flow velocity is relative small compared with the mean flow centerline velocity. By looking at these experimental profiles shown in Figures 4.2a and 4.2b, the back-flow velocity is approximate 15% or less of the centerline velocity. This condition can be expressed as

$o < U_b < 0.15 U_o$

where U_b represents the magnitude of the maximum back-flow velocity.

The mean flow distribution in this case is given by the partially linear profile

$$U(y) = \begin{cases} U_o & \text{for } o \le y < d_1 \\ U_o - \left[\dfrac{y-d_1}{d_2-d_1}\right] (U_o + U_b) & d_1 \le y < d_2 \\ U_b\left[\dfrac{y-d_2}{d_o-d_2} - 1\right] & d_2 \le y \le d_o \end{cases} \qquad (4.38)$$

with a discontinuous velocity gradient given by

$$U'(y) = \begin{cases} 0 & \text{for } o \le y < d_1 \\ -\dfrac{Uo+Ub}{d_2-d_1} & d_1 \le y < d \\ \dfrac{Ub}{do-d_2} & d_2 \le y \le do \end{cases} \qquad (4.39)$$

Assuming antisymmetric disturbances superimposed on a mean symmetrical flow the solutions to the inviscid stability equation satisfying the boundary conditions are as before

$$\phi_1(y) = A_1 \cosh ky \qquad \text{for } o \le y < d_1$$
$$\phi_2(y) = A_2 \sinh ky + B_2 \cosh ky \qquad d_1 \le y < d_2 \qquad (4.40)$$
$$\phi_3(y) = A_3 \sinh k(do-y) \qquad d_2 \le y \le do$$

Applying the displacement and the pressure interface conditions we obtain the determinant

$$(4.41)$$

$$\begin{vmatrix} -1 & \tanh kd_1 & 1 & 0 \\ -\tanh kd_1 & 1+N\tanh kd_1 & \tanh kd_1+N & 0 \\ 0 & -\sinh kd_2 & -\cosh kd_2 & \sinh k(do-d_2) \\ 0 & \cosh kd_2-T\sinh kd_2 & \sinh kd_2-T\cosh kd_2 & \cosh k(do-d_2) \\ & & & -P\sinh k(do-d_2) \end{vmatrix} = 0$$

where:

$$N = \frac{Uo+Ub}{k(d_2-d_1)(Uo-c)}, \quad P = \frac{Ub}{(Ub+c)\,k(do-d_2)} \quad \text{and}$$

$$T = \frac{Uo+Ub}{k(d_2-d_1)(Ub+c)} \qquad (4.42)$$

The solution to this determinant leads to a quadratic equation in the non-dimensional complex velocity $\bar{c} = c/Uo$, of the form.

$$\bar{c}^2 + B\bar{c} + C = 0 \qquad (4.43)$$

This equation is similar to (4.29), where $\bar{c} = \dfrac{c_r}{U_o} + i \dfrac{c_i}{U_o}$.

Defining a factor ℓ such that $Ub = \ell Uo$, where $o \le \ell \le 0.15$,

the coefficients of the quadratic equation can be sim-

plified to

$$
B = \left[\frac{1 + \ell}{k(d_2 - d_1)}\right]\left[\tanh kdo(\cosh^2 dk_1 - \cosh^2 kd_2) + 1/2 \atop (\sinh_2 kd_2 - \sinh kd_1)\right]
$$

$$
+ \ell\left[1 - \frac{\sinh k(do - d_2)\ \cosh kd_2}{k(do - d_2)\ \cosh kdo}\right] - 1
$$

$$(4.44)$$

and

$$
C = \frac{\sinh k(do - d_2)}{k^2(d_2 - d_1)^2\ \cosh kdo}\left[\cosh dk_2\left[k(d_2 - d_1)(1 + \ell) + \frac{(1 + \ell)^2}{2}\ \sinh_2 kd_1\right]\right.
$$

$$
\left. - (1 + \ell)^2\ \sinh kd_2\ \cosh^2 kd_1\right]
$$

$$
+ \ell\left[\frac{(1 + \ell)\ \cosh kd_1}{k^2(do - d_2)(d_2 - d_1)\cosh kdo}\ k(do - d_2)\ \sinh k(do - d_1) - \right.
$$

$$
\sinh k(do - d_2)\sinh k(d_2 - d_1)
$$

$$
\left. + \frac{\sinh k(do - d_2)\cosh kd_2}{k(do - d_2)\ \cosh kdo} - 1\right]
$$

$$(4.45)$$

Notice that for the case of no back-flow region ($\ell = o$)

expression (4.44) and (4.45) reduce to expression (4.36)

and (4.37) respectively for non-symmetric disturbances.

We now procede to investigate the effects on stability

produced by the presence of a back-flow velocity in the

jet mean velocity profile.

The real and the imaginary part of the complex roots of equation (4.43) are described in Figure 4.8 where they are compared with the results obtained for a similar velocity profile without a back-flow region (Profile I). The dimensionless parameter δ is the same for both cases but Profile II includes a back-flow of magnitude $\ell = 0.15$.

The wave phase velocity is less for Profile II giving small negative values of phase velocity at small wavenumbers. The growth factor is larger for the velocity profile with the back-flow velocity, but the differences are relative small; both cases reaching maximum growth at about the same wavenumber. In a real situation the magnitude of the centerline velocity for Profile II should be less than Uo and the corresponding growth factor smaller than the one described in Figure 4.8. Decreasing the magnitude of the back-flow velocity decreased the magnitude of the growth factor by a small amount if the same interface distance was maintained. Changing the interface distance while maintaining a constant back-flow velocity produced significant changes in stability. These results indicate that the presence of a back-flow produces secondary effects on stability, with the size of the interface distance d playing the dominant role.

In Figure 4.9 we show the growth factor calculated

for antisymmetric perturbations on the approximated
velocity profiles for a jet in a confined region, as
measured by Durst et al. (1974). The location of the
interface was adjusted to simulate the experimental
observations described in Figure 4.2 The decrease in
the centerline velocity as the jet velocity distribu-
tion spreads to the walls was taken into account in the
growth factor computations.

The Streamlines of the Perturbation

The stream function representing a single oscillation
of the disturbance is represented by the real part of

$$\psi(x,y,t) = \phi(y) \, e^{i(kx-\omega t)} \tag{4.46}$$

in the two-dimensional rectanglar geometry, where as ex-
plained in previous sections $\phi(y)$ represents the amplitude
of the oscillation. For the case of symmetrical perturba-
tions upon the mean flow, the amplitude of the oscillation
is described by the functions of equation (4.18), satisfy-
ing the boundary conditions (4.16) and (4.17) and the
interface conditions (4.21) and (4.22). To obtain the
streamlines of the perturbation flow alone we applied
these conditions, to solve for the constants A's and B
after choosing the disturbance wavenumber close to the
point of maximum growth rate and the geometry of the test
section as, $do=1.0$, $d_1=0.20$ and $d_2=0.30$. Substituting
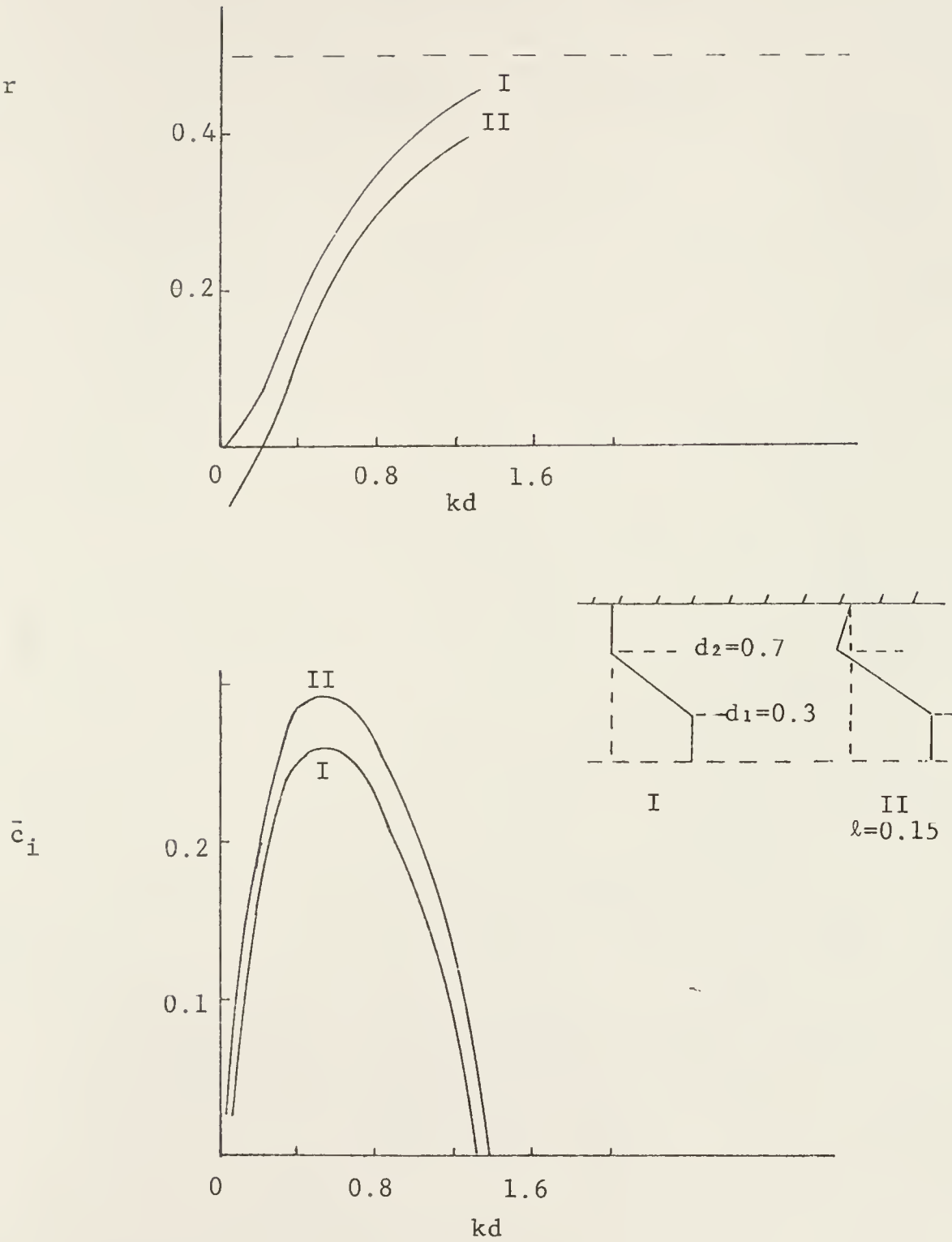
Figure 4.8   Stability of profiles with a back-flow region

$U/Uo=1$

(I) $d_1=0.15$
$d_2=0.30$

0.8

(II) $d_1=0.15$
$d_2=0.65$

0.57 0.46

(III) $d_1=0.20$
$d_2=0./5$

(IV) $d_1=0.20$
$d_2=0.95$

0.4

0.2

$\bar{c}_i$

I

II

III

IV

0 0.40 1.2
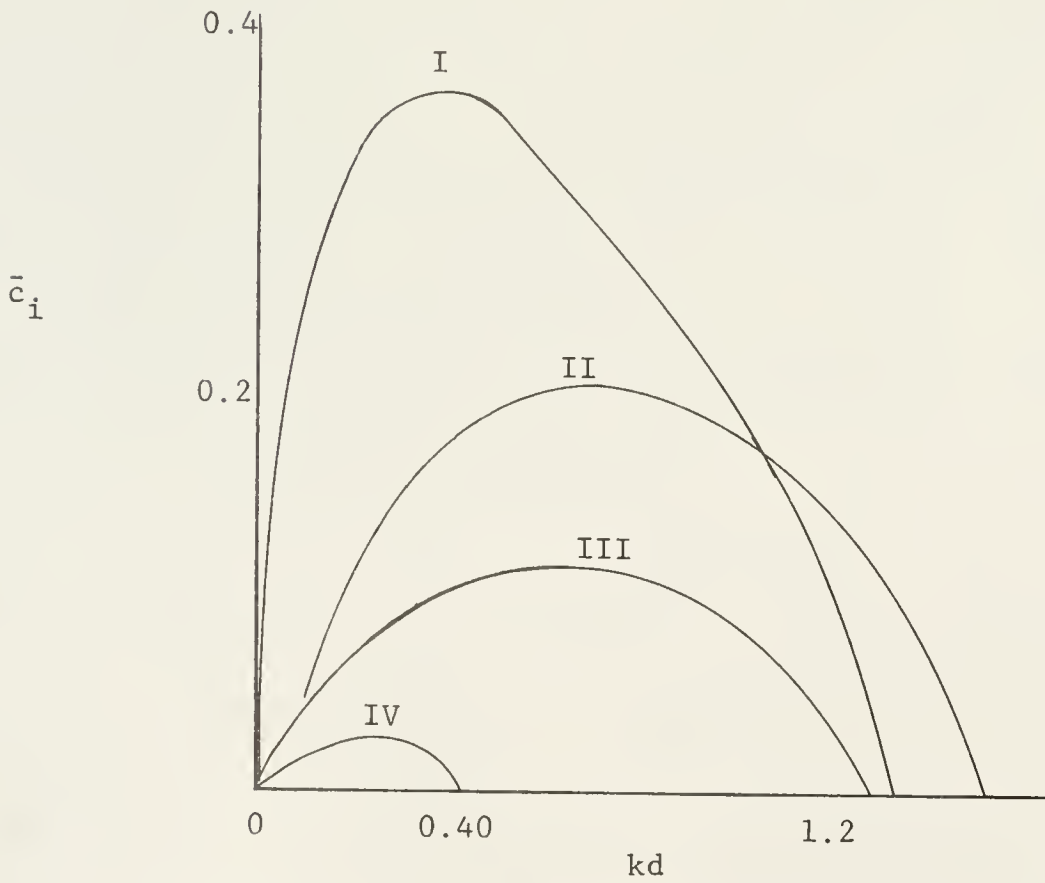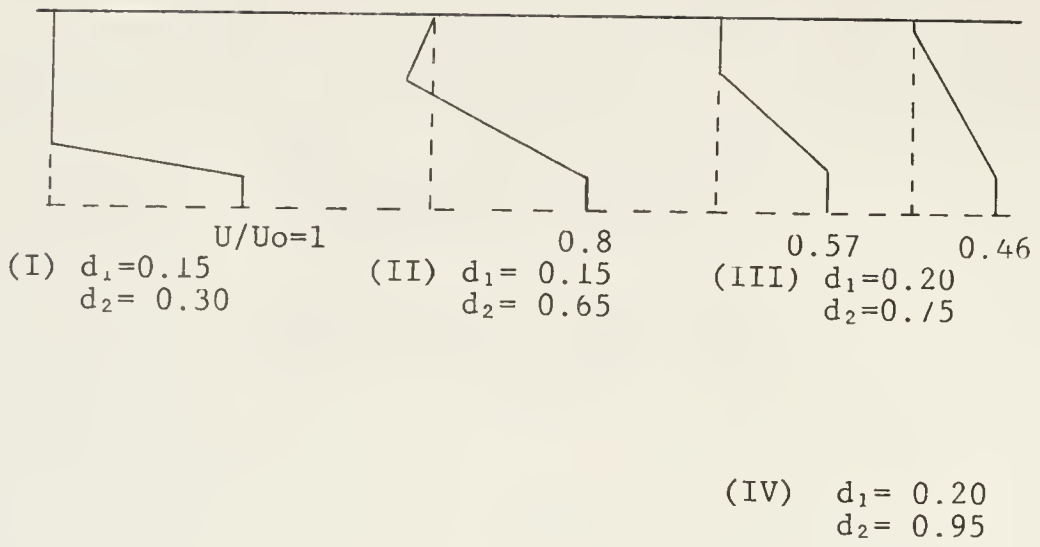
kd

Figure 4.9   Relative stability of velocity profiles
at different axial positions

the geometry parameters simplifies the algebra, which
yielded for the normalized stream function in each flow
region the following functions.

$$\Psi_{1_N}(x,y,t) = a\, e^{bkx}\, \sinh ky\, \cos(kx + \phi_1) \quad \text{for } 0 \leq ky < 1.60 \tag{4.47a}$$

$$\Psi_{2_N}(x,y,t) = e^{bkx}\, \left[f(y)\right]^{\frac{1}{2}} \cos(kx + \phi_2) \qquad 1.60 \leq ky < 2.4 \tag{4.47b}$$

$$\Psi_{3_N}(x,y,t) = d\, e^{bkx}\, \sinh k(1-y)\, \cos(kx + \phi_3) \quad 2.4 < ky < 8.0 \tag{4.47c}$$

where $a=0.077$, $b=0.471$, $d=1.371 \times 10^{-3}$, $k=8L^{-1}$

and $f(y) = \cosh^2 ky - 2.03 \cosh ky \sinh ky - 1.03 \sinh^2 ky$

and the phase angles are given by

$$\phi_1 = -0.4528 \text{ rad.}$$

$$\phi_2(y) = -\tan^{-1}\frac{0.0339}{\coth ky - 1.015} \text{ rad.}$$

$$\phi_3 = -1.532 \text{ rad.}$$

Plotting the coordinates of some of the points satisfying
the relation $\Psi(x,y,t) = $ constant, we obtain the streamlines
of the superimposed fluctuation on the jet mean flow, given
the vortex type pattern described in Figure 4.10 for the
case $\Psi = \pm 0.20$, as observed by an observer travelling with
the wave phase velocity. The functions described by equa-

tions (4.47a) are continuous at the interface boundaries where the inclinations of the perturbation streamline is produced by the complex nature of the amplitude function. The first and third layer shows constant phase angle through the layer, while in the intermediate transitional layer the phase angle is a function of the transverse coordinate y, matching at the interface boundaries with the phase angle of the inner and the outer layer.

Mathematical Formulation in Cylindrical Coordinates

In this section we wish to examine the stability of the axisymmetric jet formed downstream of a round orifice in the presence of rigid cylindrical boundaries. The fluid under consideration is again assumed to be inviscid, homogenous and incompressible. Neglecting the viscous forces in equation (4.2) we obtain Euler's equation of motion

$$\frac{\partial \vec{q}}{\partial t} + \vec{q} \cdot \vec{\nabla} \vec{q} = \frac{1}{\rho} \vec{\nabla} p \tag{4.48}$$

and the continuity equation

$$\vec{\nabla} \cdot \vec{q} = 0 \tag{4.49}$$

as the starting point for the analysis in the cylindrical coordinates (r, θ, z) with mean flow velocity components $(o, o, W(r))$ and the pressure p. To study the stability of

Figure 4.10   The streamlines of the perturbations

this system we postulate a set of solutions composed of the steady-state flow with a superimposed infinitesimal time-dependent fluctuation, namely

$$Vr = \hat{u} \ (r,\theta,z,t)$$
$$V\theta = \hat{v} \ (r,\theta,z,t)$$
$$Vz = W(r) + \hat{w}(r,\theta,z,t)$$
$$p = P(r) + \hat{p}(r,\theta,z,t)$$

(4.50)

where $\hat{u}$, $\hat{v}$ and $\hat{w}$ are the velocity fluctuation components and $\hat{p}$ the pressure fluctuation. The mean flow is again assumed to be almost parallel and only a function of the radial position at a given axial position.

Substituting the set of relations (4.50) into the equation of motion and the equation of continuity, following the linearization procedure of neglecting products of fluctuation components, we obtain after eliminating $\hat{v}$ and $\hat{w}$ out of the resultant set of differential equations, the following partial differential equations describing the stability of the system (see Fung, 1974).

$$\frac{1}{r^2} \frac{\partial^2 \hat{p}}{\partial \theta^2} + \frac{\partial^2 \hat{p}}{\partial z^2} - \rho \ d_* \ (\overset{*}{D}\hat{u}) - DW \frac{\partial \hat{u}}{\partial z} = 0 \qquad (4.51a)$$

and $\quad d_* \ (\frac{\partial \hat{p}}{\partial r}) + \rho d_*^{\ 2} \ \hat{u} = 0 \qquad (4.51b)$

where the operators are given by

$$d_* = \frac{\partial}{\partial t} + W \frac{\partial}{\partial z}$$

$$D = \frac{d}{dr}$$

$$D* = D + \frac{1}{r}$$

Following Fung and Kurzweg (1975) we assume that the perturbation components $\hat{u}$ and $\hat{p}$ are of the exponential form

$$\{\hat{p},\hat{u}\} = \{p(r), u(r)\}\, e^{i(kz + m\theta - \omega t)} \tag{4.52}$$

where $p(r)$ and $u(r)$ represent the pressure and the amplitude of the disturbance, k the axial wavenumber, m the azimuthal wavenumber and ω the complex amplification factor as described before, $\omega = \omega_r + i\omega_i$.

Due to the periodicity of the solution in the θ direction the azimuthal wavenumber m takes only integer values.

Substituting equation (4.52) into (4.51) we obtain, after eliminating the pressure amplitude p, the single second order ordinary differential equation (see Batchelor and Gill, 1962).

$$\tag{4.53}$$

$$\left[\frac{r}{m^2 + (kr)^2} \, (ru(r))' \right]' = \left[1 + \left(\frac{r}{W-c} \right) \left(\frac{rW'}{m^2 + (kr)^2} \right)' \right] u(r)$$

Where we make use of the relation $c = \omega/k$ to define the complex wave speed, and the prime indicates a total derivative with respect to the radial coordinate r.

The stability equation described by (4.53) together with the specified boundary conditions of the problem determine an eigenvalue problem for the complex wave speed c for specified values of k, m and W. As explained previously the system is unstable whenever $c_i \neq o$, and neutrally stable when $c_i = o$.

Axisymmetric Disturbances

In the case of axisymmetric perturbations (m=o) on an axisymmetric mean flow the radial perturbation component is of the form

$$\hat{u} = u(r) \ e^{i(kz-\omega t)} \tag{4.54}$$

The stability equation simplifies to the form

$$\left[\frac{r}{(kr)^2} \ (ru(r))' \right]' = \left[1 + \frac{r}{W-c} \ \left(\frac{rW'}{(kr)^2} \right)' \right] u(r) \tag{4.55}$$

To find a solution to (4.55), we expand the equation by taking the derivatives. Finally we obtain for the equation describing the amplitude of the disturbance

$$u''(r) + \frac{u'(r)}{r} - (\frac{1}{r^2} + k^2) \ u(r) = \left[W'' - \frac{W'}{r} \right] \frac{u(r)}{W-c} \tag{4.56}$$

This equation can be further reduced to a Modified Bessel's equation in the special case that the velocity distribution describing the mean flow satisfies the relation.

$$W'' - \frac{W'}{r} \equiv 0 \tag{4.57}$$

Under this condition the stability equation reduces to

$$r^2 u''(r) + ru'(r) - (1 + (kr)^2)u(r) = 0 \quad (4.58)$$

with solutions of the form

$$u(r) = AI_1 (kr) + B K_1 (kr) \quad (4.59)$$

Where I_1 (kr) and K_1 (kr) are the hyperbolic Bessel's functions of order one and of the first and second kind, and A and B are constants. According to Betchov and Criminale (1967) equation (4.57), which can be rewritten as $(\frac{W'}{r})' = 0$, represents the production of vorticity in the cylindrical geometry, taking the place of the usual term W'' as found in two-dimensional flows in rectangular coordinates. The vanishing of this term is a necessary condition for instability in axisymmetric disturbances in the inviscid limit.

The velocity profiles given by the solution to equation (4.57) are of the parabolic type

$$W(r) = ar^2 + b \quad (4.60)$$

and they can be used to approximate the development of a pipe jet with a flat entering velocity profile. Velocity distributions that develop downstream from the jet orifice are represented by a constant velocity segment close to the tube centerline, followed by a parabolic section matching the high velocity region with the almost stationary

flow as shown in Figure (4.11). Also shown in the same figure for comparison purposes is the experimentally determined profile by Iribarne et al. (1972), at an upstream Reynolds number of 389 in a cylindrical section of diameter ratio of 1/2.

For the case of two interface positions located at a radial distance of R_1 and R_2 with respect to the centerline, in a test section of radius Ro and neglecting the back-flow region the velocity distribution is described by

$$W(r) = \begin{cases} Wo & \text{for } o \leq r < R_1 \\ Wo \ \dfrac{R_2^2 - r^2}{R_2^2 - R_1^2} & R_1 \leq r < R_2 \\ 0 & R_2 \leq r \leq Ro \end{cases} \qquad (4.61)$$

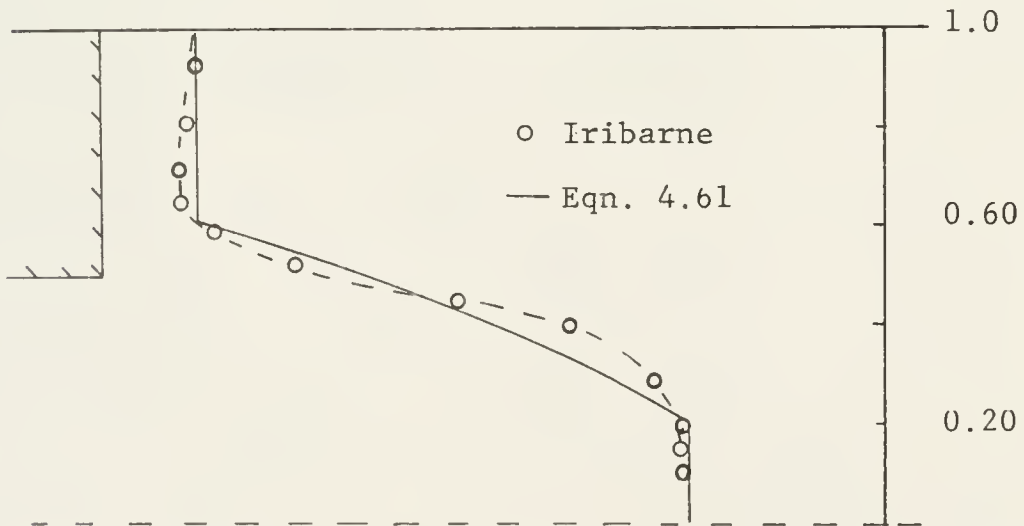as shown in Figure 4.11. The velocity gradient in the

Figure 4.11 Velocity profiles in cylindrical coordinates

radial direction is given by

$$W'(r) = \begin{cases} 0 & \text{for } 0 \le r < R_1 \\ \dfrac{-2W_0 r}{R_2{}^2 - R_1{}^2} & R_1 \le r < R_2 \\ 0 & R_2 \le r < R_0 \end{cases} \qquad (4.62)$$

The boundary conditions on the eigenfunctions of the stability equation are the vanishing of the perturbation amplitude at the walls and the finiteness of the amplitude at the centerline. Under these conditions the perturbation amplitude in each region is described by

$$u_1(r) = A_1 \, I_1(kr) \qquad \qquad \text{for } 0 \le r < R_1$$

$$u_2(r) = A_2 \, I_1(kr) + B_2 K_1(kr) \qquad R_1 \le r < R_2$$

$$u_3(r) = A_3 \left[I_1(kr) - \frac{I_1(kR_0)}{K_1(kR_0)} K_1(kr) \right] \qquad R_2 \le r \le R_0 \qquad (4.63)$$

Following Michalke and Schade (1963) we apply the interfacial conditions that the perturbation displacement and pressure are continuous at the two interface locations R_1 and R_2.

$$u(r) \text{ is continuous at } r = R_1 \text{ and } R_2 \qquad (4.64)$$

and $(W-c)\left[u'(r) + \dfrac{u(r)}{r} \right] - W'u(r)$ is continuous at

$r = R_1 \text{ and } R_2$. $\qquad (4.65)$

Substituting in the interface conditions, we obtain at $r = R_1$.

$$u_1(R_1) = u_2(R_1) \qquad (4.66)$$

and $(W_0-c)\left[u_1'(r) + \dfrac{u_1}{r} \right]_{R_1} = (W_0-c)\left[u_2' + \left| \dfrac{u_2}{r} \right| \right]_{R_1} - W'u_2 \Big|_{R_1}$

$$(4.67)$$

For the interfacial conditions at $r = R_2$, we obtain

$$u_2(R_2) = u_3(R_2) \tag{4.68}$$

and $\quad -c \left[u_2' + \dfrac{u_2}{r} \right]_{R_2} - W'u_2 \Big|_{R_2} = -c \left[u_3' + \dfrac{u_3}{r} \right]_{R_2} \tag{4.69}$

Substitution of equations (4.61) to (4.63) into (4.66) to (4.69) leads to the relations.

$$\tag{4.70}$$

$$A_2 \left[2I_1^2(kR_1) \right] + B_2 \left[2K_1(kR_1)\, I_1(kR_1) - (1-\bar{c}) \quad \left(\frac{R_2}{R_1}\right)^2 - 1 \right] = 0$$

$$\tag{4.71}$$

$$A_2 \left[I_0(kR_2) - \beta o I_1(kR_2) \right] + B_2 \left[-Ko(kR_2) - \beta o K_1(kR_2) \right] = 0$$

where $\bar{c} = c/_{Wo}$ is the non-dimensional complex velocity and

$$\beta o = \beta + \frac{2kR_2}{k^2\bar{c}\ (R_2^2 - R_1^2)} \tag{4.72}$$

where

$$\beta = \frac{Io(kR_2)\ K_1(kRo) + I_1(kRo)Ko(kR_2)}{K_2(kRo)I_1(kR_2) - I_1(kRo)K_1(kR_2)} \tag{4.73}$$

In the process of deriving these relations we make use of the Modified Bessel's function relations as described in Watson (1966)

$$\frac{dI_1(kr)}{d(kr)} = Io(kr) - \frac{I_1(kr)}{kr} \tag{4.74a}$$

$$\frac{dK_1(kr)}{d(kr)} = -Ko(kr) - \frac{K_1(kr)}{kr} \qquad (4.74b)$$

and the Wronskian relation

$$Ko(kr)\ I_1(kr) + K_1(kr)Io(kr) = \frac{1}{kr} \qquad (4.75)$$

For a non-trivial solution to exists the determinant of (4.70) and (4.71) must be zero. Expanding the determmiant we derive a quadratic equation in the complex non-dimensional wave-velocity $\bar{c}$. Complex roots in the quadratic equation will imply an exponentially growing disturbance and hence flow instability. These results are

$$A\bar{c}^2 + B\bar{c} + C = 0 \qquad (4.76)$$

where the coefficients of the quadratic equation are described by

$$(4.77)$$

$$A = (kr_1)^2 \left[\left(\frac{R_2}{R_1}\right)^2 - 1\right]^2 \left[\beta I_1(kR_2) - Io(kR_2)\right]$$

$$B = 2(k\dot{R}_1)^2 \left[\left(\frac{R_2}{R_1}\right)^2 - 1\right] \left[I_1^{\ 2}(kR_1) - Ko(kR_2) - \beta K_1(kR_2)\right.$$

$$\left. + K_1(kR_1)I_1(kR_1) \quad \beta I_1(kR_2) - Io(kR_2)\right]$$

and

$$C = (kR_2)\left[4K_1(kR_1)I_1(kR_1)I_1(kR_2) - 4I_1^{\ 2}(kR_1)K_1(kR_2)\right.$$

$$\left. -2\left[\left(\frac{R_2}{R_1}\right)^2 - 1\right]I_1(kR_2)\right]$$

The non-dimensional phase velocity is given by the real part

$$\bar{c}_r = -B/2A \qquad (4.78)$$

and the amplifications or growth factor by the imaginary part

$$\bar{c}_i = \frac{1}{2A} \sqrt{4AC-B^2} \qquad (4.79)$$

The results of the computations on the phase velocity, growth factor and growth rate are shown in Figure 4.12, 4.13 and 4.14. The wave phase velocity for different δ's are shown in Figure 4.12, where it is noticed that the general behavior is the same when compared with the corresponding case of symmetric perturbations in rectangular coordinates. For large wavenumbers the perturbation velocity approaches half of the mean flow velocity for profiles with a sharp interface transition (high δ's), whereas those at low δ's are above half of the mean flow velocity. The cylindrical geometry produced higher phase velocity for the same δ and kd.

The growth factors shown in Figure 4.13 are of lower magnitude in the cylindrical geometry, they also show for small interface distances a peaking effect not noticed in the rectangular geometry, but again the general behavior is the same, giving a non-vanishing growth factor in the same range of wavenumbers, approximate $o<kd<1.30$.

The growth rate as defined by

$$\sigma = kR \left(\frac{c_i}{c_r}\right) \quad , \text{ where } R = R_2 - R_1 \qquad (4.80)$$

is shown in Figure 4.14. The stabilizing effect upon symmetrical perturbations is so great that for $\delta = 0.75$ only a weakly growing instability disturbance remained which disappeared with increasing interfacial distance. The maximum growth rate calculated ($\delta = 30$) was about 0.39 occurring at a wavenumber kd = 0.80.

The disturbances whose amplitude is increased the most in a given time, is the one for which the growth rate is a maximum. This maximum amplification occurred for an instability wavenumber (kd) of approximate 0.80, with increasing deviation toward smaller wavenumbers for large interface distances.

Non-axisymmetric Disturbances in an Unbounded Jet

In examining the formation and development of instabilities in a partially obstructed pipe, some of our preliminary observations (Lopez and Kurzweg, 1977) using birefringent Bentonite solution indicated that the onset of disturbances and transition to turbulence of the laminar jet formed downstream from the contraction was characterized by the appearance of axisymmetric perturbations near the constriction but often by helical modes of instability further down-stream but prior to the appearance of decaying
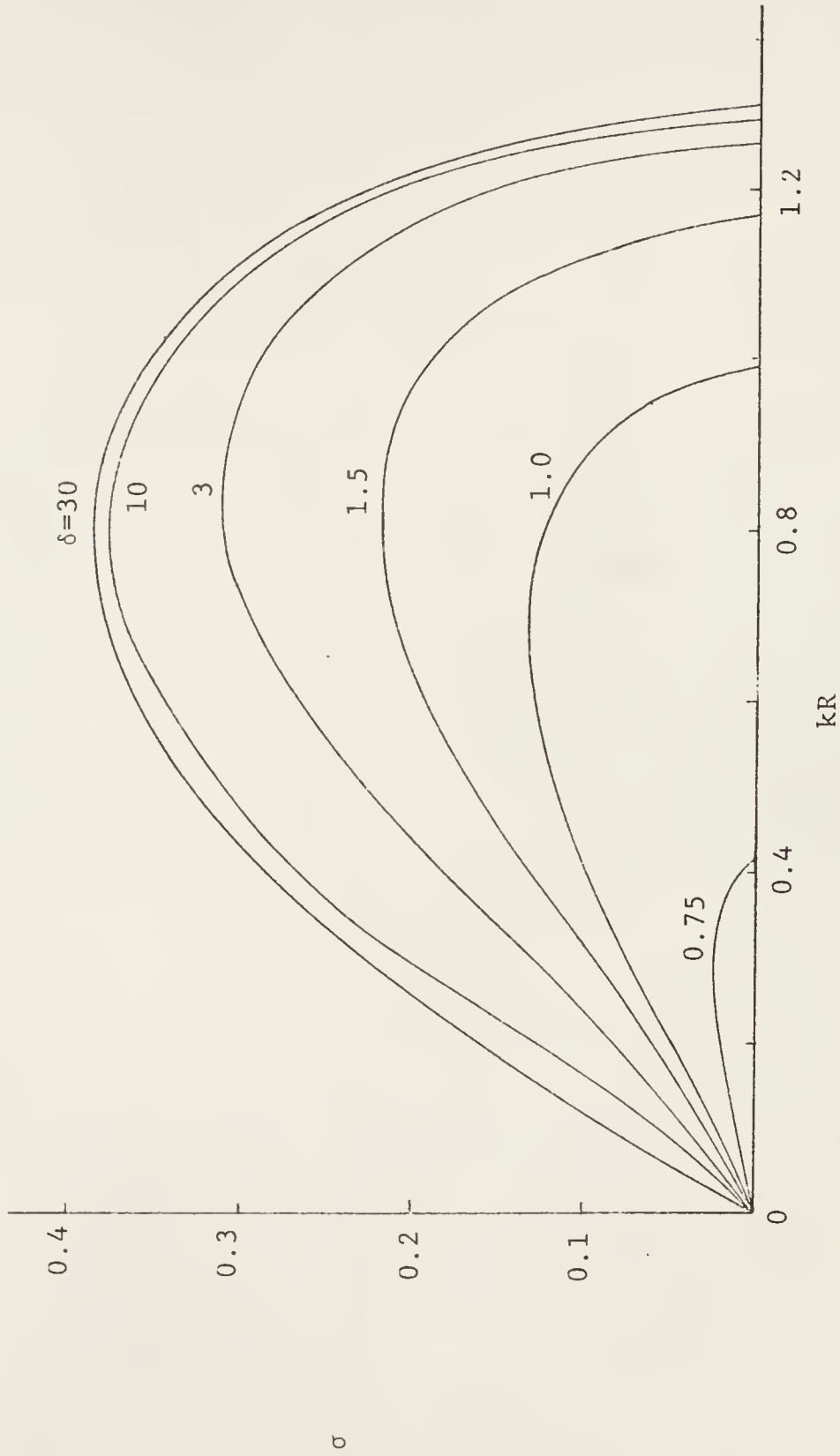
Figure 4.12   Wave phase velocity (m=o)

Figure 4.13   Growth factor curves (m=o)
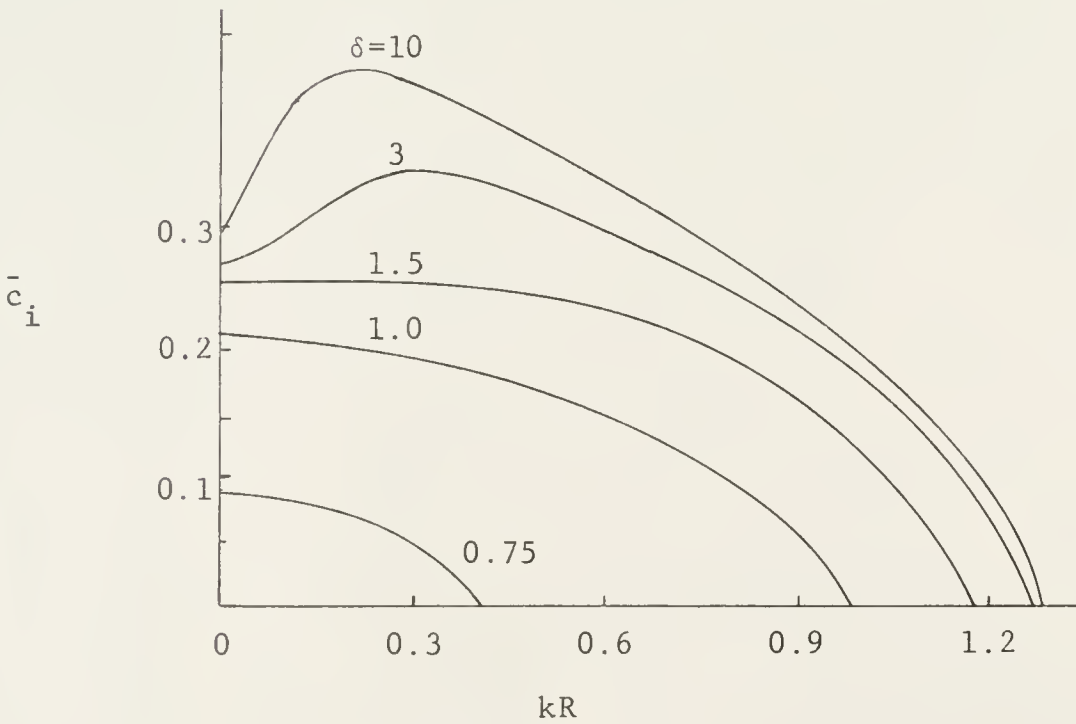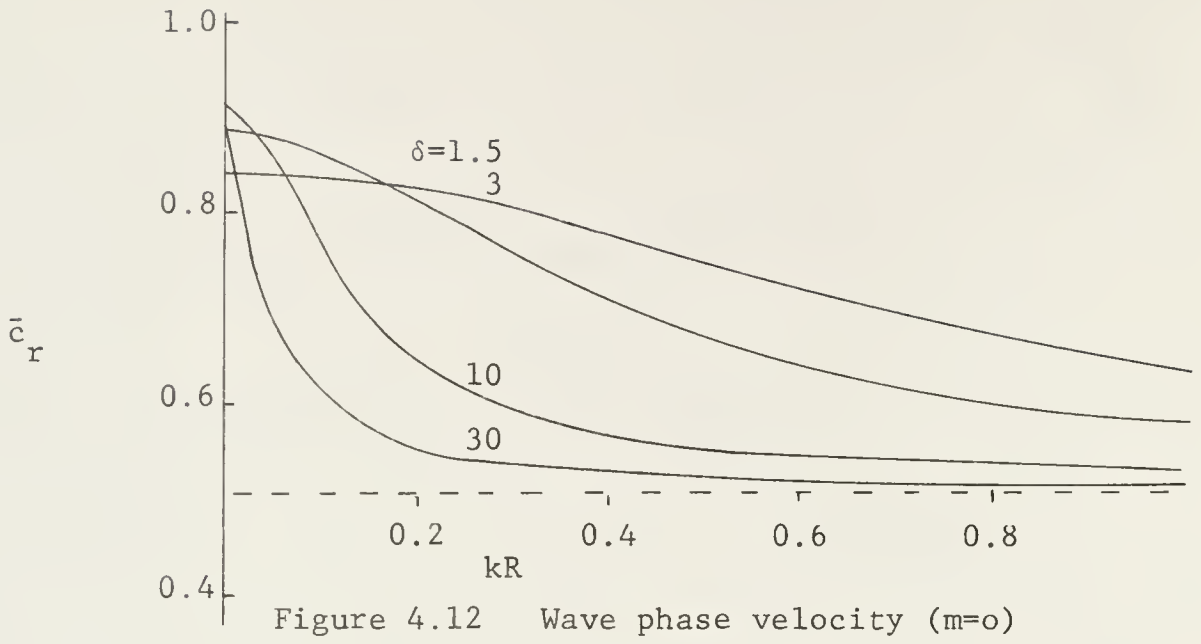
Figure 4.14   Growth rate curves for axisymmetric disturbances (m=o)

turbulence. Some of these observations are shown in
figure 3.2a, where a form of non-axisymmetric perturbation
can be detected in the right hand corner about 10 cm down-
stream from the constricted region. Another example is
shown in figure 3.3a where a three dimensional propagation
can be observed.

Similar observations of helical disturbance had been
previously reported by Reynolds (1962) for an unbounded
jet, and suggest the breakdown phenomenon to turbulence is
essentially the same in the two cases. Batchelor and Gill
(1962) have examined the invisicid stability of jets in
unbounded media for arbitrary infinitesimal disturbances
for the steady-state velocity profile corresponding to the
axial velocity component of the classical similarity solu-
tion for the round jet. Their calculation at a fixed
axial position indicated that the only amplified distur-
bance possible is of helical type with large axial wave-
length and an angular wavenumber of unity. Pure axisym-
metric disturbances do not grow for the special case con-
sidered by them.

It is our purpose here to extend their analysis by
examining the inviscid instability of an axisymmetric un-
bounded jet to infinitesimal non-axisymmetric perturba-
tions, at various axial positions, and to compare the rate
of amplification of these disturbances with the corres-

ponding growth of axisymmetric perturbations. Finally we
will show in agreement with experimental observations,
that the early stages of laminar jet transition to turbu-
lence are characterized by axisymmetric disturbances but
that propagation of non-axisymmetric modes is also possible,
having comparable growth rates at positions further down-
stream from the orifice.

In order to simplify our calculations we assume that
the jet is discharging in an unbounded medium and neglect
the wall effects. We know from previous calculations that
the presence of the walls will not significantly modify
our results.

Mathematical Formulation

The governing eigenvalue equation describing the
inviscid stability of the jet for infinitesimal disturb-
ances of axial wavenumber k and angular wavenumber m is
given by equation (4.53) and repeated below.

$$(4.81)$$

$$\left[\frac{r}{m^2+(kr)^2} \ (ru(r))' \right]' -u(r) =\left(\frac{ru(r)}{W-c} \right)\left[\frac{rW'}{m^2+(kr)^2} \right]'$$

with the boundary conditions

$$u(r)\Big|_{r=0} =\text{finite}, \ u(r)\Big|_{r\to\infty} =0 \qquad (4.82)$$

where the amplitude of the radial velocity perturbation
described by u(r) and W(r) is the steady state axial

velocity component. For the case of non-axisymetric per-
turbations the angular wave number m can take integer
values, m>1.

Closed form solutions to the stability equation are
possible for $W(r)$ constant or for velocity distributions
where the term in the square bracket in the right of
equation (4.81) is constant.

The general solution is given by the velocity profile

$$W(r) = a \, \tfrac{1}{2}(kr)^2 + m^2 \ell nr + b \tag{4.83}$$

where a and b are adjustable constants depending on the
conditions imposed on the problem. One such steady-state
profile which accomplishes this and also resembles the
diffusing laminar jet under consideration is

$$W(r) = \begin{cases} Wo & \text{for } o \leq r < R_1 \\ \\ Wo \, \dfrac{\tfrac{1}{2}k^2(R_2{}^2 - r^2) + m^2 \ell n (R_2/r)}{\tfrac{1}{2}k^2(R_2^2 - R_1{}^2) + m^2 \ell n \dfrac{R_2}{R_1}} & R_1 \leq r < R_2 \\ \\ 0 & R_2 \leq r < \infty \end{cases} \tag{4.84}$$

where Wo is the centerline velocity and R_1, R_2 are as
before the interface positions at which the radial velo-
city gradient is discontinuous. As accomplished in pre-
vious sections the jet profile at various axial positions
can be approximated by moving the second interface point
(R_2) away from the centerline. According to the steady
state similarity solution for this jet, valid everywhere

except in the immediate vicinity of the orifice, the half-width of the jet is approximately proportional to the axial distance z from the orifice and inversely to the entrance Reynolds number. So as the jet profile develops downstream the spreading of the velocity distribution is simulated by increasing the relative interface distance $R=R_2-R_1$. Notice that the shape of the velocity profile described by equation (4.83) is a function of the disturbance asymmetry parameter $s={}^m/_{kr}$.

For the profile described by (4.84), the stability equation has a closed from solution given in terms of the derivative of the Modified Bessel functions $I_m(kr)$ and $K_m(kr)$, as obtained by Michalke and Timme (1967).

$$u(r) = Akd\frac{Im(kr)}{d(kr)} + Bkd\frac{Km}{d(kr)}(kr) \qquad (4.85)$$

where the derivative is taken with respect to the argument of the Bessel function, and A and B are arbitrary constants satisfying the boundary conditions.

To satisfy the boundary condition at r=0 requires $B_1=0$, while the condition at infinite requires $A_3=0$, giving for the different regions

$$u_1(r) = A_1 Im'(kr) \qquad\qquad \text{for } o \leq r < R_1$$
$$u_2(r) = A_2 I'm(kr) + B_2 K'm(kr) \qquad R_1 \leq r \leq R_2 \quad (4.86)$$
$$u_3(r) = \qquad\qquad B_3 K'm(kr) \qquad R_2 \leq r < \infty$$

Applying the interfacial conditions that the perturbation displacement and pressure are continuous at the two interface locations R_1 and R_1.

$$\langle u(r)\rangle \Big|_{R_1,R_2} = 0 \tag{4.87}$$

and

$$\langle W'u(r) - (W-c)(u'(r) + \frac{u(r)}{r})\rangle \Big|_{R_1, R_2} = 0 \tag{4.88}$$

we obtain the determinant.

$$\tag{4.89}$$

$$\begin{vmatrix} I'm\ (kR_1) & I'm(kR_1)K'm(kR_1) - \dfrac{[m^2+(kR_1)]^2}{R_1^3}\ \dfrac{(Wo-c)}{W'} \\[2ex] K'm(kR_2)I'_m(kR_2) - \dfrac{[m^2+(kR_2)^2]\,c}{R_2^3 W'(kr_2)} & K'^2_m(kR_2) \end{vmatrix} = 0$$

Where use was made of the relation for the second derivative of the Modified Bessel Function (Watson, 1966) as described below

$$\frac{d_2}{d(\overline{k}r)^2} I_m(kr) = \left[1 + (\tfrac{m}{\overline{k}r})^2\right] I_m - \frac{1}{2\overline{k}r}\left[I_{m-1} + I_{m+1}\right]$$

$$\frac{d^2}{d(\overline{k}r)^2} K_m(kr) = \left[1 + (\tfrac{m}{\overline{k}r})^2\right] Km + \frac{1}{2\overline{k}r}\left[K_{m=1} + K_{m+1}\right] \tag{4.90}$$

The determinant described by (4.90) was non-dimensionalized with respect to the jet centerline velocity Wo and the dimensionless coordinate kr. The solution to the determinant is then represented by a quadratic equation in the non-dimensional complex wave speed $\bar{c}$, of the form

$$A\bar{c}^2 + B\bar{c} + C = 0 \tag{4.91}$$

where the non-dimensional coefficients can be evaluated
from the expressions

$$A = \left[\frac{1}{(kR_1)(kR_2)}\right]\left[1 + \frac{m}{k\bar{R}_1}^2\right]\left[1 + \frac{m}{k\bar{R}_2}^2\right]$$

$$B = \frac{1}{kR_2}\left[1 + \left(\frac{m}{k\bar{R}_2}\right)^2\right]\bar{W}_{R_1}I'm(kR_1)K'm(kR_1) \tag{4.92}$$

$$- \frac{1}{kR_1}\left[1 + \left(\frac{m}{kR_1}\right)^2\right]\bar{W}_{R_2}K'_m(kR_2)I'_m(kR_2) - A$$

and

$$C = \bar{W}_{R_1}'\bar{W}_{R_2}'\left[\left[(Im(kR_1)K'_m(kR_2)\right]^2 - K'_m(kR_2)K'_m(kR_1)\right.$$

$$\left. I'_m(kR_2)I'_m(kR_1)\right]$$

$$+ \frac{1}{kR_1}\left[1 + \left(\frac{m}{kR_1}\right)^2\right]\bar{W}'(kR_2)K'_m(kR_2)I'_m(kR_2)$$

where $\bar{W}(r) = \frac{W(r)}{W_0}$ is a non-dimensional velocity distribu-
tion and the prime in this case indicates a derivative
with respect to the non-dimensional variable (kr). Flow
instability is being characterized by a $\bar{c}_i$ different from
zero (complex roots). A measure of the amplification or
growth rate of a given infinitesimal disturbance between
two axial positions is given by

$$\sigma = kR\left(\frac{c_i}{c_r}\right) \tag{4.93}$$

We have evaluated equation (4.93) numerically up to m=5 for the special case Wo = 1 and R_1 = 1. The results are summarized in Figures 4.15a through 4.15f where the growth rate is plotted as a function of the angular wavenumber and the non-dimensional axial wavenumber kR for several interfacial distances.

Increasing R corresponds to increasing axial distance downstream from the orifice where the jet has widened. Since the flux of momentum is conserved the centerline velocity must decrease with increasing axial distance in an actual jet, and our calculated growth rate will generally be in excess of these existing at various axial positions.

It is clearly seen from these figures that for small interfacial distance R, the least stable modes expected are axisymmetric although the maximum growth rate for non-axisymmetric modes is almost as large and sometimes even larger as in the case of very small disturbance wavelengths. These results for a sharp interface with the second interface position located at R_2 = 1.10 are shown in Figure 4.15a, and they are representative of the stability of velocity profiles closer to the jet orifice.

As the interface distance R increases the growth rate is seen to decrease implying a more stable jet configura-

tion showing a trend for m mode suppression with increasing R as shown in Figure 4.15b for R = 0.20. Upon further increasing the interfacial distance the m = 1 mode shows more instability that the corresponding axisymmetric mode implying that as the jet spreads the optimum growth rate will be characterized by helical disturbances, while higher m modes suppression continues as illustrated in Figure 4.15c and 4.15d for interface distance of 0.50 and 1.0 respectively.

For a distance R = 1 only the m = 0, 1 modes are present with the non-axisymmetric mode (m = 1) showing higher instability growth rate. At a distance of 2.5 shown in Figure 4.15e the instability growth rate have been largely reduced, but both modes of instability are still present and of the same magnitude. For approximately R = 2.75, (Figure 4.15f) only a weakly growing axisymmetric instability disturbance remained which disappeared with increasing interfacial distance.

The non-dimensional phase velocity (c_r / W_o) for the case of R = 0.20 is shown in Figure 4.16. These results show that long waves with axial symmetry travel with the speed of the center of the jet, whereas those not having axial symmetry travel with about half that speed, as previously reported by Batchelor and Gill (1962) for an interface of zero-thickness.

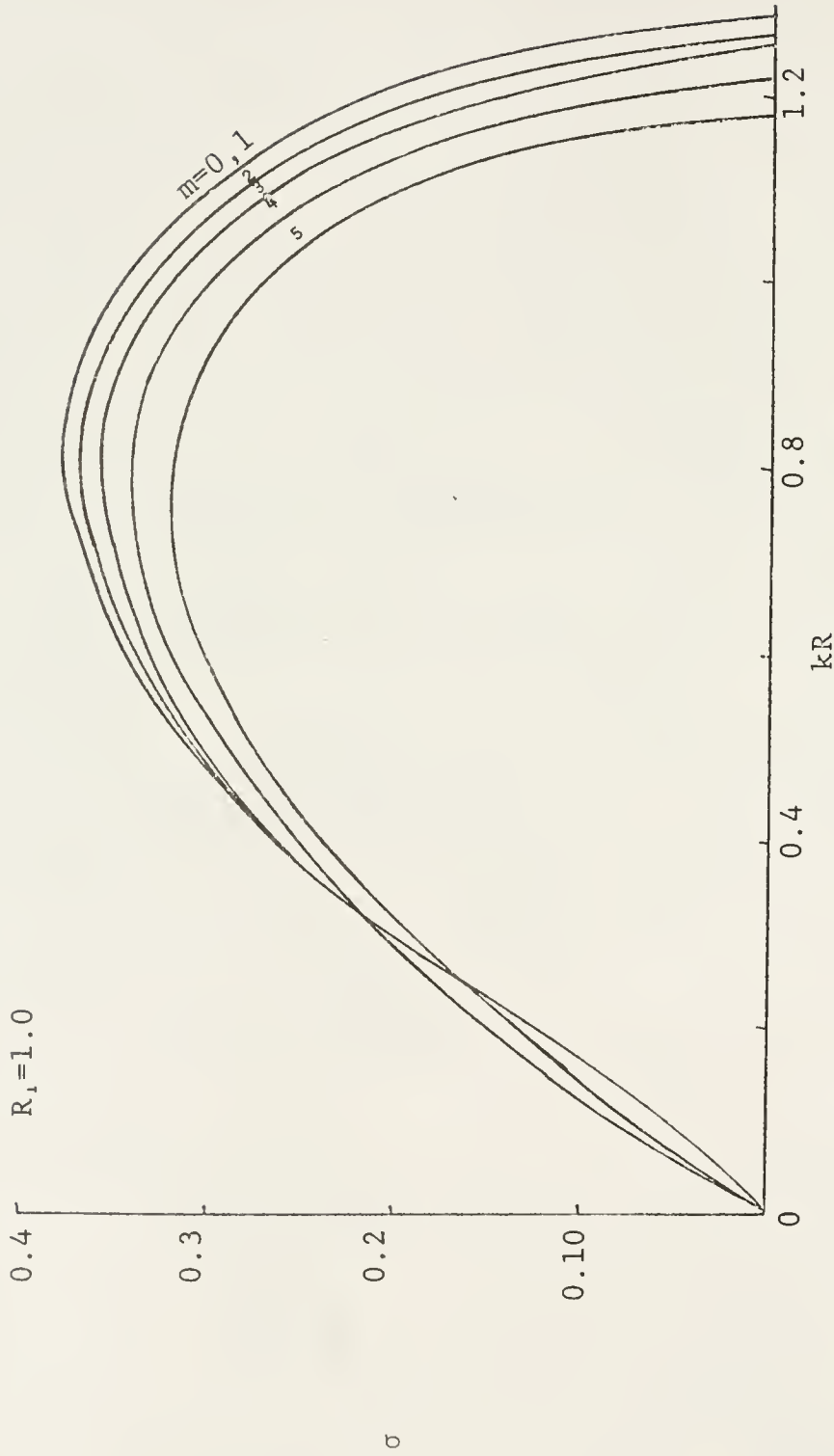The imaginary part or growth factor (c_i / W_o) is shown

156

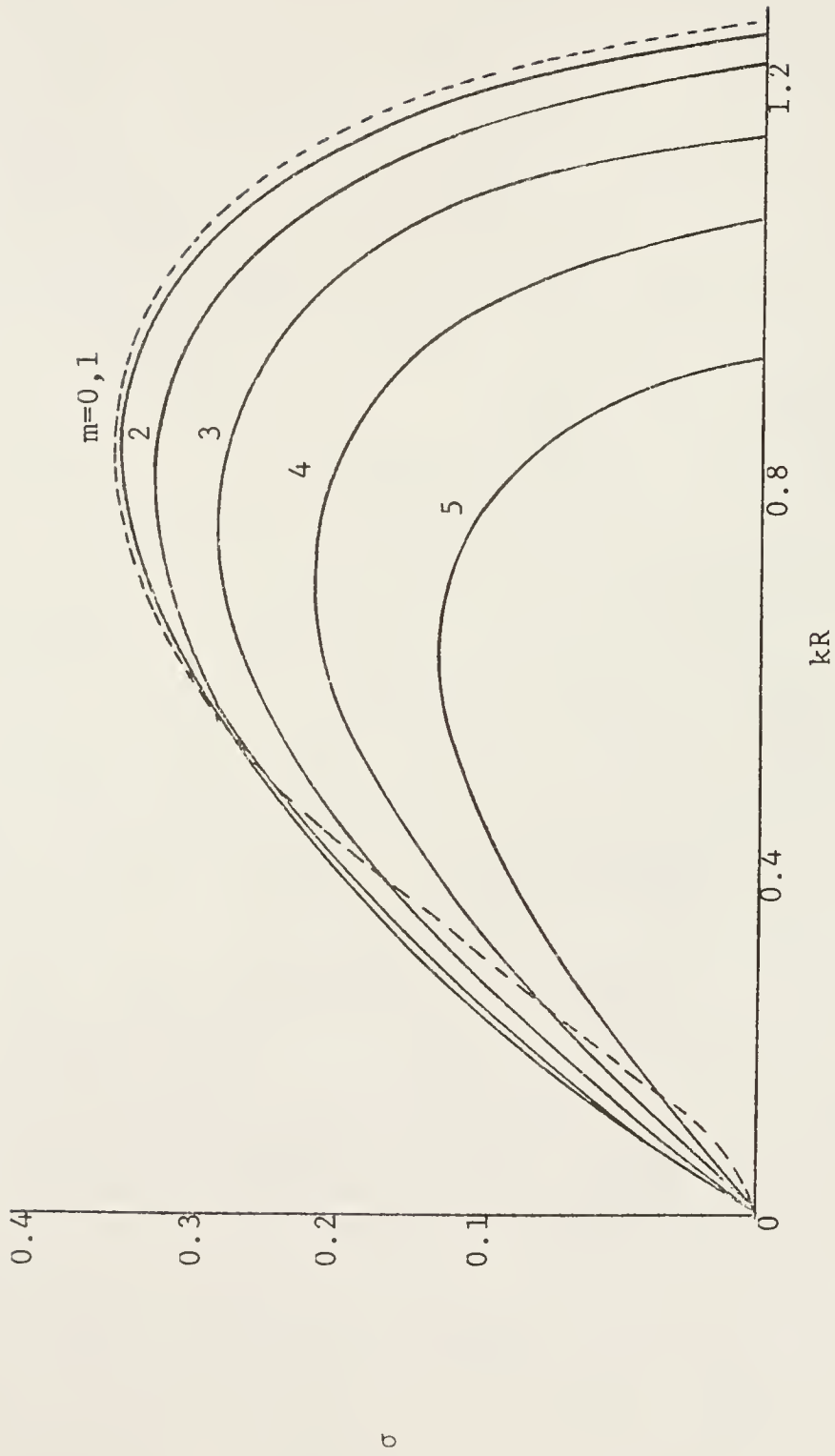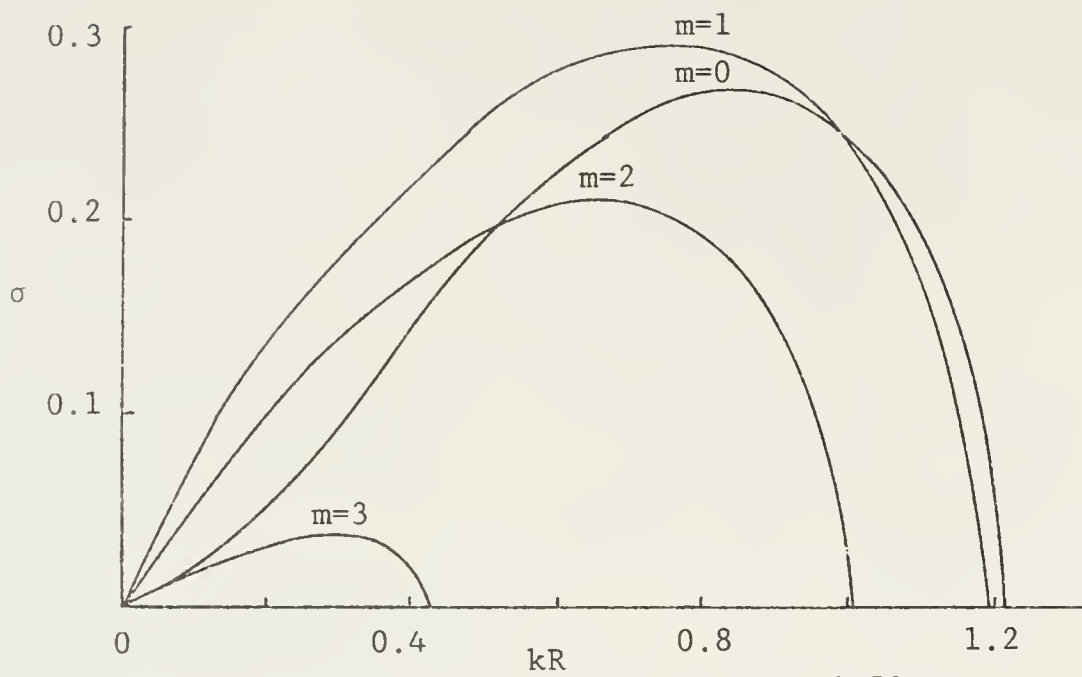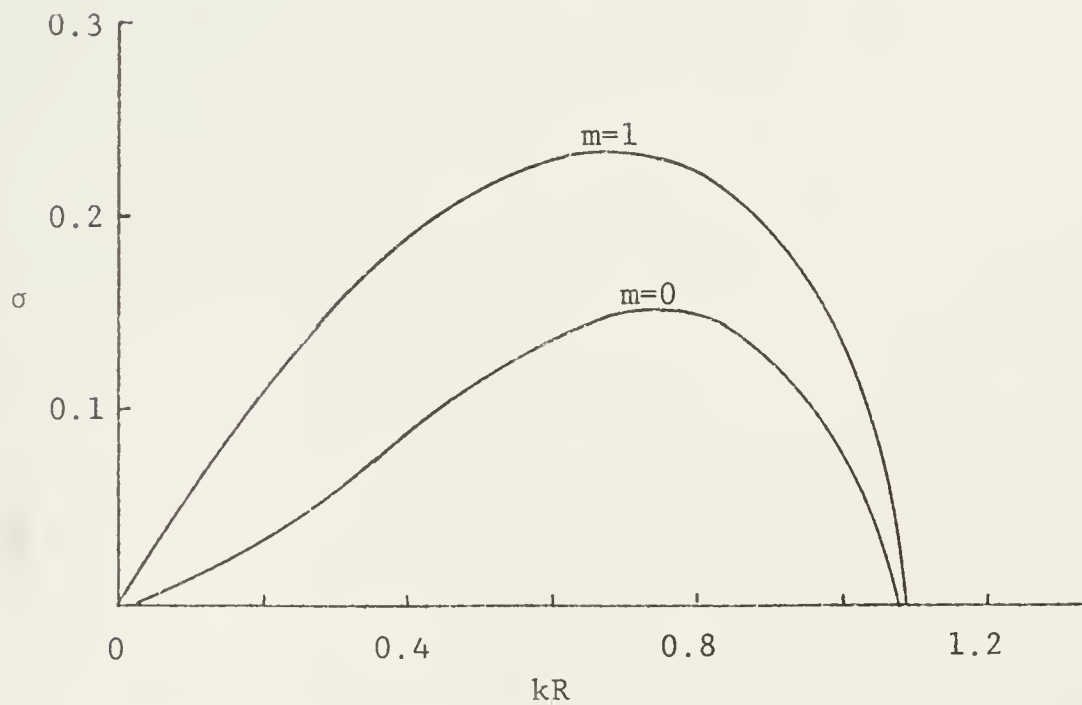Figure 4.15a   Growth rate curves for non-axisymmetric disturbances.
R=0.10

Figure 4.15b   Growth rate curves for non-axisymmetric disturbances.
R=0.20

Figure 4.15c   Growth rate curves.   R=0.50

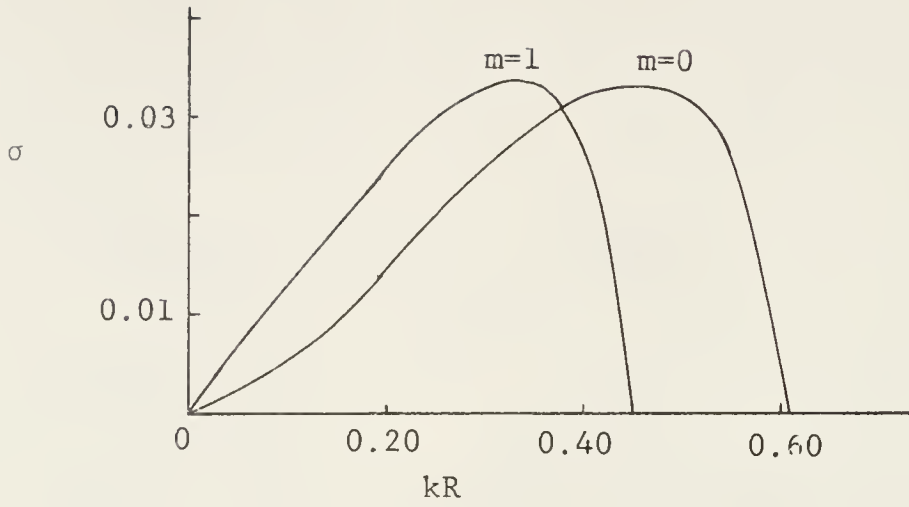Figure 4.15d   Growth rate curves.   R=1.0

Figure 4.15e   Growth rate curves.   R=2.5

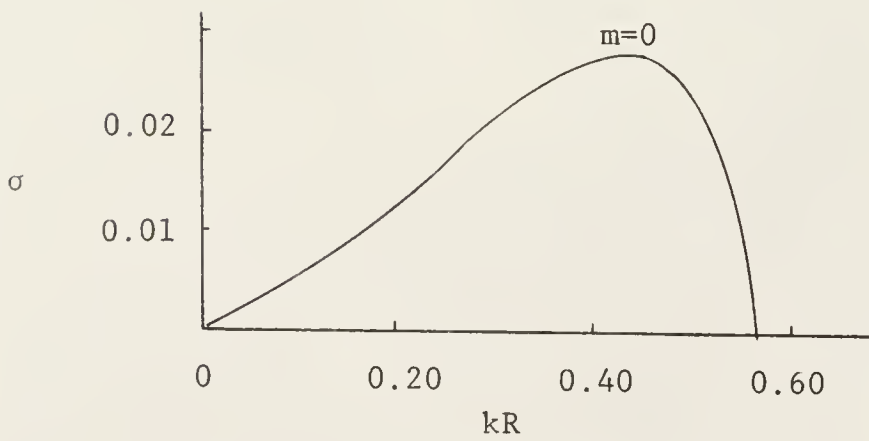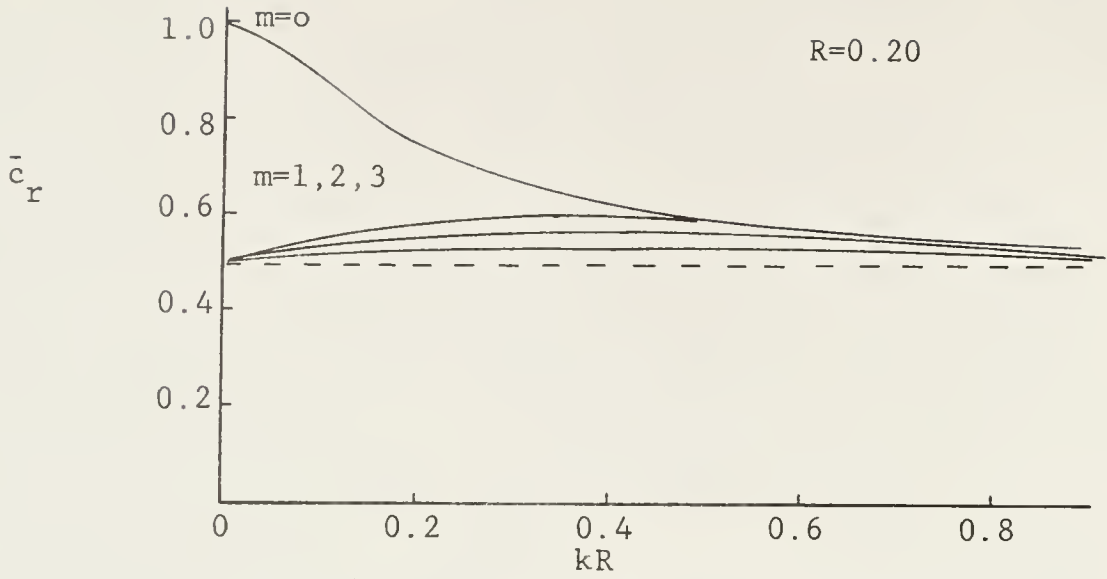
Figure 4.15f   Growth rate curve.   R=2.75

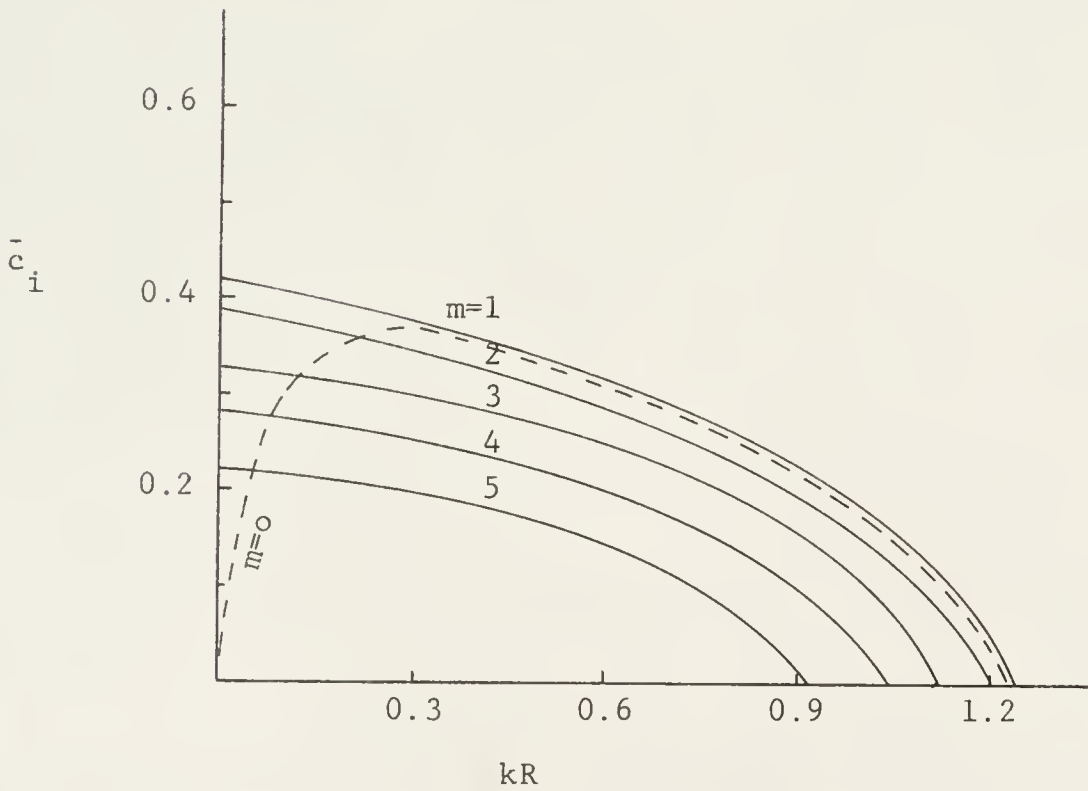Figure 4.16   Wave phase velocity curves

Figure 4.17   Growth factor curves

in Figure 4.17 for the same case.

The somewhat unexpected result than non-axisymmetric instability modes occur in the laminar jet profile considered is quite interesting as it suggests that more detailed analysis involving viscous and non-linear effects should consider such helical modes as a starting point. It may also be that the breakdown phenomenon in boundary layer flow is characterized by the propagation of non-axisymmetric instabilities. The experiments of Kim, Kline and Reynolds (1971) indicate that the bursting process of low speed streaks in boundary layer flow at transition is characterized by the appearance of streamwise vortex motions.

Correlation With Experimental Observations

In this section we try to correlate some of the experimental observations as obtained from the flow visualization experiments with the results predicted by the inviscid stability analysis of axisymmetric perturbations in cylindrical coordinates. The perturbations that shows the largest growth rate is the most likely to appear during an experiment, since it grows faster than any other disturbance. In some of the experiment photographs the existence of a wave-like motion is obvious, like the ones shown in Figures 3.1b and 3.6. We measured the disturbance wavelength from

the photographs using the line marks on the surface of the pipe (separated at 1 cm). This method is not exact but provides a good approximation to the actual disturbance wavelength.

The growth rate for two profiles whose interface positions were adjusted to simulate the actual profiles for the models with diameter ratio 1/6 and 1/2 are shown in Figures 4.18a and 4.18b. The location of the interfaces were approximated by looking at experimentally determined profiles from previous investigations. In the same figure the location of the observed wavenumbers are also shown (broken lines). In both cases the observed disturbances are very close to the wavenumber at maximum growth rate, as predicted by analysis. Similar satisfactory correlations were carried out with the experimental observations in rectangular models, using the milling yellow solution. This good agreement between inviscid theory and experiment is very encouraging.

Effects Produced by the Boundaries

All of the results derived in previous sections assumed a fixed wall position at 1 unit of length from the centerline. In order to study the effects of the boundaries in flow stability the wall position was changed, and placed away from the centerline. The growth factor was then computed for the rectangular and cylin-
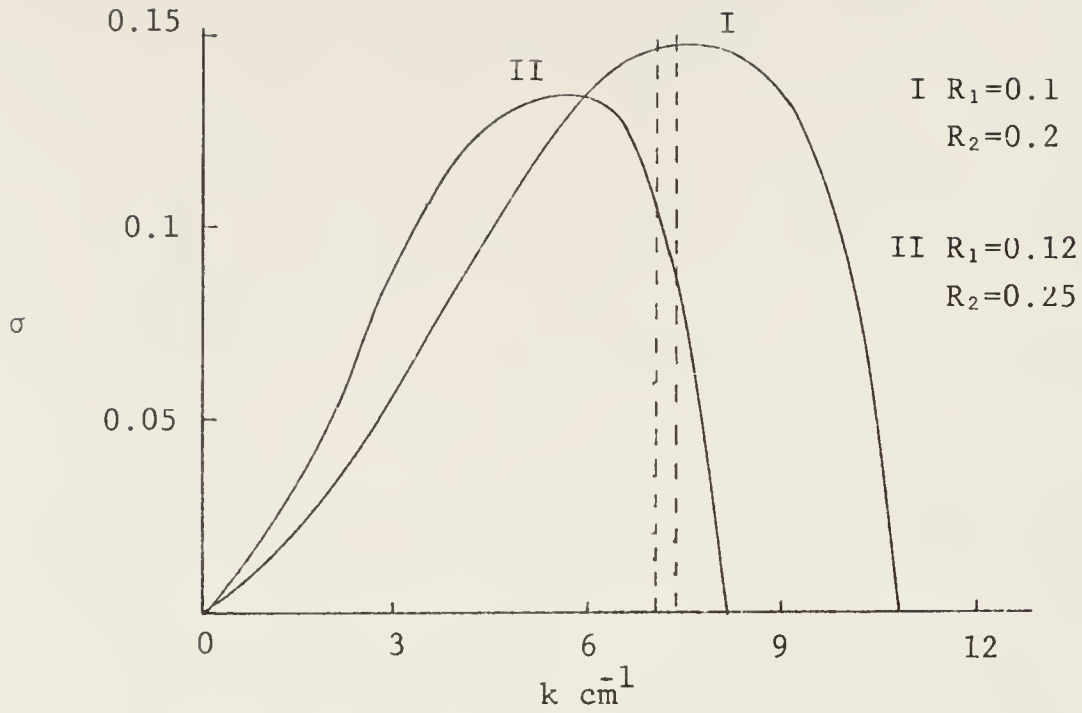
Figure 4.18a   Correlation with experiment.
$D_1/Do=1/6$
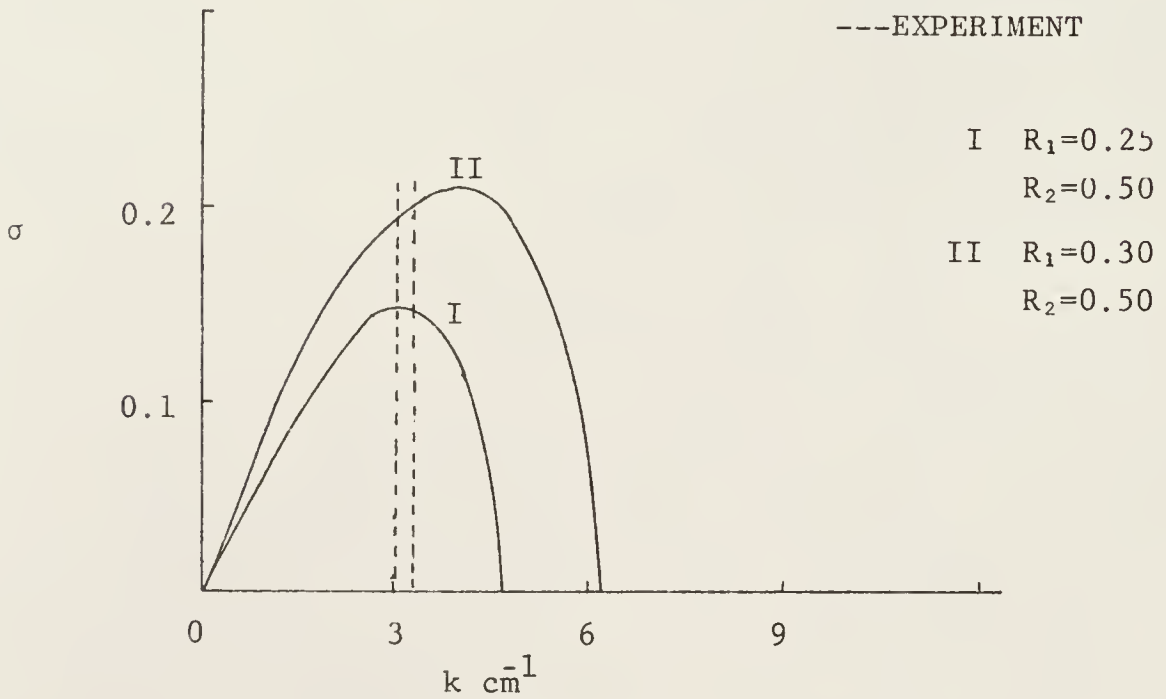
Figure 4.18b   Correlation with experiment.
$D_1/Do=1/2$

drical geometry. Calculations were made for the case of
symmetric disturbances acting in a mean symmetric flow.
These results are described in Figure 4.19a for rectang-
ular coordinates, and in Figure 4.19b for the cylindrical
geometry. As we notice from these results the presence
of solid boundaries tend to stabilize the flow for small
disturbance wavenumber as they are moved away from the
centerline. The destabilization of the flow produced by
the proximity of the boundaries is unexpected. There
was no noticeable effects on stability at large wave-
numbers.

Do=1,5,10,20,30

$d_2=0.6$

$d_1=0.3$

Ro=1

0.3

5

10

0.2

20,30

0.1

| 0 | 0.3 | 0.6 | 0.9 | 1.2 |

kd
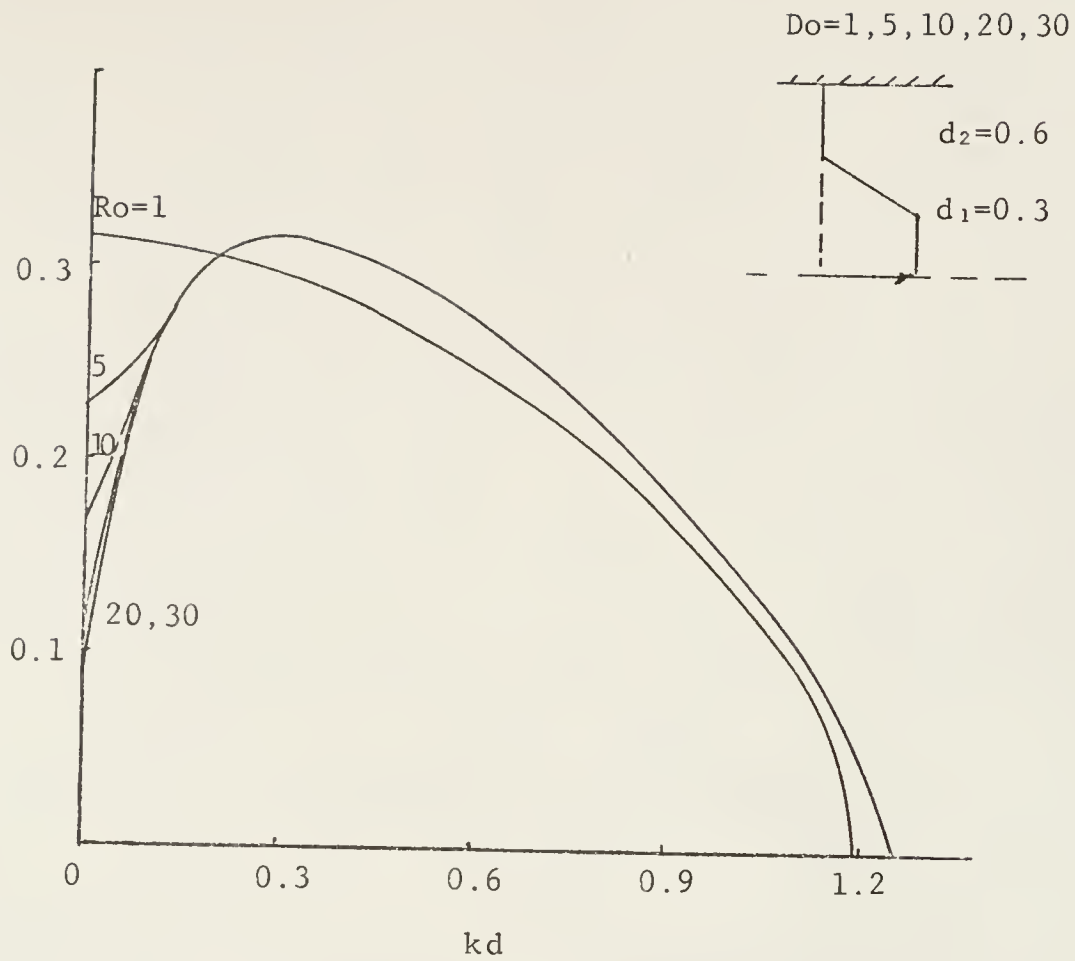
Figure 4.19a   Effects of boundaries (rectangular)

Ro=1,5,10,∞

$R_2=0.6$

$R_1=0.3$

Ro=1

0.2

5

0.1

∞

| 0 | 0.3 | 0.6 | 0.9 |

kR
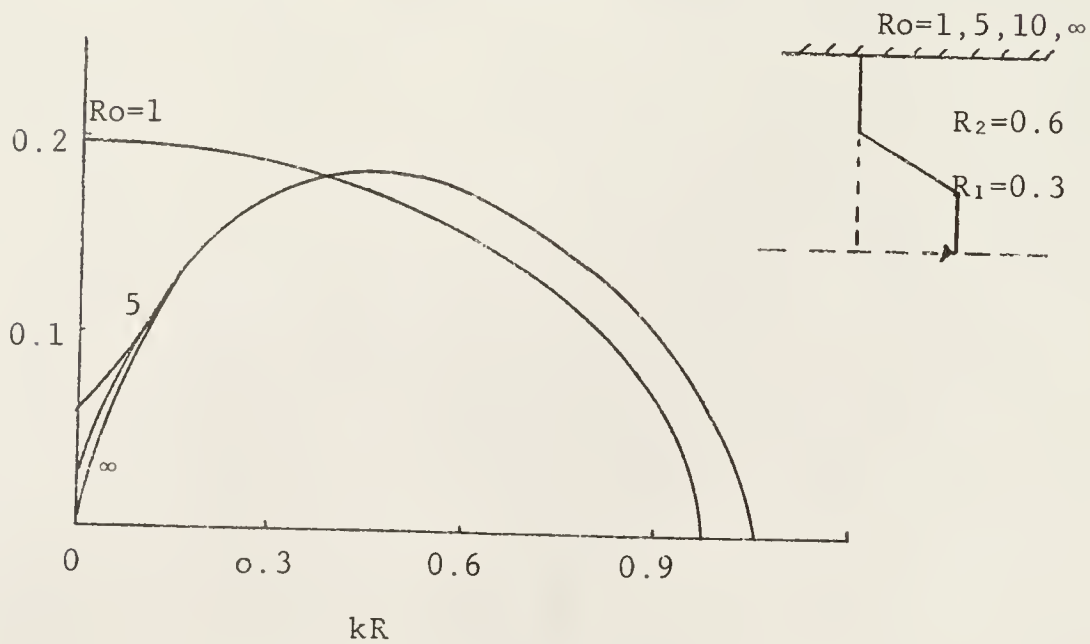
Figure 4.19b   Effects of boundaries (cylindrical)

CHAPTER 5

CONCLUSIONS

This investigation has consisted mainly of two
sections in which experimental and analytical techniques
were employed to investigate some of the properties of a
confined liquid jet at low Reynolds numbers. The investi-
gation was motivated by the lack of observational data on
the Reynolds number at which such jets become unstable,
and the flow characteristics in the transition region to
turbulent flow. The experimental approach consisted of a
series of flow vizualization experiments based on the
"streaming-double refraction" properties of bentonite
solutions.

These experiments were primarily directed to determine
the Reynolds number at the onset of disturbances and to
study the stationary turbulent region formed downstream of
a constriction in a pipe. Also as part of the experimental
section, pressure drop measurements were taken across the
constricted region to determine the added resistance to
flow as a function of the constriction to pipe area ratio
and its geometrical properties. It was noticed, as deter-
mined by previous investigations in unbounded media, that

such jets are unstable and capable of producing strong
mixing at very low Reynolds numbers. It was also observed
that the jet formed downstream of the constriction was
characterized by the appearance of axisymmetric instabili-
ties near the orifice but often by the non-axisymmetric
mode of propagation further downstream, with character-
istics very sensitive to the fluid velocity.

These interesting observations motivated the second
section, or analytical portion of this investigation,
which was an attempt to determine the mode of instability
propagation that grows most rapidly at a very large
Reynolds number and its correlation with observed wave-
like disturbances.

The major findings and conclusions derived in the
experimental section and inviscid stability analysis
may be summarized as follows:

(1) The Reynolds number for transition is constricted
     tubes occurred well below the value of 2000 normally
     associated with turbulence in unconstricted tubes.
     The value of the critical Reynolds number at the
     onset of instabilities decreased with decreasing
     constriction to pipe area ratio.

(2) The Transition region from a steady laminar jet, the
     appearance of disturbances and the final breakdown
     into localized turbulence was not instantaneous but

occurred over a small range of Reynolds number, with flow
characteristics showing a large sensitivity to changes in
flow rate.

(3) The laminar jet disintegrated into turbulent flow
     at sufficiently high velocities. Turbulence appeared
     to be localized over a relative small region down-
     stream of the jet orifice, while the upstream flow
     remained undisturbed. Due to the low mean flow
     energy (small Reynolds number) turbulence decayed
     rapidly to laminar flow.

(4) The orifice to pipe diameter ratio had a strong
     influence on the Reynolds number at the onset of in-
     stabilities. This behavior was generally non-linear
     but a linear region was noticed at intermediate area
     ratios. As also determined by Kim and Corcoran, the
     flow fluctuations at very small area ratios appeared
     to be more intense and composed of higher frequency
     oscillations.

(5) The constricted geometry appeared to play a second-
     ary role in the transition phenomenon. The shape of
     the constricted region produced minor affects on the
     critical Reynolds number which appeared to be domi-
     nated by the high shear layer formed between the
     emerging high velocity fluid and the stationary fluid,
     as in the Kelvin-Helmholtz instability mechanism.

(6) There was a definite correlation between the onset of sounds determined by previous investigations and the onset of turbulence; but the onset of sounds usually occurred at higher flow rates than the onset of disturbances as determined by this study, especially when the sensor was located outside the tube. This seems to indicate that sounds will be detected at a more advanced stage of turbulence development when the fluctuations are of sufficient amplitude and frequency to cause wall vibrations. The effects of unsteady flow, wall elastic properties and boundary conditions must also be considered in determining the degree of stenosis or tube contraction by means of sound detection.

(7) The experimental observations in rectangular and cylindrical test sections also showed different possible modes of disturbance propagation. These modes of propagation were later identified with the axisymmetric and non-axisymmetric modes of propagation. The symmetric mode appeared to occur more frequently closer to the jet orifice, while the appearance of some kind of turning helical motion was noticeable further downstream of the orifice.

(8) Experimental results showed a very strong influence of geometry, both the size and shape, on the pressure

drop across the obstructed section. Pressure drops across severly constricted models were more than an order of magnitude larger than in the moderately constricted models at the same Reynolds number. The laminar pressure drop was negligible compared with the total drop across the obstructed section. The shape of the constriction, while not producing large effects on the onset of instabilities, had a strong influence on the pressure drop. The abrupt transition models caused twice the pressure drop associated with the models with rounded edges.

(9) Partial pressure recovery usually occurred between 4 and 6 pipe diameters downstream of the jet orifice. Slight increases in the recovery distance were noticed at lower Reynolds number (above transition). This effect can be noticed in Figure 3.25a, where partial recovery occurred at about 6.5 pipe diameters from the orifice at a Reynolds number of 411 and, at 4.5 diameters for a Reynolds number of 2067. These results correlate with Back and Roschkes (1972) measurements which indicated a decrease in reattachment length with an increase in Reynolds number above the transition point to turbulence.

(10) At low Reynolds numbers viscous losses play an important role and the dimensionless pressure drop

decreases with increasing Reynolds number. Once
turbulence begins to develop the pressure drop
becomes independent of the Reynolds number and turbu-
lent losses are dominant. The onset of disturbances
usually produced a change in slope of the dimension-
less pressure drop versus Reynolds number curve.
Projecting the slope of the first few pressure mea-
surements (at low Re) onto the Re axis provided a
good approximation to the value at the onset of dis-
turbances. Similar correlation characteristics be-
tween pressure measurements and features of the flow
pattern had been reported previously by Johansen in
his experiments on orifice plates.

(11) Numerical calculations showed a non-vanishing instabil-
ity growth rate in the dimensionless wavenumber range
$o<kd<1.30$, where d is the thickness of the layer. The
instability growth rate showed a strong sensitivity to
the shear layer thickness, indicating that the fluid
behavior is largely dominated by the velocity gradient
in the layer. This large amplification rate for axi-
symmetric instabilities in velocity profiles showing a
sharp velocity transition appears to be the mechanism
producing very low experimental critical Reynolds num-
bers, as observed for the small area ratio models.
Maximum value of growth rate usually occurred for a

dimensionless wavenumber kd of order 1 (kd≈0.80)

(12) The presence of a back-flow region in the jet velocity distribution was slightly destabilizing. The effect was secondary when compared with the effect produced by changing the transition layer thickness.

(13) The effects produced by the presence of the boundaries were destabilizing for small disturbance wavenumbers. The destabilization of the flow was noticed in the rectangular and the cylindrical geometry. There were no significant effects at large disturbance wavenumbers.

(14) The direction of the disturbance phase velocity was the same as the main flow except for the case including a back-flow region, which showed a small negative phase velocity at small wavenumbers. At large disturbance wavenumbers both the symmetric and the anti-symmetric modes of propagation produced a disturbance phase velocity of magnitude close to half of the mean flow velocity. For small wavenumbers, symmetric perturbations in rectangular coordinates travelled above half the mean flow velocity, while non-symmetric perturbations travelled below that value, approaching zero with decreasing wavenumber.

(15) The action of the dimensionless parameter δ or the
flow instability to small periodic disturbances was
very strong. There was a significant stabilizing
effect upon symmetrical disturbances produced by a
decrease in δ (larger interface distance), however
it was destabilizing under non-symmetrical distur-
bances. For a very sharp velocity transition (large
δ) the instability growth rate approached the value
of 0.40, for both types of disturbances in the
rectangular geometry.

(16) The results of the inviscid analysis for cylindrical
unbounded jets showed that such jets are least
stable for low number (m=1) non-axisymmetric distur-
bances at intermediate distances from the orifice,
but the preferred mode of instability at very small
and large axial positions are axisymmetric. These
results can also be expected for the bounded jet as
observed experimentally (see Conclusion No. 7).

(17) The growth rate for the unbounded jet was found to
be a monotonically decreasing function of distance
from the jet orifice. Except for the m=1 mode
higher angular modes showed smaller growth rate,
with higher m mode suppression as the interfacial
distance increased. At sufficiently large values of
m the axisymmetric jet profile was stable.

(18) Axisymmetric disturbance of small wavenumber
     travelled close to the maximum speed of the flow,
     whereas non-axisymmetric disturbances travelled with
     about half that speed, as previously reported by
     Batchelor and Gill, for profiles with zero interface+
     thickness

While the relatively low transition Reynolds numbers ob-
served experimentally can not be predicted by inviscid
analysis, the technique does provide a good representa-
tion of the fluid instability characteristics, and the
possible unstable modes of propagation at large Reynolds
number. It also appears that the inviscid approach using
approximated velocity profiles is able to predict with a
fair degree of confidence the instability wavenumber that
is amplified the most for a given mean flow profile; and
within the limitations of the inviscid analysis the
approach can be used to study the instability character-
istics of a jet in a bounded medium.

APPENDIX A
VISCOSITY MEASUREMENTS

The Hoppler-Rheo-Viskometer

Viscosity measurements of various bentonite solutions samples were performed on several occasions using a Hoppler-"Rheo-Viskometer," with the purpose of determining the viscosity dependency on increasing rates of shear and temperature variations.

According to the instruction manual provided by the manufacturer of the instrument, the viscosity of a fluid is given by the formula

$$\mu(cp) = CPt \tag{A.1}$$

where C is the calibration constant, P is the load per unit area of the cross section of the tube, and t is the measured time for the glass ball to travel a certain distance.

The Rheo-Viskometer consists of a vertical glass tube of about 16mm diameter in which a glass ball fastened to a rod is forced to travel by the action of different weights. The distance travelled (30mm) is continuously indicated by an indicator clock, and the time of fall measured with chronometer (stop watch).

175

Temperature control was provided by a Haake Constant Temperature Circulator, Model F423. To provide ambient cooling (below room temperature) a partially insulated container of ice water was immersed in the bath of the Haake Circulator, and replaced at regular intervals.

To obtain reliable readings the instrument must be cleaned according to the manufacturer's instructions. The test tube as well as the measuring glass ball were thoroughly cleaned with alcohol and ethyl ether, and afterwards rinsed in distilled water. To prevent the formation of air bubbles, every sample of bentonite solution was heated for a period of 20 minutes at a temperature of 35-40°C, and carefully introduced into the test tube and, left overnight at room temperature (22°C), for the air bubbles to disappear.

Calibration

Although both cylinder and ball have dimensions which are specified to a few thousandths of a centimeter, the closeness of fit requires calibration for each combination of test tube and ball (for this test the 0.01 test tube), also it is necessary to maintain the same relative position each time the test tube is removed and replaced.

To calibrate the instrument a fluid of known viscosity is needed. In this case, pure water was used and the viscosity obtained from the Handbook of Chemistry and Physics. The results of the calibration procedure are a

plot of the calibration constant versus the reciprocal of the load per unit area at a constant temperature of $20^{\circ}C$.

To obtain the magnitude of the calibration constant at large fluid deformation $(P \to \infty)$, the linear relationship can be extrapolated to the ordinate axis. The nearest measured value of 0.00527 cp-cm^2/gr-sec was considered more reliable and used as the calibration constant for this particular tube. Knowing the calibration constant, the viscosity can be found by means of expression (A1).

Viscosity of Bentonite Solutions

The Bentonite solutions viscosity were measured in the same was as the calibration measurements and obtained for a temperature range between 20 and $26^{\circ}C$.

The results for a 0.20% solids concentration solution are shown in Figure A-1a. Water viscosity in the same temperature range (Handbook of Chemistry and Physics) is also shown for comparison purposes. In all cases a data point represents the average of four separate time readings.

The Bentonite solution showed a slightly higher viscosity than pure water (about 10%), with a decrease in viscosity as the fluid deformation increased from 5 to 10 gr/cm^2. Readings at load per unit area higher than

15.0 gr/cm^2 were not considered reliable. The viscosity for a concentration of 0.10% is shown in Figure A-1b again in the same temperature range. Notice the reduction in solution viscosity as the amount of solids in suspension decreased, approaching the viscosity of water.

Viscosity for large deformation was obtained by plotting the apparent viscosity versus the inverse of the load per unit area, at a temperature close to the average temperature during the flow visualization experiments ($\approx 24.5^oC$). The results are described in Figure A-2 for P=2.5, 5.0, 10.0, 15.0 and 20.0 gr/cm^2. It is evident that the flow structure undergoes a rapid transition at about P=15 gr/cm^2, probably produced by turbulence or flow separation behind the falling glass ball (E. Schonblom, 1974). Instead of extrapolating to the ordinate axis (P→∞), the magnitude at the last reliable point μ = 1.025cp was selected to be used as the viscosity of a 0.20% solid concentration Bentonite solution at a temperature of 24.5^oC.

The kinematic viscosity calculated according to the definition

$$\nu = \mu/\rho = 1.032 \times 10^{-2} \ cm^2/sec \qquad (A.2)$$

For a more extensive research on the viscosity and physical properties of Bentonite solutions of different solid concentration the reader is referred to Lindgren (1957).
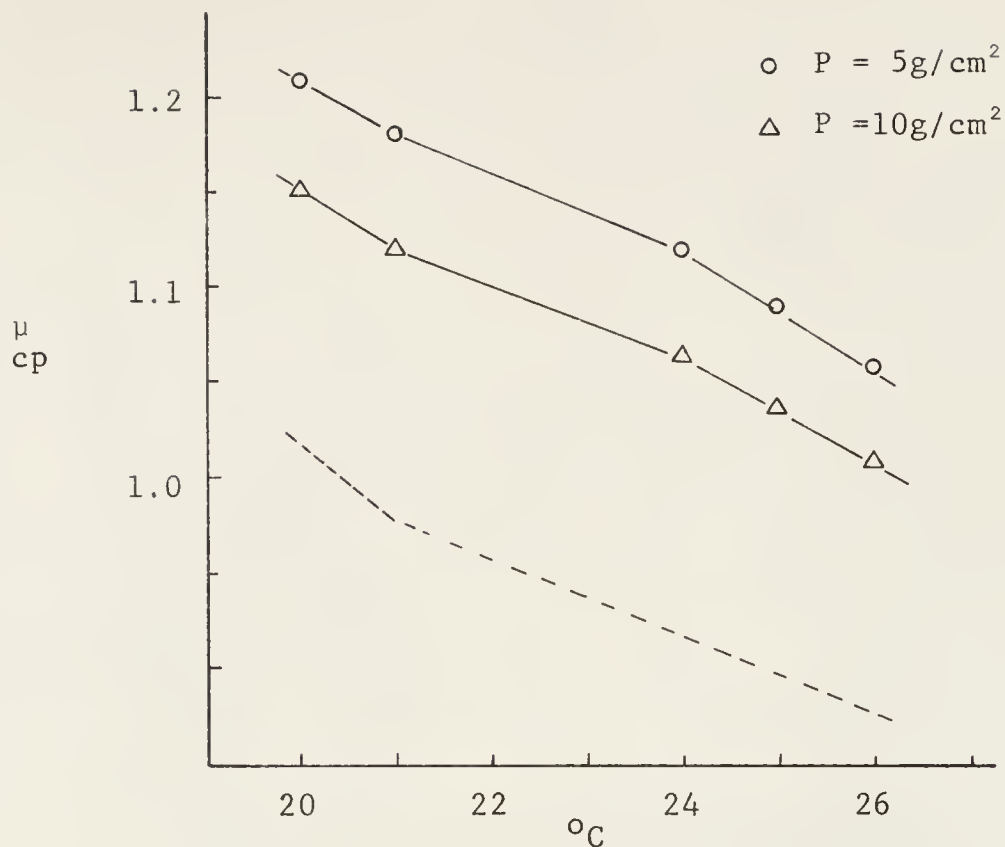
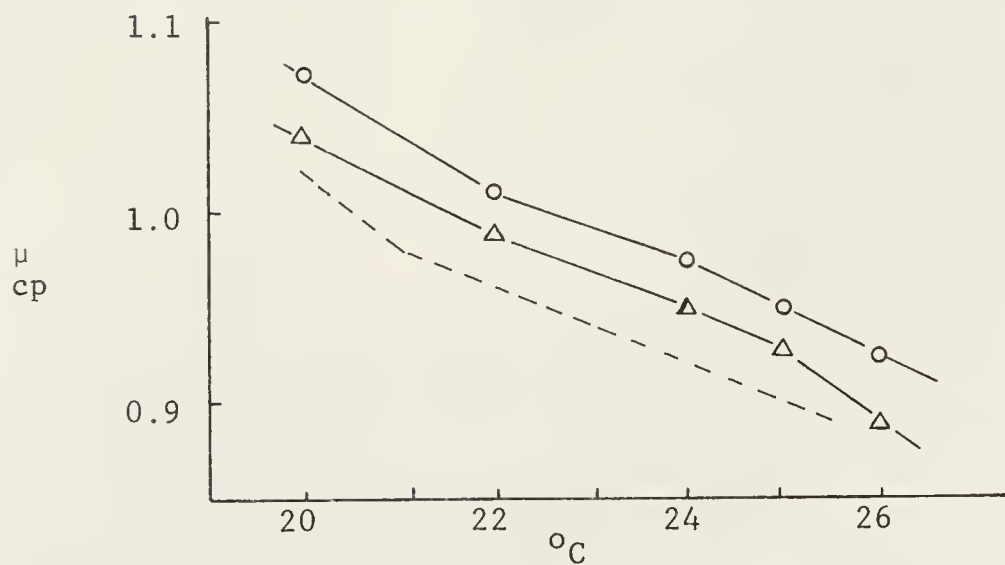Figure A.1a   Bentonite solution viscosity (0.2%)

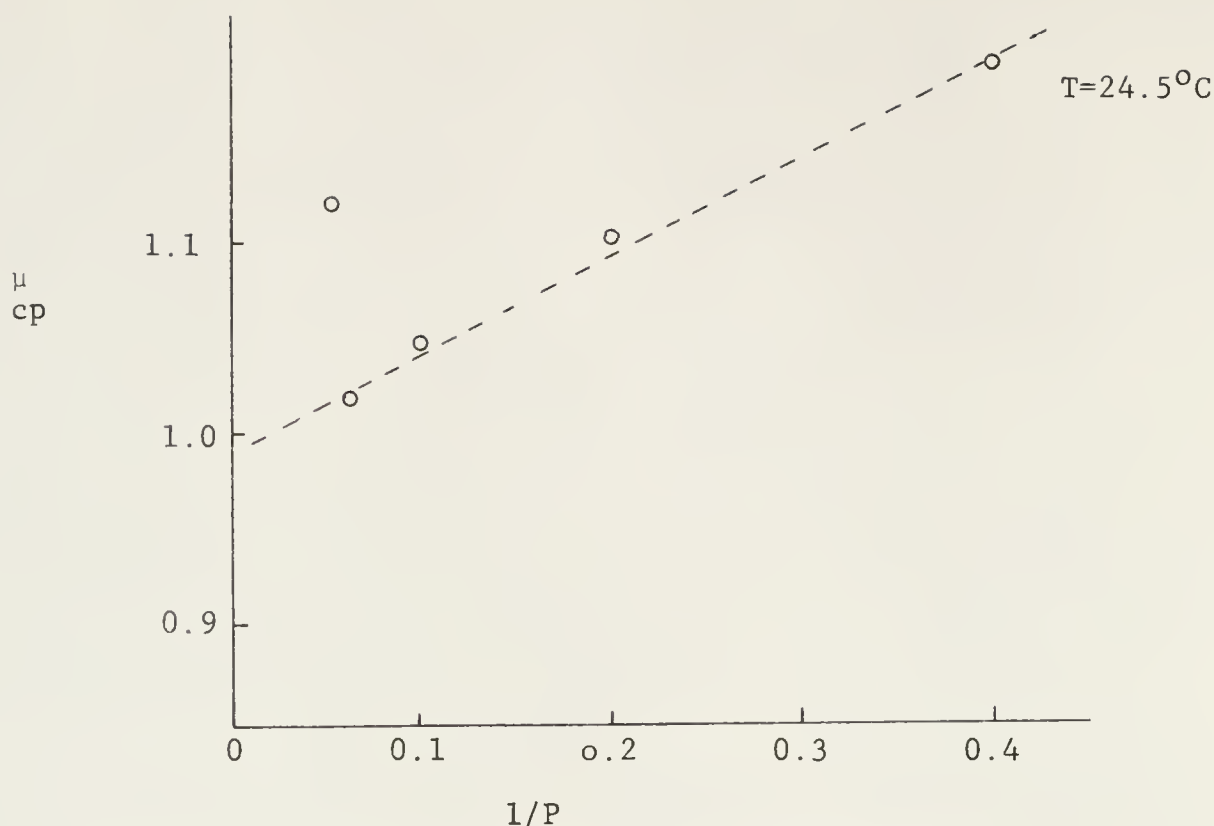Figure A.1b   Bentonite solution viscosity (0.1%)

Figure A.2   Fluid viscosity at large deformation

Viscosity of Polymer Solutions

The present experiments concern the viscosity measure-
ments of weak solutions of polyethlenoxide (Union Carbide
WSR-301) of molecular weight approximate 4,000,000.   The
viscosity of two samples of the polymer solution were deter-
mined by the method described previously, except that in
this case the polymer solution samples were not heated to
eliminate air bubbles.   The samples were taken from the
working solution of 0.01% concentration (100 PPM), prepared
by adding distilled water to the stock solution (1%) until
the proper concentration was reached.

The viscosity of the first sample was measured one week after preparation of the working solution, and the same fluid sample used to take all the readings of viscosity variations due to changes in load and temperature. The results of this investigation are described in Figure A-3 for a temperature range between 20 and 26°C. Water viscosity is also shown for comparison purposes.

The second sample viscosity was measured about 3 hours after preparation of the working solution, and the fluid sample changed every time the temperature was incremented. The idea was to determine if the shear rate degradation produced by the falling glass ball inside the
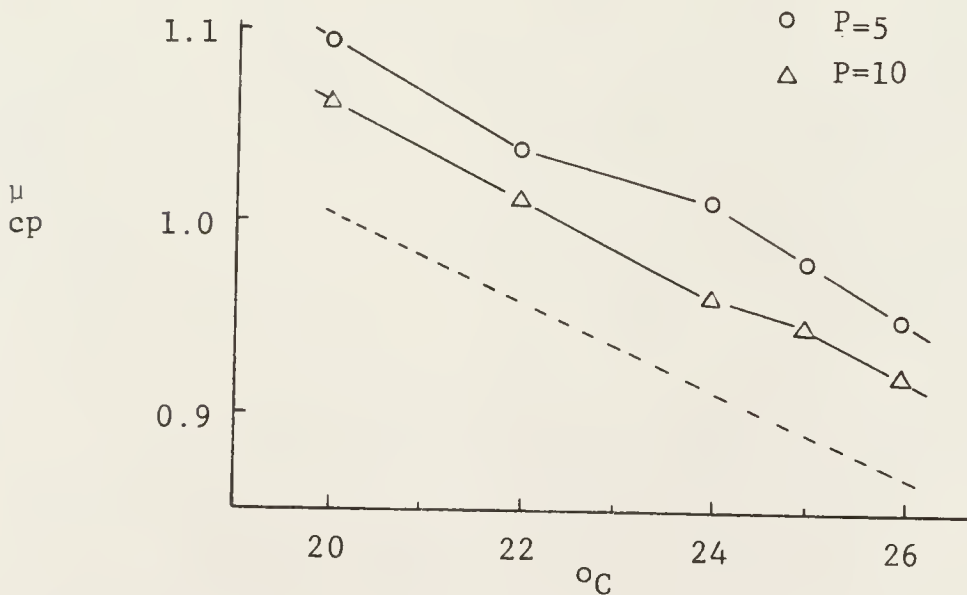

Figure A.3   Polyox solution viscosity (100PPM)

test tube was a significant factor. The viscosity of the polymer solution was slightly higher than water for both cases but the difference between the two was relatively small. The viscosity of the polymer solution appeared to be between 5 an 10% above the viscosity of water for a solution concentration of 100PPM. These measurements are in agreement with previous experiments on Polyox solutions done by Lindgren (1965) and by Paterson and Abernathy (1970).

BIBLIOGRAPHY

Abbot, D.E., and Kline, S.J., "Experimental investigation of subsonic turbulent flow over single and double backward facing steps," Trans. of the Asme, J. of Basic Eng. Sept. (1962, pp. 317-325).

Aillo, G.A., and Trefil, J.S., "The generalized entry flow problem and the establishment of Poiseuille flow in locally constricted tubes," J. Biomechanics, Vol. 9 (1976, pp. 49-54).

Andrade, E.N., "The velocity distribution in a liquid-into-liquid jet. The plane jet," Proc. Phys. Soc., London, 51 (1939, pp. 784-793).

Archer, W.J., Trans. ASCE. 76, (1913, p. 999).

Back, L.H., and Roschke, E.J., "Shear-layer flow regimes and wave instabilities and reattachment lengths downstream of an abrupt circular channel expansion." Trans. of the ASME, J. of App. Mech., Sept. (1972, pp. 677-681).

Batchelor, G.K., and Gill, A.E., "Analysis of the stability of axisymmetric jets," J. of Fluid Mech., Vol. 14 (1962, pp. 529-551).

Betchov, R., and Criminale, W.O., "Stability of Parallel Flows," App. Mth. and Mech., Vol. 10. Academic Press, New York and London (1967, p. 229).

Bickley, W., "The plane jet," Phil. Mag. Ser. 7, 23 (1939, pp. 727-731).

Binnie, A.M., "A double-refraction method of detecting turbulence in liquids," Proc. Phys. Soc. Lond. 57, 390 (1945).

Binnie, A.M., and Fowler, J.S., "A study by a double-refraction method of the development of turbulence in a long cylindrical tube," Proc. Roy. Soc. 192, 32, (1947).

Bruns, D.L., "A general theory of the causes of murmurs in the cardiovascular system," Amer. J. Med. 27 (1959, pp. 360-374).

Caro, C. G., Fitz-Gerald, J. M., and Schroter, R. C., "Atheroma and arterial wall shear observation, correlation and proposal of a shear dependent mass transfer mechanism for athero genesis," Proc. Roy. Soc. Lond. B 177 (1971, pp. 109-159).

Castro, W., and Squire, W., "The effect of polymer additives on transition in pipe flow," App. Sci. Res. 18, Sept. (1967, pp. 81-96).

Chandrasekhar, S., "Hydrodynamic and Hydromagnetic Stability," Clarendon Press, Oxford, (1961, p. 482).

Charm, S. E., and Kurland, G. S., "Blood Rheology in Cardiovascular Fluid Mechanics," D. H. Bergel, editor, Academic Press, Vol. 2 (1972, pp. 163-164).

Durst, F., Melling, A., and Whitelaw, J. H., "Low Reynolds number flow over a plane symmetric sudden expansion," J. of Fluid Mech., Vol. 64 (1974, pp. 111-128).

Fabula, A. G., Lumley, J. L., and Taylor, W. D., "Some interpretations of the Toms Effect" in Modern Developments in the Mechanics of Continua, Academic Press, N. Y. (1966).

Foreman, J. E. K., and Hutchison, K. J., "Arterial wall vibration distal to stenoses in isolated arteries of dog and man," Circulation Res. 26 (1970, pp. 583-590).

Fry, D. L., "Acute vascular endothelial changes associated with increased blood velocity gradients," Circulation Res. 22 (1968, pp. 165-197).

Fung, Y., "Stability of heterogeneous swirling flows," Ph. D. dissertation, Univ. of Florida (1974, pp. 12-17).

Fung, Y., and Kurzweg, U. H., "Stability of swirling flows with radius dependent density," J. Fluid Mech., Vol. 72 (1975, pp. 243-255).

Gonzalez, F., "The origin of Korotkoff Sounds and their role in Sphygmomanometry," Ph. D. dissertation, Univ. of Florida (1974, pp. 42-57).

Greene, H. L., Nokes, R. F., and Thomas, L. C., "Drag reduction phenomena in pulsed blood flow," Flow Its measurement and control in Science and Industry, Vol. 1, part 3, Inst. Soc. of America (1974, pp. 1459-1464).

Hagen, G., "Vebor die Bewengung des Wassers in engen cylindrischen Rohren," Ann.d. Ph.und Ch. (Pogg. Ann.) (2) 46 (1839, p. 423).

Handbook of Chemistry and Physics, 55th Edition, published by CRC Press (1975, p. F-49).

Helmholtz, H., "Über discontinuirliche Flüssigkeits-Bewegungen," Akad. Wiss. Berlin, Monatsber. 215 (1868).

Hershey, D., and Smolin, R., "Laminar retime transition for blood flow in tubes," Biorheology, 4:61 (1967, pp. 61-67).

Hoyt, J. W., and White, W. D., "High-Polymer Additive effects on turbulent flow of dextran, saline solution, and plasma," Proceedings 19th Annual Conference on Engineering in Medicine and Biology (1966, p. 49).

Hoyt, J. W., "The effect of additives on fluid friction," Trans. of the ASME, J. of Basic Eng. June (1972, pp. 258-285).

Iribarne, A., Frantisak, F., Hummel, R. L., and Smith, J.W., "An experimental study of Instabilities and other flow properties of a laminar pipe jet," AICHE Journal, Vol. 18, No. 14 (1972, pp. 689-698).

Johansen, F. C., "Flow through pipe orifices at low Reynolds numbers," Proc. R. Soc. London (Math, Phy. Sci.) 126 (1929, pp. 231-245).

Kelvin, Lord, "On a disturbance in Lord Rayleigh's solution for waves in a plane vortex stratum," Mathematical and Physical Papers, Vol. 4, Cambridge Univ. Press, London and New York (1880, pp. 186-187).

Kim, B. M., and Corcoran, W. H., "Experimental measurements of turbulence spectra distal to stenoses," J. of Fluid Mech., Vol. 7 (1974, pp. 335-342).

Kim, H. T., Kline, S. J., and Reynolds, W. C., "The production of turbulence near a smooth wall in a turbulent boundary layer," J. of Fluid Mech., Vol. 50 (1971, p. 133).

King, H. W., and Brater, E. F., "Handbook of Hydraulics" McGraw-Hill Book Co., New York (1963, pp. 6-21).

Lee, J.S., and Fung, Y.C., "Flow in locally constricted tubes at low Reynolds numbers," J. Appl. Mech., 37 (1970, pp. 9-16).

Lees, R.S., and Dewey, C.F., "Phonoangiography: A new non-invasive diagnostic method for studying arterial disease," Proc. Nat. Acad. Sci. 67 (2) (1970, pp. 935-942).

Lin, C.C., "On the stability of two dimensional parallel flows." Parts I, II, III. Quart. App. Math. 3 (1945, pp. 117-142, 218-234, 277-301).

Lindgren, E.R., "The transition process and other phenomena in viscous flow", Arkiv for Fysik, Band 12 nr 1 (1957, pp. 11-29).

Lindgren, E.R., "Viscosity studies on distilled water and weak sols. of Polyethylenoxide using the falling cylinder viscometer," Bureau of Ships Gen. Hydro. Res. Prog. S-R009 01 01, Oct. (1965, pp. 24-32).

Lopez, J.L., and Kurzweg, U.H., "Amplification of helical disturbances in a round jet," Physics of Fluids (to appear June 1977).

Macagno, E.O., and Hung, T., "Computational and experimental study of a captive annular eddy," J. of Fluid Mech., Vol. 28 (1967, pp. 43-64).

McDonald, D.A., "Blood Flow in Arteries," Ed. Arnold, London, (1960).

Michalke, A., and Schade, H., "Zur Stabilitat von freien Grenzschichten," Ingenieur - Archiv, 33 (1963, pp. 1-23).

Michalke, A. and Timme, A., "On the inviscid instability of certain two-dimensional vortex-type flows," J. Fluid Mech., Vol. 29 (1967, pp. 647-666).

Morgan, B.E., and Young, D.F., "An Integral method for the analysis of flow in arterial stenoses," Bull. of Math. Biology, Vol. 36 (1974, pp. 39-53).

Orr, W.M.F., "The stability or instability of the steady motions of a perfect liquid and of a viscous liquid. Part II: A viscous liquid," Proc. Roy. Irish Acad. 27 (1907, pp. 9-68, and pp. 69-138).

Paterson, R.W., and Abernathy, F.H., "Turbulent flow drag reduction and degradation with dilute polymer solutions," J. of Fluid Mech., Vol. 43 (1970, pp. 689-710).

Prados, J.W., and Peebles, F.N., "Two dimensional laminar-flow analysis utilizing a doubly refracting liquid," A.I.Ch.E. Journal, Vol. 5, No. 2 (1959, pp. 225-234).

Rayleigh, Lord, "On the stability, or instability, of certain fluid motions." Proc. of the London Math. Soc., XI (1880, pp. 57-70).

Rayleigh, Lord, "On the stability or instability of certain fluid motions" II, Proc. of the London Math Soc., XIX (1887, pp. 67-74).

Reynolds, A.J., "Observations of a liquid-into-liquid jet," J. Fluid Mech., 14 (1962, pp. 552-556).

Reynolds, O., "An experimental investigation of the circumstances which determine whether the motion of water shall be direct or sinuous, and of the law of resistance in parallel channels," Scientific Papers, Vol. 2, Cambridge Univ. Press (1883, pp. 51-105).

Roach, M.R., "An experimental study of the production and time course of poststenotic dilatation in the femoral and carotid arteries of adult dogs." Circulation Res. 13 (1963a, pp. 537-551).

Roach, M.R., "Changes in arterial distensibility as a cause of poststenotic dilatation," Amer. J. Cardiol. 12 (1963b, pp. 802-815).

Robbins, S.L., and Bentov, I., "The kinetics of viscous flow in a model vessel," Laboratory Investigation, Vol. 16, No. 6 (1967, pp. 864-874).

Robertson, J.M., and Herrick, J.F., "Turbulence in Blood Flow," Dept. of Theoretical and App. Mech. Univ. of Illinois, T. & A.M. Report No. 401 (1975).

Robicseck, F., Sanger, P.W., Taylor, F.H., Magistro R., and Foti, E., "Pathogenesis and significance of post-stenotic dilatation in great vessels," Ann. Surg. 147 (1958, pp. 835-844).

Rodbard, S., Ikeda, K., and Montes, M., "An analysis of mechanisms of poststenotic dilatation," Angiology 18 (1967, pp. 349-369).

Ruden, P., "Turbulente Ausbreitung im Freistrahl," Naturwissenschaften, 21 (1933, pp. 375-378).

Sacks, A. H., Tickner, E. G., and MacDonald, I. B., "Criteria for the onset of vascular murmurs," Circulation Research, Vol, XXIX (1971, pp. 249-256).

Schiller, L., "Experimentelle Untersuchungen zum Turbulenz problem," ZAMM 1 (1921, p. 436).

Schlichting, H., "Über die Stabilitat der couetteströmung," Ann. d. Phys. V (1932, pp. 905-936).

Schlichting, H., "Laminare Strahlausbreitung," ZAMM 13 (1933, pp. 260-263).

Schlichting, H., "Boundary Layer Theory," Sixth Edition, McGraw-Hill Book Co., New York (1963, pp. 439-444).

Schonblom, J. E., "Rheology and streaming birefringence of an anisotropic fluid," Ph. D. diss. Univ. of Florida (1974, pp. 205-208).

Seeley, B. D., and Young, D. F., "Effect of geometry on pressure losses across models of arterial stenoses," J. Biomechanics, Vol. 9 (1976, pp. 439-448).

Sommerfeld, A., "Ein Beitrag zur hydrodynamischen Erklärung der turbulenten Flussigkeitsbewegung," Atti del 4. Congr. Internat. dei Mat. Vol III, Roma (1908, pp. 116-124).

Tatsumi, T., "Stability of the laminar inlet-flow prior to the formation of Poiseuille regime, I and II," J. Ph Soc.. Jap. 7 (1952, pp. 489-495).

Tatsumi, T., and Kakutami, T., "The stability of a two-dimensional laminar jet." J. Fluid Mech. 4 (1958, pp. 261-275).

Taub, H. H., "Investigation of nonlinear waves on liquid jets," The Physics of Fluids, Vol. 19, No. 8 (1976, pp. 1124-1129).

Tollmien, W., "Berechnung turbulenter Ausbreitungsvergange," ZAMM 6 (1926, pp. 468-478).

Tollmien, W., "Über die Entstehung der Turbulenz," 1. Mitteilung. Nachr. v.d. Gesellschaft d. Wiss. zu Gottingen, Mat.-Ph. Kl., Heft 1 (1929, p. 21).

Toms., B. A., "Some observations on the flow of linear polymer solutions through straight tubes at large Reynolds numbers," Proc. Int. Congress on Rheology," Vol. III, North Holland Pub. Co., Amsterdam (1949, p. 135).

Union Carbide Brochure F-42933. "How to dissolve Polyox water-soluble resins," (1970).

Viilu, A., Preliminary report of MIT. (Dep. of Aeron. and Astron.) for NASA. Grant No. NSG-31-60, (1960).

Virk, P. S., Merrill, E. W., Mickley, H. S., and Smith, K. A., "The critical wall shear stress for reduction of Turbulent drag in pipe flows by Poly (Ethylene Oxide) in Dilute Solution," Mod. Devep. in the Mech. of Continua, Acad, Press Inc., N.Y. (1966).

Watson, G. N., "A Treatise on the theory of Bessel Functions," 2nd Edition, Cambridge Univ. Press, Cambridge (1966, pp. 79-80).

Whitaker, S., "Introduction to Fluid Mechanics," Prentice-Hall, Inc., N.J. (1968, p. 235).

Young, D. F., and Tsai, F. Y., "Flow characteristics in models of arterial stenoses-I Steady Flow," J. of Biomechanics, Vol. 6 (1973, pp. 395-409).

Zimm, W., "Über die Strömungsvorgänce im freien Luftstrahl," VDI-Forschungsheft 234 (1921).
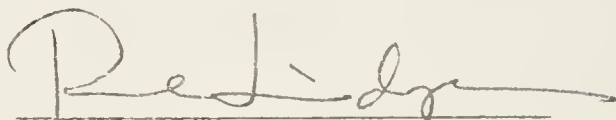
BIOGRAPHICAL SKETCH

The author was born on 27 January 1941 in Habana, Cuba, where he received his elementary and high school education. After attending the School of Physics at Habana University for a period of two years he came to the United States where he entered the University of Miami from which he received a Bachelor of Science degree in Mathematics in 1968, and a Master of Science degree in Physics in 1970. Upon graduation, he accepted employment at the Air Force Armament Laboratory at Eglin Air Force Base, Florida, where he is presently employed.

I certify that I have read this study and that in my opinion it conforms to acceptable standards of scholarly presentation and is fully adequate, in scope and quality, as a dissertation for the degree of Doctor of Philosophy.
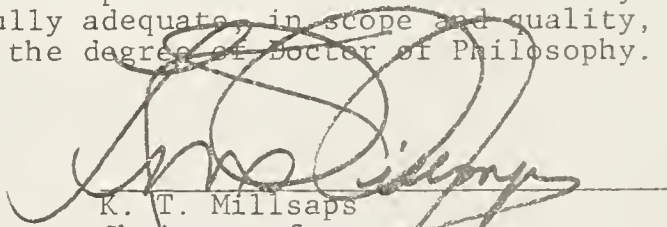
U. H. Kurzweg, Chairman
Professor of
Engineering Sciences

I certify that I have read this study and that in my opinion it conforms to acceptable standards of scholarly presentation and is fully adequate, in scope and quality, as a dissertation for the degree of Doctor of Philosophy.
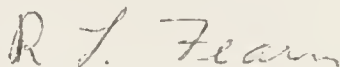
E. R. Lindgren
Professor of
Engineering Sciences

I certify that I have read this study and that in my opinion it conforms to acceptable standards of scholarly presentation and is fully adequate, in scope and quality, as a dissertation for the degree of Doctor of Philosophy.

K. T. Millsaps
Chairman of
Engineering Sciences

I certify that I have read this study and that in my opinion it conforms to acceptable standards of scholarly presentation and is fully adequate, in scope and quality, as a dissertation for the degree of Doctor of Philosophy.

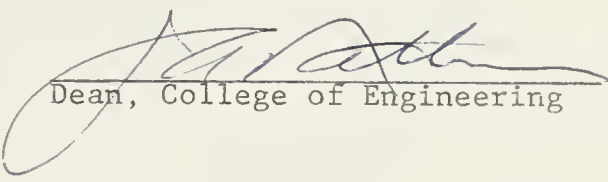R. L. Fearn
Associate Professor of
Engineering Sciences

I certify that I have read this study and that in my opinion it conforms to acceptable standards of scholarly presentation and is fully adequate, in scope and quality, as a dissertation for the degree of Doctor of Philosophy.

R. J. Gordon
Associate Professor
of Chemical Engineering

This dissertation was submitted to the Graduate Faculty of the College of Engineering and to the Graduate Council, and was accepted as partial fulfillment of the requirements for the degree of Doctor of Philosophy.

June, 1977

Dean, College of Engineering

Dean, Graduate School